GAS PHASE STUDIES OF ORGANIC AND BIOLOGICAL SPECIES USING

MASS SPECTROMETRY

by

MU CHEN

A dissertation submitted to the

Graduate School-New Brunswick

Rutgers, The State University of New Jersey

in partial fulfillment of the requirements

for the degree of

Doctor of Philosophy

Graduate Program in Chemistry and Chemical Biology

written under the direction of

Professor Jeehiun K. Lee

and approved by

_____

_____

_____

_____

New Brunswick, New Jersey

May, 2014

ABSTRACT OF THE DISSERTATION

GAS PHASE STUDIES OF ORGANIC AND BIOLOGICAL SPECIES USING MASS SPECTROMETRY

By MU CHEN

Dissertation Director:

Professor Jeehiun K. Lee

This dissertation focuses on the study of gas phase properties of several organic and bioorganic species, using experimental (mass spectrometry) and computational (Gaussian) methods.

Damaged nucleobases are from oxidation or methylation of normal nucleobases. These damaged bases are linked with diseases, aging, and cell death. They can be excised by enzymes such as DNA glycosylases. However the mechanism is still unknown. Tautomerism, proton affinity, and acidity of a damaged base xanthine have been studied to understand the mechanism of AlkA, the enzyme that excises xanthine.

1,2,3-triazoles are novel compounds that have various applications, especially in synthetic and catalytic chemistry. The fundamental properties of these triazoles could potentially be useful in understanding their binding to metals. Tautomerism, proton affinity, and acidity of several 1,2,3-triazoles have been studied by using computational and experimental methods. The results indicate that PA of the triazoles correlate with their binding ability to metals such as gold.

N-Heterocyclic carbenes (NHCs) are good electron donors and are used as ligands in organometallic complexes. However, unlike the traditional carbenes (methylene), NHCs are not electrophilic. *N,N'*-Diamidocarbenes (DACs) display not only nucleophilic but also electrophilic properties. The proton affinity of several DACs were studied and found to be close to proton affinity of the NHCs. The electrophilic reactivities of DACs can be attributed to their low-lying LUMO orbitals.

Nucleophilicity and electrophilicity in the gas phase are important reactivity parameters of organic species. Gas phase calculations and experiments can exclude the influence of solvents and reveal the intrinsic properties of nucleophiles and electrophiles. Classic physical organic approaches, including Hammett plots, kinetic isotope effect, and H/D exchange, have been employed to study the gas phase reactions between nucleophiles and electrophiles.

RNA oligonucleotides (2-5nt) are found to play important roles in the transcription of DNA. However, the specific RNA species and their sequences are unknown. An LC-MS method has been developed for the separation and quantification of these oligonucleotides. Collision induced dissociation (CID) patterns of the oligonucleotides are found to be useful in the characterization of these biologically significant species.

DEDICATION

To my wonderful parents for their love and everything

ACKNOWLEDGEMENTS

TABLE OF CONTENTS

LIST OF FIGURES

LIST OF TABLES

Chapter 1. Introduction

1.1 Overview

1.1.1 Gas phase acidity and proton affinity of xanthine

Deoxyribonucleic acid (DNA) carries genetic information[1] and it has a "double-helix" structure that consists of two complementary strands (polynucleotide). The basic structure of the polynucleotide is nuclecotide. The nucleotide contains a five-membered sugar (deoxyribose) ring which are connected by phosphodiester bonds. Each sugar ring has a nucleobase connected via an *N*-glycosidic bond. Figure 1.1 illustrates the basic structure of DNA (cytosine is used as an example).
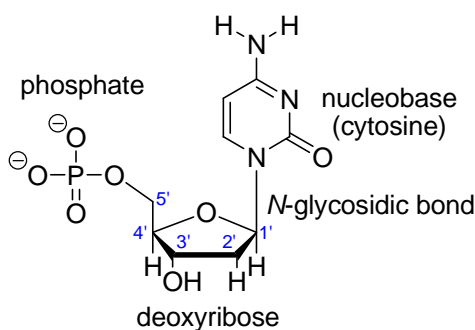
Figure 1.1. Basic structure of DNA (nucleotide).

The nucleobases that normally exist in DNA are purines and pyrimidines. Structures of these nucleobases (and uracil in RNA) are shown in Figure 1.2.
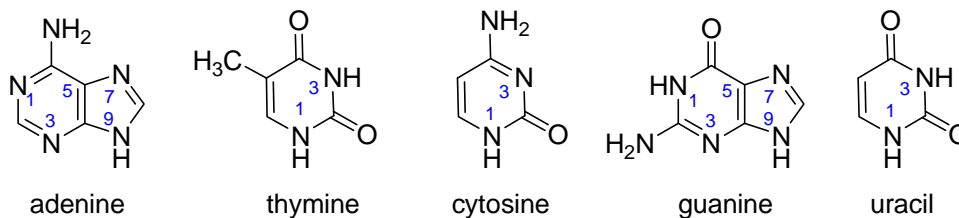
Figure 1.2. Structures of normal DNA and RNA nucleobases.

In human body, DNA can be attacked by cellular metabolites, various chemicals, UV light, and radiation. The attack of DNA can cause DNA modifications, one example of which is the nucleobase modification. This nucleobase modification process generates damaged nucleobases (see Figure 1.3 for several examples) which are related to cancer, aging, and cell death.[2-7]

7-methyladenine   3-methyladenine   7-methylguanine   3-methylguanine

O-methylguanine   1,N^6-ethenoadenine
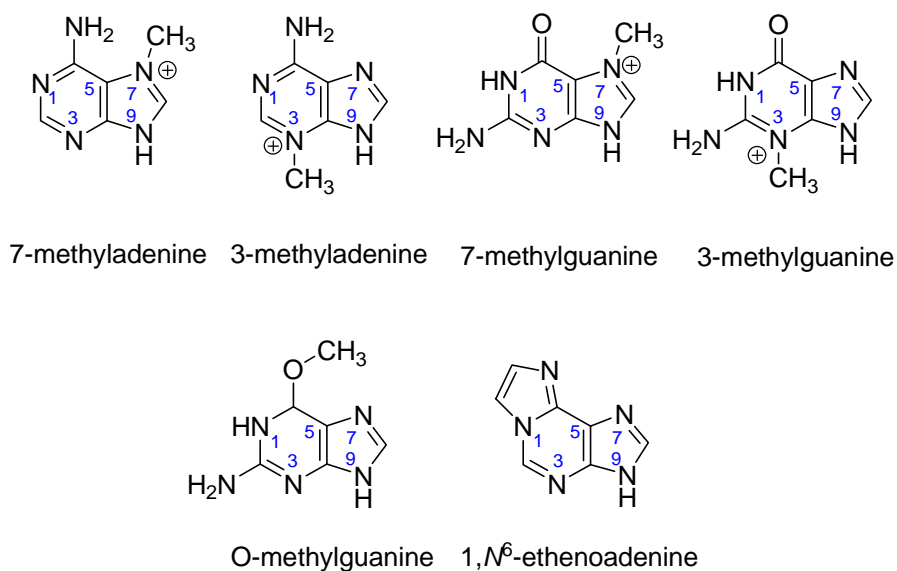
Figure 1.3. Structures of some damaged nucleobases.

The damaged nucleobase can be fixed by a BER mechanism. In this pathway, the DNA repair enzyme recognizes and excises the damaged nucleobases. However, the mechanism by which the enzyme, *N*-glycosylase, recognizes and excises the damaged bases is unknown.[4,7,8] To study the mechanism of the BER pathway, it is important to

study the intrinsic acidity and proton affinity of the nucleobases because these properties are significantly relevant to the mechanism.

The gas phase environment is a very useful place to study the properties of nucleobases for several reasons. First, the gas phase environment excludes the influence of solvents and reveals the intrinsic properties of the subject under study. Second, many biological systems are non-aqueous or non-polar, including the active sites of the DNA repair enzymes.[9-13] The gas phase provides properties of molecules in the non-polar environment, which can be employed to study the biological media under discussion.[9-12,14-16]

The acidity ($\triangle H_{acid}$) of an acid in the gas phase, HA, is the delta enthalpy of the deprotonation of HA into its conjugate base. The gas phase proton affinity (PA) of a base (B) is the negative value of the enthalpy change of the protonation reaction of the base (Eq. 1.1 and Eq. 1.2).

$$HA \longrightarrow H^+ + A^- \; ; \Delta H = \Delta H_{acid, AH} \quad \text{Eq. 1.1}$$
$$B + H^+ \longrightarrow BH^+ \; ; -\Delta H = PA_B \quad \text{Eq. 1.2}$$
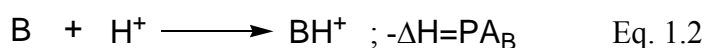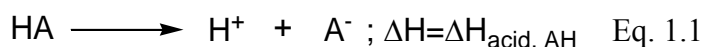
The differences between the intrinsic properties of normal nucleobases and damaged nucleobases are used to understand the mechanism of *N*-glycosylases and BER pathways.[9-11,14,17-21] In Chapter 1, an experimental and computational study of a damaged nucleobase, xanthine, is described. Xanthine is cleaved by an enzyme named 3-methyladenine-DNA glycosylase II AlkA. The acidity and PA of xanthine are studied. These studies support a hypothesized mechanism of AlkA.

1.1.2 Gas phase acidity and proton affinity of 1,2,3-triazoles

1,2,3-Triazoles have the basic five-membered ring structure with three nitrogen atoms adjacent to each other (Figure 1.4). As stable compounds in physiological conditions, 1,2,3-triazoles have been under close investigation for decades[22]. With the development of "click chemistry" discovered by Sharpless and coworkers in 2001[23], different 1,2,3-triazoles were prepared for various purposes and applications, including energetic materials[24], drug-delivery[25], dyes for bioimaging[26], and chemotherapy for cancer[27].
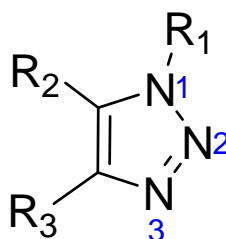
Figure 1.4. Structures of 1,2,3-triazole

The other very important application of 1,2,3-triazoles is that they can be used as ligands to transition metals. Organometallic catalysts in which 1,2,3-triazoles coordinate to various metals, including Cu(II)[28], Zn(II)[29], Pd(0)[30], and Au(I)[31], were reported capable of catalyzing many useful organic transitions.

Since 1,2,3-triazoles can bind to metals as both cations (protonated) and anions (deprotonated), their proton affinity (PA), acidity, and tautomerism are essential for the better understanding of their organometallic bonding to metals. The acid-base properties of 1,2,3-triazoles have been studied in different solvents; however, not many studies have looked at the fundamental properties of the 1,2,3-triazoles in the gas phase.[32-35] In Chapter 2, the characterization of the gas phase PA, acidity, and tautomerism of

1,2,3-triazoles is described. These studies are potentially informative for the understanding and application of 1,2,3-triazole ligands.

1.1.3 Proton affinities of *N*-heterocyclic carbenes and *N,N'*-diamidocarbenes

A carbene is an organic molecule with a neutral carbon that has a valence of two and two unshared valence electrons[36] (Figure 1.5). The two unshared valence electrons can occupy the sp^2 orbital with opposite spin (singlet) or occupy the sp^2 and the empty p orbital with parallel spin (triplet) (Figure 1.5). Depending on the atoms bonded to the carbon and the electronic structures of the molecule, carbenes can exist in either singlet or triplet ground state.
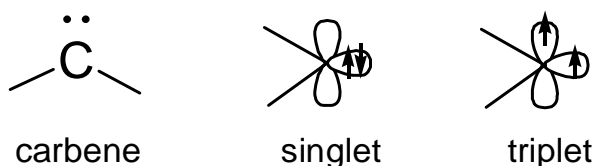
Figure 1.5. Structure of carbene and its two spin states

The classic example of the traditional carbene is methylene (CH_2:). It has a triplet ground state. Traditional carbenes display various electrophilic reactivities[37-40]. However, traditional carbenes such as CH_2: are quite reactive and short-lived. Their application is thus limited.

N-Heterocyclic carbenes (NHCs) were isolated by Arduengo *et al.* and Igau *et al.* in 1991[41,42] as the first stable carbene (Figure 1.6). These NHCs have singlet ground states and have been widely studied and utilized in many aspects of chemistry, especially as ligands to transition metals such as ruthenium, palladium, and nickel.[43-49] NHCs are

known as the second generation ligands in the catalysts for the Grubbs ruthenium olefin metathesis and perform better than the first generation ligand, PCy_3.[50] The intrinsic properties of the NHCs such as their proton affinity and acidity can help better understand the reactivities of NHCs.
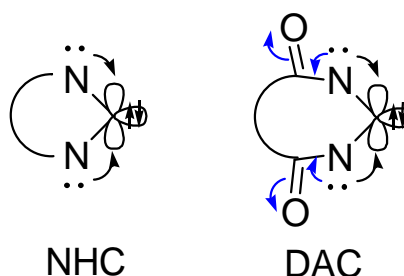
Figure 1.6. *N*-Heterocyclic carbene (NHC) and *N,N'*-diamidocarbene (DAC)

The two electron-donating amino groups that stabilize the divalent carbon nucleus render the NHCs more nucleophilic than traditional carbenes (such as methylene). However, NHCs are not able to undergo the typical electrophilic reactions of the traditional carbenes (CH_2:), such as C-H insertion, CO affixation and so forth.[51] By attaching a carbonyl group to the nitrogen atoms of a NHC, our collaborator managed to remove the electron density from the empty *p* orbital on the carbon nucleus to the low-lying π^* orbitals of carbonyls (Figure 1.6).[52,53] These carbenes, named *N,N'*-diamidocarbenes (DACs), exhibit not only nucleophilic properties, such as binding effectively to transition-metals, but also electrophilic reactivity.

In order to study the intrinsic properties of the NHCs and DACs, I characterized their proton affinity in the gas phase by using both computational and experimental methods. Chapter 3 describes this work and discusses how PA and other properties of DACs can be used to explain the similarity and differences between the reactivity of

NHCs and DACs. Steric hindrance from the substituents on the nitrogens is also studied for the gas phase reactivity of these carbenes.

1.1.4 Covalent bond versus hydrogen bond in gas phase clusters

The mechanisms of organic reactions involve the transfer of electrons. For example, in the S_N2 mechanism of nucleophilic substitution of an alkyl halide, a nucleophile donates an electron pair to the carbon center of the substrate to form a new covalent bond. The leaving groups leaves with a pair of electrons at the same time (Figure 1.7). In the S_N1 mechanism, the leaving group leaves to form a carbocation first, which subsequently accepts a pair of electrons from a nucleophile. In this case, the carbocation is considered as an electrophile (Figure 1.7). The strength of a nucleophile is usually referred to as the nucleophilicity. In the same way, the strength of an electrophile is referred to as the electrophilicity.[54-57]
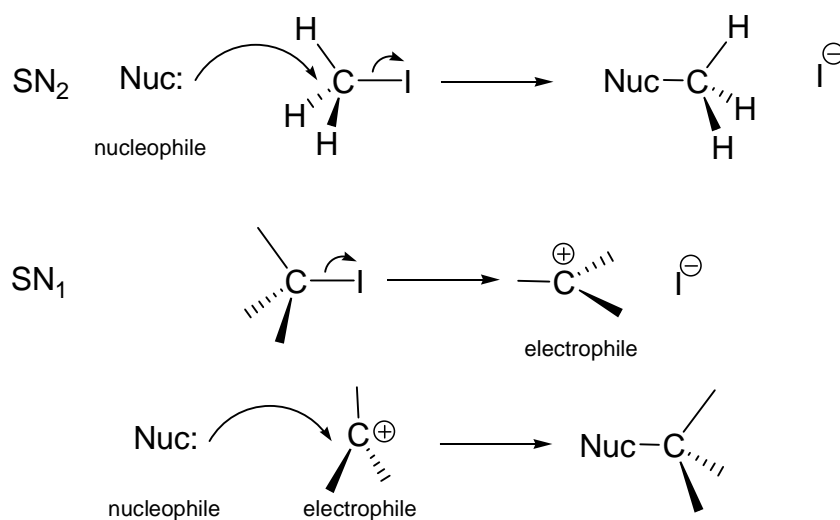
Figure 1.7. Nucleophile and electrophile in SN_1 and SN_2 reactions

Many factors could influence nucleophilicity and electrophilicity, including the nature of the nucleophile or electrophile, solvent, and temperature of the reaction. There are many attempts to describe these two kinetic parameters quantitatively by assigning parameters to different nucleophiles and electrophiles.[58-61] Among these studies, the nucleophilicity and electrophilicity parameters reported by Mayr and coworkers in 1994 is the most systematic.[62] They demonstrated that the relative rate constants of a nucleophilic reaction can be described by the following equation (Eq. 1.3), in which two parameters are used for the nucleophile (s, N) and one parameter for the electrophile (E). These parameters cover a large range of reactivity and provide satisfactory predictions on many nucleophilic reactions.

$$\log k = s(N+E) \qquad \textbf{Eq. 1.3}$$

However, all these parameters developed to describe the nucleophilicity and electrophilicity are in the solution phase. With the presence of the solvent, the parameters do not represent the intrinsic properties of the nucleophiles and electrophiles. Gas phase can provide a vacuum environment which excludes the influence of the solvents. Thus, the characterization of the nucleophilicity and elctrophilicity in the gas phase could help better understand the relationship between structure and reactivity. Denekamp and coworkers reported the first characterization of nucleophilic and electrophilic parameters in the gas phase.[63] However, some fundamental questions remain unsolved in their study. Chapter 4 describes our preliminary study of these parameters in the gas phase. The gas phase ion-molecule reactions of a series of diphenylmethylium cations and neutral electrophiles are monitored in a 3D ion trap mass spectrometer. Both computational and

experimental physical organic methods have been used to probe the nature of the clustering in between the cations and neutral nucleophiles in the gas phase.

1.1.5 Collision induced dissociation of RNA oligonucleotides in the gas phase

Transcription is the first step of gene expression[64], during which RNA polymerase initiates the synthesis of *m*RNA. When the RNA polymerase recognizes the first gene, RNA transcripts with 2-15 nucleobases are sometimes synthesized. This process competes with the formation of full-length mRNA transcripts and is referred to as "abortive initiation". It is believed to play important functional roles in regulating transcription.[65]

Our collaborator Nickels and coworkers reported the first detection of abortive transcripts *in vivo*.[66] Their work supported the possible important functional roles played by these short abortive nucleotides. However, due to the lack of information about their identities, the functions of these abortive RNAs are largely unknown. It is significantly important to develop a method to analyze short RNA nucleotides (nanoRNAs) to help understand the abortive transcription.

Mass spectrometry and tandem mass spectrometry are powerful tools that can be used for the characterization of RNA oligonucleotides.[67,68] In chapter 5, the characterization of simple oligonucleotides using a quadrupole ion trap mass spectrometer is described. The collision induced dissociation (CID) fragmentation patterns of the oligonucleotides are studied in both positive and negative ion modes and are analyzed. This fragmentation information is potentially useful in characterizing abortive transcripts in vivo and understanding their biological functions.

1.2 Instrumentation

1.2.1 FTMS

The Fourier transform ion cyclotron resonance mass spectrometer (FT-ICR, or FTMS) is a mass analyzer, which detects ions based on the relationship between mass-to-charge ratio (m/z) and frequency (ω) of a cyclotron in a magnetic field. [69]

For a positively charged particle, its circular motion in a magnetic field, B can be depicted in Figure 1.8, in which v is the velocity of the particle, r is radius of the trajectory, F_L is magnetic force (or Lorentz force), F_c is centrifugal force.
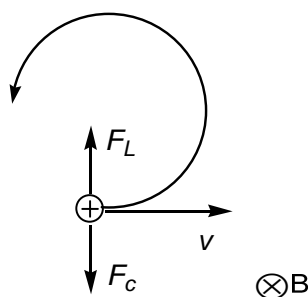
Figure 1.8. The motion of a positively charged ion in a magnetic field[69,70]

The Lorentz force F_L is the product of the charge, velocity, and field strength:

$$F_L = qv\text{B} \qquad \textbf{Eq. 1.4}$$

The centrifugal force is proportional to the mass of the particle, square of the velocity and inversely proportional to the radius of the gyration:

$$F_c = mv^2/r \qquad \textbf{Eq. 1.5}$$

When the centrifugal force is balanced with the Lorentz force, the cyclotron can be stabilized on a circular trajectory:

$$qv\text{B} = mv^2/r \qquad \textbf{Eq. 1.6}$$

Since the frequency ω and the velocity have the following relationship:

$$\omega r = v \qquad\qquad \textbf{Eq. 1.7}$$

Thus:

$$\omega = \frac{e\text{B}}{\frac{m}{z}} \text{ , } e\text{=Faraday constant, B=magnetic field strength, } \textbf{Eq. 1.8}$$

Equation 1.8 shows that for a given magnetic field, the frequency of the cyclotron is solely depended on the mass-to-charge ratio.

In our FTMS instrument, the cyclotron is trapped in a magnetic field in an "analyzer cell". One typical analyzer cell is a cubic cell (Figure 1.9). The cubic cell consists of three pairs of metal plates named "trapping plates", "detection plates", and "excitation plates". All three pairs of plates are placed in a fixed magnetic field with the trapping plates perpendicular to the magnetic field, and the other two pairs of plates parallel to the magnetic field.[69,70]
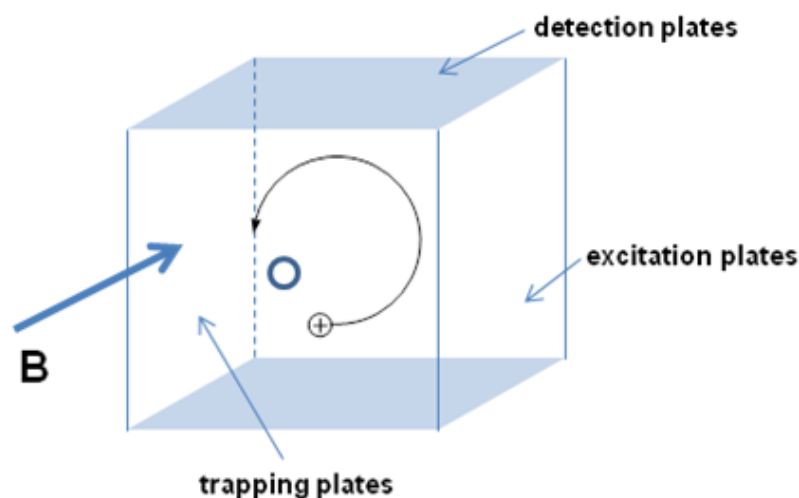
Figure 1.9. Plates in the cubic analyzer cell of FTMS

The charged particle enters the cubic cell from the holes on the trapping plates and starts the circular motion in the magnetic field. A radio frequency is then applied. When

the radio frequency has the same frequency as the cyclotron, the cyclotron absorbs the radio frequency and get excited to another trajectory which has a larger radius. When the excited ions are near the detection plates, they induce an alternating current or the "image current", which can be interpreted in frequency signals. The frequency signals will eventually be translated into the mass-to-charge ratio information of the detected ions.[69]

1.2.2 Electrospray ion source

Electrospray ionization (ESI) is a widely used ion source for mass spectrometry, especially for the analysis of biological macromolecules. ESI ionizes samples at atmospheric pressure and is a considered as a "soft ionization" method, since the process often generates a molecular ion or pseudo molecular ion without fragmentation. The electrospray mass spectrometry (ESI-MS) technique was developed by John Bennett Fenn in the 1980s.[71,72]

The process of electrospray ionization can be illustrated in Figure 1.10. Under atmospheric pressure, an electrospray is generated by applying a strong electric field to a flow of solution (usually slow flow rate). The analyte of interest is usually dissolved in a volatile solvent such as methanol, and injected into a stainless steel or silica capillary. The solution is pushed through the capillary by a pump at a speed of 1-1000 uL/min and comes out at the end of the capillary tip. Between the capillary tip and the counter electrode (in our instrument, a heated metal capillary), a potential difference of 3-6 kV is applied. The capillary tip and the counter electrode is usually separated by 0.3-2.0 cm, thus a very strong electric field is generated in the atmospheric region between the tip and counter electrode.[73]
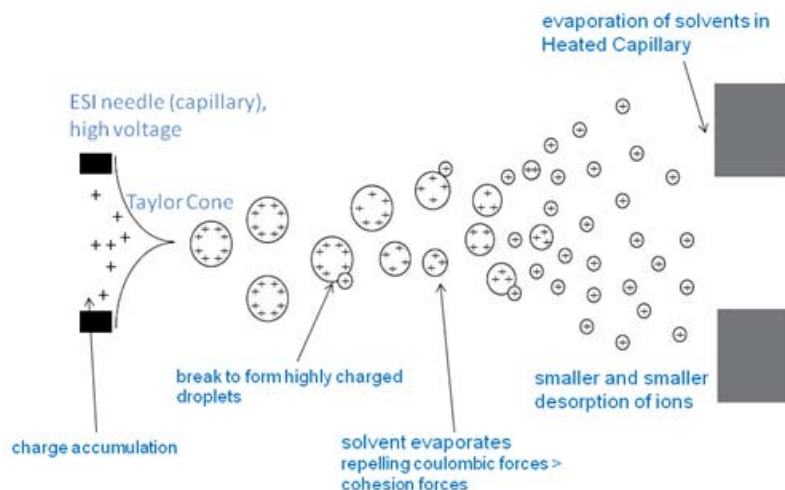
Figure 1.10. Process of electrospray ionization[74] (adapted from ref75 and other pictures)

Due to the strong electric field, charged ions accumulate at the end of the capillary tip and form a conical shape named "Taylor cone". The solution can break to form highly charged droplets at the Taylor cone.[75-77] Being directed by the electric field, the charged droplet can travel from the capillary to the heated capillary. During this process, the evaporation of solvents from the droplet can increase the repelling coulombic force to reach the Rayleigh limit, at which the droplet becomes unstable can break into smaller droplets. With further evaporation of solvents, the smaller droplet becomes unstable and breaks into even smaller droplets. Eventually, all the solvents will be evaporated and the ions will be released.

1.2.3 Quadrupole mass spectrometers

The quadrupole device separates and analyzes ions based on their mass-to-charge ratios by utilizing the stability of the ions' trajectories. Paul and Steinwegen discovered

the principle of quadrupole in the 1950s.[78] Shoulders, Finnigan, and Story later developed the quadrupole into a commercially available instrument.[79]

A quadrupole analyzer is made up of four rods with the set up shown in Figure 1.11. A pair of rods that are opposite to each other has the same polarity. If a positively charged ion enters the space between the four rods, it will be driven to a rod with negative potential. Before it hits the negative rod, the polarity of the rods can be changed and the positively ion will be driven away from the rod. An alternative electric field is applied on the two pairs of rods to allow ions of certain mass-to-charge ratios to go through the space in between while other ions get discharged. Based on this, the ions can be separated and analyzed.[80]
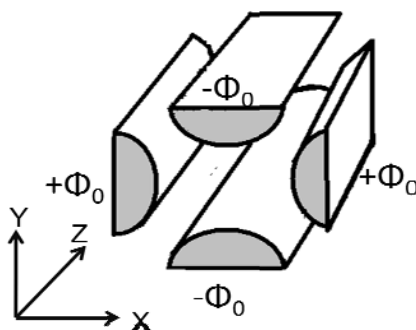
Figure 1.11. Four rods in the quadrupole analyzer[81]

One configuration of the quadrupole analyzer is the linear ion trap (2D ion trap, Figure 1.12). The linear ion trap has three sections and ions from the ion source enters the ion trap from the front section and get trapped in the middle section. By manipulating the RF frequency on the hyperbolic electrodes and the DC voltages on the two end electrodes, the ions can be trapped or released from the ion trap according to their mass-to-charge ratio. The LTQ instrument that I used in the RNA project (chapter 6) is a linear ion trap mass spectrometer.[82]
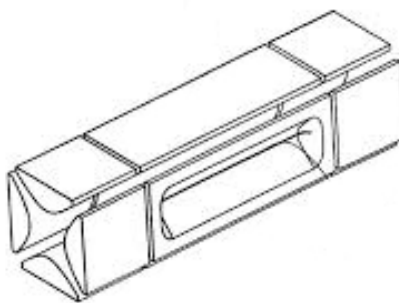
Figure 1.12. Structure of the linear ion trap mass spectrometer[82]

Another configuration of the quadrupole analyzer is the quadrupole ion trap (QIT, also known as 3D ion trap, Paul trap, or Quistor). It is first described by Paul and Steinwedel in 1960[83] and later developed into commercial mass spectrometer by Stafford and coworkers.[84] Due to its high sensitivity, capability of tandem mass, low cost, and many other advantages, QIT has become a very popular mass spectrometer.

The quadrupole ion trap has three electrodes: one circular electrode, one cap on the top and one cap at the bottom (Figure 1.13). Inert gas (usually helium, ~1 mTorr) is introduced into the ion trap in order to prevent the ions from repelling each other and provide a collision gas for the collision induced dissociation. The trajectory of the ions can be manipulated by applying different alternate radio frequency. The ions can thus be activated and ejected through the openings in the endcap electrodes and separated according to their mass-to-charge ratios.
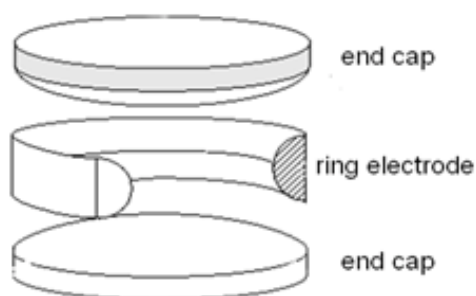
Figure 1.13. Structure of the 3D ion trap mass spectrometer

1.2.4 Modified Finnigan LCQ instrument for the bracketing method in ion trap

A Finnigan LCQ classic instrument is used for many experiments in this dissertation. The LCQ instrument is a mass spectrometer with a 3D ion trap mass analyzer which is described in 1.2.3. The damping gas used for the ion trap in the LCQ is He and it is introduced into the ion trap through a pressure regulator and a capillary restrictor, which controls the flow at about 1 mL/min. The ion trap is also pumped by a turbomolecular pump to make the partial pressure of the He gas around 1 mtorr.

In order to introduce vapor of neutral compounds into the ion trap, the metal tubing that carries He gas is modified as shown in Figure 1.14. The neutral compound is added into a glass vial which is connected to the inlet system using a Cajon connection. A cooling bath is used to control the temperature of the glass vial to maintain an appropriate constant pressure of the compound in the glass vial. The metering valve is used to adjust the amount of vapor that goes into the cross region in which the He flow (from A) carries the vapor into the ion trap (D). A convectron gauge is connected at position C in order to monitor the total pressure of the gas that goes into the ion trap.
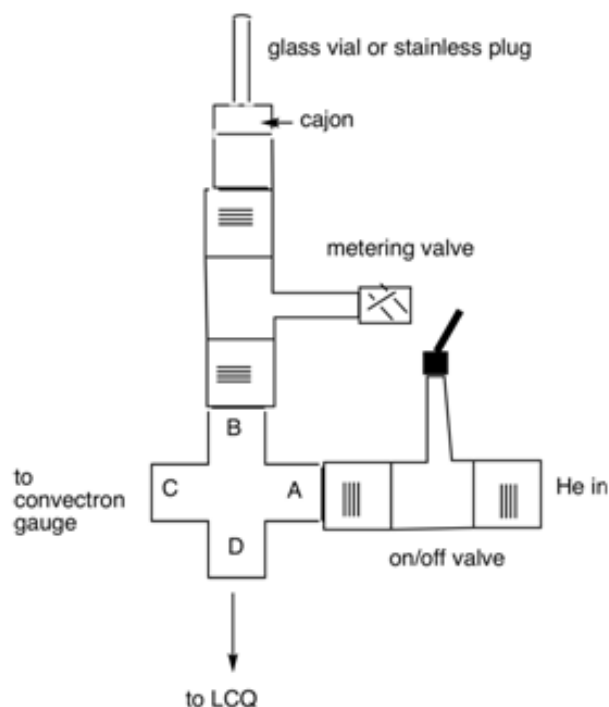
Figure 1.14. Modified gas inlet on our LCQ mass spectrometer

1.3 Methodology

1.3.1 Bracketing method

Bracketing method is used to measure the proton affinity and acidity. A Finnigan 2001 FT-ICR with a dual cell setup is used for the experiments in this dissertation. By changing the voltages of the parallel metal plates, gas phase ions can be transferred through a hole in the middle plate, from the cell on the left (we name it "source cell") to the cell on the right ("analyzer cell") or in the opposite direction. The transferred ions are then cooled by argon pulsed in via pulse valves. Solid samples are introduced by using the solids probe (can be heated) and evaporate into the gas phase. Vapors of liquid samples are introduced by using the heated batch inlet, leak valve, or pulsed valve. All reactions were conducted at room temperature.

The bracketing method uses bases or acids with known proton affinity or acidity as reference bases or acids.[12,14,17,19] By chemical ionization (reaction with H_3O^+ or OH^- ions), protonated or deprotonated compound under study (analyte) is generated in the source cell and transferred to the analyzer cell to react with the neutral reference base or acid in the analyzer cell (Figure 1.16 a). In the opposite direction, protonated or deprotonated ions generated from the reference base or acid can react with the neutral analyte in the source cell (Figure 1.16 b). By monitoring the proton transfer reactions between the analyte and references, proton affinity and acidity of the analyte can be compared to that of the reference base or acid. For example, if protonated analyte can be deprotonated by a reference base, PA of the analyte should be lower than the PA of the reference base. By using a series of reference bases and acids, PA and acidity of the analyte can be "bracketed" into a narrow range and can thus be measured.

Source Cell   Analyzer Cell   Source Cell   Analyzer Cell

| protonated /deprotonated analyte | Neutral reference | | Neutral analyte | protonated /deprotonated reference |

transfer   transfer

a   b
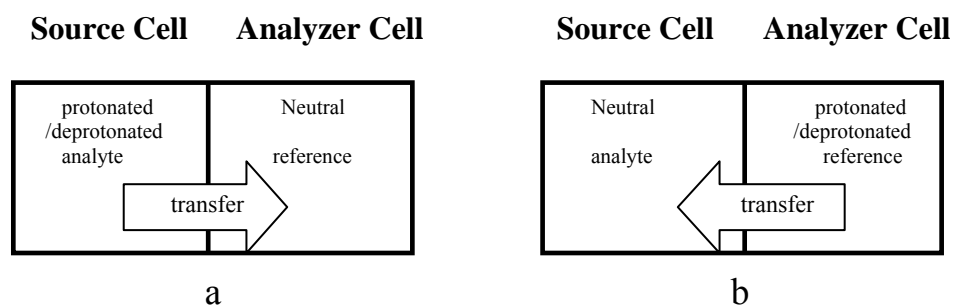
Figure 1.15. Proton transfer reactions in the dual cell setup

The organic compounds described in this dissertation have several tautomers and multiple basic and acidic sites. We developed a method to measure the less basic or less acidic sites of these compounds[18]. The PA measurement of xanthine is used as an example herein. When xanthine is protonated by hydronium cation (H_3O^+), several different cations of the analyte can be generated due to the protonation at multiple basic

sites. The cation at the less basic site will tautomerize into the cation at the more basic site due to neutral catalyzed isomerization (Scheme 1.1). The neutral catalyzed isomerization can be avoided by transferring the cations into the other cell immediately after their generation. The proton transfer reaction between the transferred less basic cation and neutral reference bases is monitored to measure the PA at the less basic site. The measurement of acidity at less acidic site can be carried out by following the same procedure.
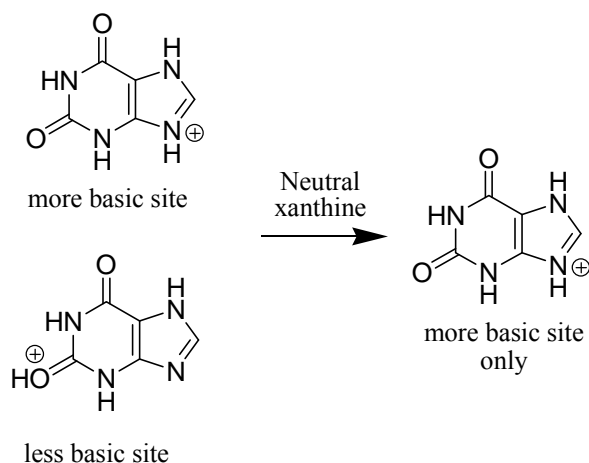
Scheme 1.1. Neutral catalyzed isomerization

1.3.2 Cooks Kinetic Method

The Cooks kinetic method is also used to measure the thermodynamic properties of several organic compounds described in this dissertation. This method was developed by Cooks and coworkers in the 1970s to obtain thermodynamic data from kinetic experiments.[85,86] Our Cooks method experiments are carried out in 3D ion trap mass spectrometers (Thermo Finnigan LCQ classic or duo).

The Cooks kinetic method requires the formation of a hydrogen bonded dimer. For

example in the proton affinity measurements, the base under study (B) forms a hydrogen bonded dimer with a reference base (Scheme 1.2). This dimer is isolated in the gas phase and subject to collision induced dissociation (CID). It is assumed that only two fragmentation pathways can occur upon CID which gives the protonated base (BH^+) and the protonated reference $(refH^+)$ respectively.[87-89] With these assumptions, the kinetic features of the two pathways can be used to calculate the thermodynamic properties of the base under study. The measurement of acidity using Cooks method follows the same principles.

$$\left[B \cdots H \cdots Ref \right]^{\oplus} \overset{k_1}{\underset{k_2}{<}} \begin{array}{c} BH^{\oplus} + Ref \\ \\ RefH^{\oplus} + B \end{array}$$
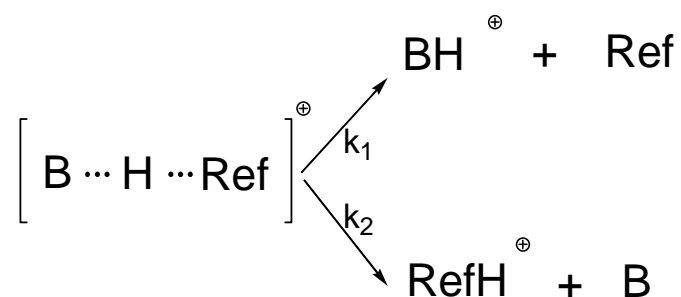
Scheme 1.2. CID of proton-bound complex of a base under study and reference base

In Scheme 1.2, the rate constants for the two fragmentation pathways are k_1 and k_2 respectively. The ratio (k_1/k_2) can be represented by the relative ion abundance of the product ions. Proton affinity or acidity of the compound under study relative to the references can be calculated by Eq. 1.9[86], in which T_{eff} is the effective temperature of the proton-bound dimer in Kelvin. By plotting $\ln(k_1/k_2)$ versus the known proton affinity or acidity for a series of references, proton affinity or acidity of the compound under study equals to the intercept of the resulting straight line.

$$ln(k_1/k_2) = - (PA_{Ref} - PA_B)/RT_{eff}$$

$$ln(k_1/k_2) = (\Delta H_{acid,Ref} - \Delta H_{acid,A})/RT_{eff}$$

$$\left.\right\} \quad \textbf{Eq. 1.9}$$

1.3.3 Computational method

Computational methods are used to calculate the thermodynamic properties of the molecules described in this dissertation, such as their proton affinity, acidity, and tautomerism. In addition, calculations are also used to predict the thermodynamic features of gas phase reactions.

The GAUSSIAN03[90] and GAUSSIAN09[91] programs are used. GaussView software is used to build the molecules and view the computational results. B3LYP/6-31+G(d)[92-96] level of theory is generally used. Geometries are fully optimized and vibrational frequencies are calculated. No scaling factor is applied. All calculated thermodynamic properties are at 298 K.

In chapter 2, M062X/6-311+G(2df,2p)[97,98], MP2(full)/6-31+G(d,p)[99-104], and CBS-QB3[105,106] levels of theory are also used to calculate the tautomerism, proton affinity, acidity of xanthine and other damaged nucleobases. Conductor-like polarizable continuum solvent model (CPCM) is used with UAKS cavity for the solution phase calculations.[107-109]

In chapter 4 and 5, GaussView 5.0 is used to generate the electrostatic potential (ESP) maps. Density isovalues are set to 0.0004. Color range is set to -0.19-+0.19.

Note: Major parts of the this chapter have been published: A. Z. Michelson, M. Chen, K. Wang, J. K. Lee, "Gas Phase Studies of Purine 3-Methyladenine DNA Glycosylase II (AlkA) Stubstrates", *J. Am. Chem. Soc.*, **2012**, *134*, 9622-9633.

Reprinted (adapted) with permission from A. Z. Michelson, M. Chen, K. Wang, J. K. Lee, "Gas Phase Studies of Purine 3-Methyladenine DNA Glycosylase II (AlkA) Stubstrates", *J. Am. Chem. Soc.*, **2012**, *134*, 9622-9633. Copyright 2012 American Chemical Society (see end of the dissertation for the permission)

Chapter 2 Gas Phase Studies of Xanthine

2.1 Introduction

Fundamental properties of nucleobases (PA, acidity, and tautomerism) are biologically important. These properties have been studied both theoretically and experimentally to help understand the mechanisms by which certain important enzymes work.[9,12,13,17-19,110-113]

As described in chapter 1, the damaged nucleobases can cause mutations during gene expression and can be repaired by base excision repair (BER) mechanisms. The enzymes which cleave the damaged bases are called glycosylases. Xanthine is a damaged nucleobase from the oxidative deamination of guanine and oxiguanine and is excised by 3-methyladenine glycosylase II (AlkA) in *E*-coli cells.[4,7] Different from most

glycosylases which specifically cleave only one nucleobase, AlkA is "broadly specific" and it cleaves a wide range of substrates (Figure 2.1).[4,7]
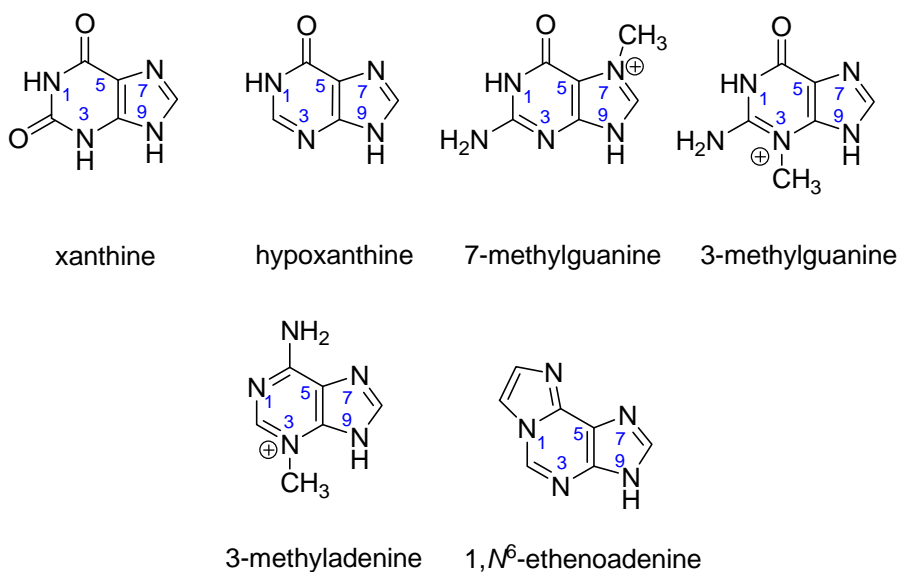
Figure 2.1. Xanthine and other substrates of AlkA

In our previous studies, fundamental properties of several substrates of AlkA were used to study how damaged nucleobases are recognized against normal nucleobases. We proposed that the lower *N*-glycosylic bond stabilities of damaged nucleobases in relative to that of normal nucleobases are caused by their higher leaving abilities in anion forms[9,20]. For example, the N9H acidities of damaged nucleobases hypoxanthine and 1,N^6-ethanoadenine are higher than that of normal nucleobases adenine and guanine (Figure 2.2).[9,10] This indicates that the anions of hypoxanthine and 1,N^6-ethanoadenine can be better leaving groups than the anions of adenine and guanine.
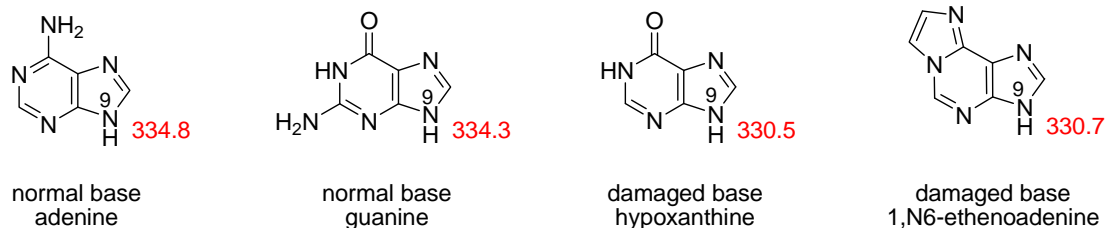
Figure 2.2. Calculated acidity (ΔH_{acid}) of damaged and normal bases, B3LYP/6-31+G*, 298 K, in kcal mol^{-1} [9,10]

In addition, the acidity difference between the damaged nucleobases and normal bases in the gas phase are higher than that in the solution phase. This might indicate that the non-polar environment in the active site of AlkA might enhance the acidity difference between damaged and normal nucleobases and thus facilitates the recognition of the damaged bases.[9-13] To further prove our hypothesis, fundamental properties of xanthine such as acidity, PA, and tautomerism are studied and discussed using both computational and experimental methods in this chapter.

2.2 Experimental

Gas phase properties (proton affinity and acidity) of xanthine are measured by both bracketing method in a Fourier transform mass spectrometer (FTMS) and Cooks kinetic method in a Finnigan LCQ 3D ion trap mass spectrometer. Theoretical gas phase calculations are conducted as guidance and reference for experiments. All compounds are commercially available (Sigma Aldrich) and are used without further purification.

The detailed set up of our FTMS instrument and the typical protocol for bracketing experiments have been described in chapter 1. Solid xanthine is introduced into the cell

via a solids probe, which is heated up to 290 ℃. Hydroxide or hydronium ions are generated from water pulsed into the cell via pulsed valves, and ionized by an electron beam [typically 8 eV (for OH⁻), or 20 eV (for H_3O^+) and 6 μA, ionization time 0.5 s]. Liquid reference acids or bases are introduced via a batch inlet or a leak valve, and allowed to react with either hydroxide (for acidity measurement) or hydronium ions (for proton affinity (PA) measurement).

For the Cooks kinetic method, xanthine is first dissolved in formic acid and then mixed with reference bases with known proton affinity or acidity in MeOH. The mixed solutions have concentrations from 100-500 uM and are subject to electrospray ionization (ESI). An electrospray needle voltage of 4.5 kV and a flow rate of 25 μL/min are applied. The proton-bound complex ions are isolated and then subject to collision-induced dissociation (CID); the complexes are activated for about 30 ms. A total of 20 scans are averaged for the product ions.

Relative energies of different tautomers of xanthine were calculated using the B3LYP method with the 6-31+G(d) basis set in Gaussian 03[90] and Gaussian 09[91]. Gas phase properties (proton affinity and acidity) of the two most stable tautomers were calculated at three different levels: M062X/6-311+G(2df,2p)[97,98], MP2(full)/6-31+G(d,p)[99-104], and CBS-QB3.[105,106]

2.3 Results

2.3.1 Computational Results

Xanthine has 33 possible tautomers with different stabilities. Four of these tautomers are within 15 kcal mol⁻¹ (Figure 2.3, numbers under each structure indicate H positions in

the ring system). Calculations done by Sponer *et al.* show that tautomers X137 and X139 are the predominant species at room temperature in both the gas phase and the aqueous phase.[114]
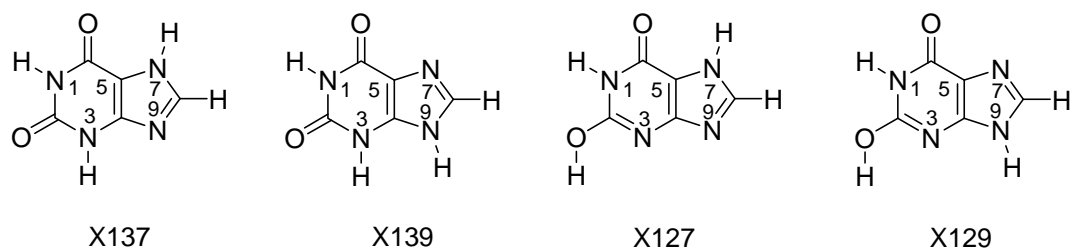
Figure 2.3. Four most stable tautomers of xanthine (numbers indicate positions of hydrogens in the purine ring system)

Table 2.1. Relative stabilities of xanthine tautomers calculated by Sponer and coworkers[114], numbers in kcal mol^{-1}

Tautomer	MP2/6-311G**//HF/6-31+G **	SCRF HF/6-31G**
X137	0.0	0.0
X139	9.0	4.0

Relative stabilities of these four tautomers are calculated by us at B3LYP/6-31+G(d) (Table 2.2). X137 is also the most stable tautomer at this level of theory. X139 is less stable than X137 by 9.1 kcal mol^{-1}. This is consistent with Sponer's result at MP2/6-311+G**//HF/6-31G** (Table 2.1). The third most stable tautomer is X127 which is 12.3 kcal mol^{-1} higher than X137.

Table 2.2. Relative energies of four most stable tautomers of xanthine, B3LYP/6-31+G(d), 298K

Tautomer	Relative Energies kcal mol^{-1}
X137	0.0
X139	9.0
X127	12.3
X129	13.8

Proton affinity and acidity of these four most stable tautomers, X137, X139, X127, and X129 are also calculated at B3LYP/6-31+G(d) (Figure 2.4). The most basic site for tautomer X137 is N9 with a PA of 205 kcal mol^{-1}, for tautomer X139 is N7 with a PA of 214 kcal mol^{-1}. The most acidic site of X137 is N7H with acidity of 325 kcal mol^{-1} (N7H) and for X139 it is the N9H site with acidity of 316 kcal mol^{-1}.
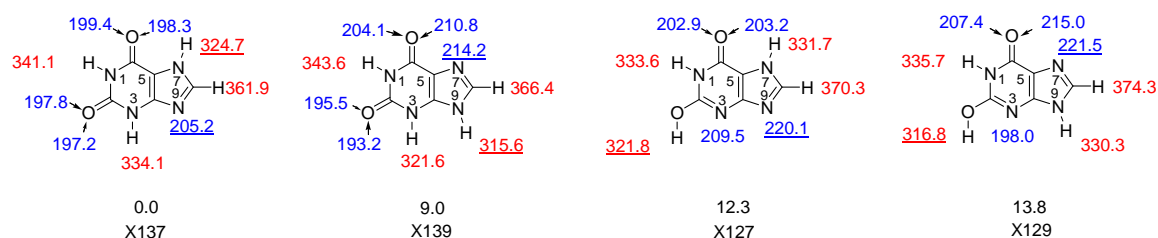
Figure 2.4. Calculated proton affinity and acidity of xanthine at B3LYP/6-31+G(d), 298 K, in kcal mol^{-1}

2.3.2   Cooks Method Results

Before the Cooks experiments are conducted, I first analyzed how tautomerism of xanthine could influence the Cooks method results. If only one tautomer, either X137 or X137, is present in the gas phase, one expect to obtain a single straight line for the Cooks plot (Figure 2.5, curve 1 or 2). The curves 1 and 2 are only different for the horizontal intercept, which is the PA of the predominant tautomer. Based on our calculations at B3LYP/6-31+G(d), we would expect curve 1 if X137 predominates or curve 2 if X139 predominates.
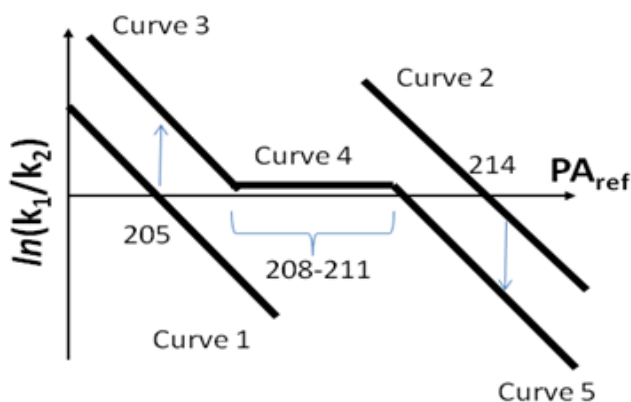
Figure 2.5. Cooks plot can be influenced by tautomerism of xanthine

If both tautomers X137 and X139 are in significant amounts in the gas phase, the Cooks plot would not be a straight line due to the existence of two different dimers (Figure 2.6). For references whose PAs are lower than 208 kcal mol^{-1}, dimer N7H gives a normal Cooks plot similar to curve 1. However, dimer N9H dissociates to form almost only protonated xanthine, since X139 is more basic than the reference bases by at least 6 kcal mol^{-1}. Due to the increased k_1/k_2 ratio, curve 3 would be observed. For similar reason, curve 5 would be observed when references higher than 211 kcal mol^{-1} are used. For references with PAs between 208 and 214 kcal mol^{-1}, dimerN7H (dimerN9H) dissociates into only protonated reference (protonated xanthine). Assuming the ratio of dimer N7H

and dimer N9H is a constant value, $\ln(k_1/k_2)$ would also be a constant within this region. The Cooks plot in this region would be a straight horizontal line (Figure 2.5, curve 4).
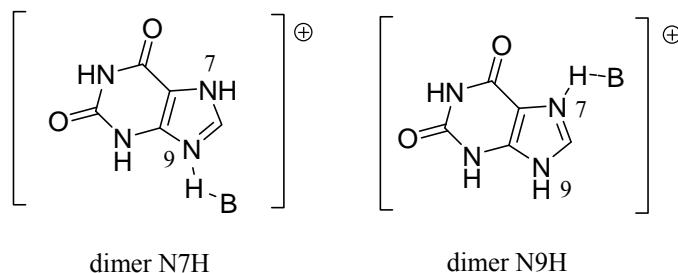
Figure 2.6. Dimers formed by X137 and X139 with reference base B

Similarly, in the Cooks plot for acidity of xanthine, a straight line would indicate only one tautomer is present, while a curved Cooks plot would imply both tautomers might be present.
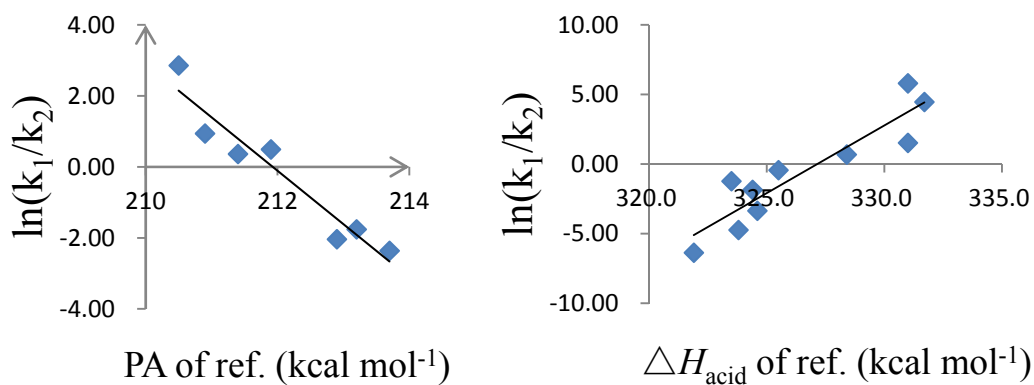
Figure 2.7. Experimental Cooks plot for PA and acidity of xanthine

Experimentally, the Cooks plot for both PA and acidity measurements of xanthine are straight lines (Figure 2.7). Curved Cooks plot in Figure 2.5 are not observed. This

indicates that only one tautomer is present in the gas phase.

For PA of xanthine, seven reference bases are used. They are pyrazole (PA=213.7 ± 2.0 kcal mol^{-1}), benzamide (PA=213.2 ± 2.0 kcal mol^{-1}), o-toluidine (PA=212.9 ± 2.0 kcal mol^{-1}), glycine (PA=211.9 ± 2.0 kcal mol^{-1}), DMSO (PA=211.4 ± 2.0 kcal mol^{-1}), aniline (PA=210.9 ± 2.0 kcal mol^{-1}), thymine (PA=210.5 ± 2.0 kcal mol^{-1}). PA of xanthine is measured to be 211.9 ± 3.0 kcal mol^{-1}.

For acidity of xanthine, ten reference acids are used. They are L-asparagine (ΔH_{acid}=331.6 ± 3.1 kcal mol^{-1}), L-histidine (ΔH_{acid}=328.6 ± 1.9 kcal mol^{-1}), difluoroacetic acid (ΔH_{acid}=331.0 ± 2.2 kcal mol^{-1}), dichloroacetic acid (ΔH_{acid}=328.4 ± 2.1 kcal mol^{-1}), o-hydroxy-benzoic acid (ΔH_{acid}=325.5 ± 2.2 kcal mol^{-1}), 3,5-bis(trifluoromethyl)-pyrazole (ΔH_{acid}=324.6 ± 2.1 kcal mol^{-1}), 3,5-bis(trifluoromethyl)-benzoic acid (ΔH_{acid}=324.4 ± 2.1 kcal mol^{-1}), trifluoroacetic acid (ΔH_{acid}=323.8 ± 2.9 kcal mol^{-1}), hydrobromic acid (ΔH_{acid}=323.5 ± 0.1 kcal mol^{-1}), heptafluorobutyric acid (ΔH_{acid}=321.9 ± 2.2 kcal mol^{-1}). Acidity of xanthine is measured to be 326.8 ± 3.0 kcal mol^{-1}.

2.3.3   Bracketing Method Results

Before bracketing PA and acidity of xanthine experimentally, I also analyzed how the proton transfer reactions in our gas phase experiments could be influenced by the tautomerism of xanthine. As described in chapter 1, a specific proton affinity PA value can be bracketed when only one tautomer predominates in the gas phase. If both X137 and X139 tautomers are present in significant amount, both two could get protonated and transferred to the second cell to react with the neutral reference base. Based on the

calculated PAs at B3LYP/6-31+G(d), proton transfer takes place between protonated xanthine and neutral reference base as long as PA of the reference base is larger than 205 kcal mol^{-1}. In the other direction, proton transfer can happen when reference base is less basic than the PA of X139 (214 kcal mol^{-1}). Consequently, proton transfer in both directions take place when reference bases within a certain PA region are used. Based on this, the bracketing method results could potentially indicate whether there is only one xanthine tautomer in the gas phase or both X137 and X139 are present.

Experimentally, ten reference bases are used in the PA bracketing of xanthine (Table 2.3). Reaction with 4'-tert-butyl-acetophenone (PA = 210.9 ± 2.0 kcal mol^{-1}) proceeds in both directions, placing the PA at 211 ± 3 kcal mol^{-1}.

Table 2.3. Summary of results for proton affinity bracketing of xanthine.

Reference compound	PA[a]	Proton transfer[b]	
		Ref. base	Conj. acid
m-toluidine	214.1 ± 2.0	+	−
o-toluidine	212.9 ± 2.0	+	−
DMSO	211.4 ± 2.0	+	−
4'-tert-butyl-acetophenone	210.9 ± 2.0	+	+
2,4-pentanedione	208.8 ± 2.0	−	+
m-chloroaniline	207.5 ± 2.0	−	+
ethyl sulfide	204.8 ± 2.0	−	+
4-methylcyclohexanone	201.9 ± 2.0	−	+
3-pentanone	200.0 ± 2.0	−	+

| | acetone | 194.0 ± 2.0 | – | + |

For acidity of xanthine, five reference acids are used (Table 2.4). Neutral xanthine can be deprotonated by 1,1,1-trifluoro-2,4-pentanedione anion. However, in the other direction, deprotonated xanthine anion cannot deprotonate neutral 1,1,1-trifluoro-2,4-pentanedione. Bromine anion is not able to deprotonate xanthine. Reaction of xanthine anion with neutral hydrobromic acid is not conducted, because the pressure of hydrobromic acid in the analyzer cell is not stable (HBr is pulsed in from the analyzer pulse valve). Collectively, the more acidic site of xanthine is bracketed to be 323.5-328.3 kcal mol^{-1}. No reference acid in between this region is used herein, because they are not volatile enough for the FTMS experiments.

Table 2.4. Summary of results for acidity bracketing of xanthine.

Reference compound	ΔH_{acid}[a]	Proton transfer[b]	
		Ref. acid	Conj. base
perfluoro-*tert*-butanol	331.6 ± 2.2	–	+
difluoroacetic acid	331.0 ± 2.2	–	+
3,5-bis(trifluoromethyl) phenol	329.8 ± 2.1	–	+
1,1,1-trifluoro-2,4-pentanedione	328.3 ± 2.9	–	+
hydrobromic acid	323.5 ± 0.1	N/A	–

We also tried to bracket the less basic site of xanthine (Table 2.5). However, it was not successful. Reference bases with PAs as low as 187.3 kcal mol^{-1} can deprotonate protonated xanthine. According to the calculated PA of X137 and X139, both of which are at least 10 kcal mol^{-1} higher than 187.3 kcal mol^{-1}, reference bases with such low PA are not expected to deprotonated protonated xanthine. The bracketing of less acidic site of xanthine experienced the same problem. Reasons for these unexpected proton transfer reactions are currently under investigation.

Table 2.5. Summary of results for less basic site of xanthine

Reference compound	PA kcal mol^{-1}	Protonated xanthine + neutral Ref
acetic acid	187.3	+
butylaldehyde	189.5	+
2-butanone	197.7	+
ethyl sulfide	204.8	+
aniline	210.9	+

To conclude, PA of xanthine is measured to be 212 $\pm$ 3 kcal mol^{-1} by Cooks kinetic method and 211 $\pm$ 3 kcal mol^{-1} by bracketing method. Acidity of xanthine is 327 $\pm$ 3 kcal mol^{-1} by Cooks kinetic method and between 323.5-328.3 kcal mol^{-1} by bracketing method.

2.4 Discussion

2.4.1 Calculated versus experimental values.

The calcualated and experimental PA of xanthine is not consistent. The calculated PA is 205.2 kcal mol^{-1} yet we measure a PA of 211 kcal mol^{-1} (by bracketing). It is possible that this is because we have a mixture of the two most stable xanthine tautomers X137 and X139. X139 tautomer is also more basic by calculation (214.2 kcal mol^{-1}) and possibly could influence the experimental PA measurement.

To investigate this discrepancy, we calculated the relative enthalpies of X137 and X139 using CBS-QB3 and MP2(full)/6-31+G(d,p) methods, because non-DFT methods could possibly yield different results. The enthalpy differences are 8.7 kcal mol^{-1} for CBS-QB3; 8.6 kcal mol^{-1} for the MP2 calculation. These values are both comparable to the B3LYP value. This is again consistent with the IR-UV double resonance spectroscopy experiments in the gas phase (X137 is predominant)[116].
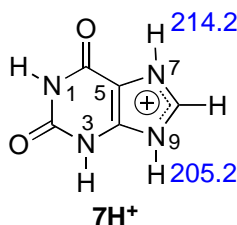
Figure 2.8. Structure of protonated xanthine

Similar discrepancy between calculated (B3LYP/6-31+G(d)) and experimental values was also observed by a former group member, when nucleobase uracil was investigated (Figure 2.9).[18] Proton affinity of uracil was calculated to be 202.0 kcal mol^{-1} at the most basic site (O4) at B3LYP/6-31+G(d). The experimental value is 209 ± 3 kcal mol^{-1}, which is 7 kcal mol^{-1} higher than the calculated value. The calculated value for the less basic site is 192.4 kcal mol^{-1} but the experimental value is 201 ± 3 kcal mol^{-1}.

202.0 *(209 ± 3)*

192.4 O *(201 ± 3)*
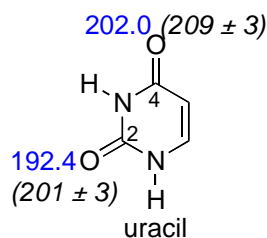
uracil

Figure 2.9. B3LYP/6-31+G(d) calculated PA (blue) values for uracil; values in parentheses are from bracketing method. All values are enthalpy in kcal mol^{-1} at 298 K.

In order to find a method or level of theory that calculates the PA of xanthine accurately, M06-2X/6-311+G(2df,2p), CBS-QB3 and MP2(full)/6-31+G(d,p) are used (Table 2.6).[38,39,105,106,117-119] However, neither the DFT or non-DFT methods can correctly predict the PAs of xanthine and uracil. I am not sure why the PAs of all the nucleobases can be accurately calculated except for xanthine and uracil. Xanthine and uracil are similar in that all the basic sites are at the β position to an N-H group (N9 for xanthine X137, O2 and O4 sites for uracil). Such structure is not seen in the other substrates. However, I am still not sure why this structure would cause the discrepancy. This discrepancy with uracil and xanthine indicates that neither DFT nor non-DFT methods is always reliable for the calculation of PAs for nucleobases.

Table 2.6. Comparison of calculated and experimental values for the N9 proton affinity of xanthine tautomer X137 and O2 and O4 proton affinities of uracil.

Method/Level	PA (N9, xanthine X137)	PA (uracil O4)	PA (uracil O2)
B3LYP/6-31+G(d)	205.2	202.0	192.4

M06-2X/6-311+G(2df,2p)	205.6	204.7	196.2
CBS-QB3	206.8	204.4	196.8
MP2(full)/6-31+G(d,p)	206.4	203.2	195.3
Experimental value	211-212	209	201

All PA values are ΔH in kcal mol^{-1} at 298 K.

To justify the above discussion that my PA calculations are poor for xanthine, 7-methylxanthine (Figure 2.10) is studied both computationally and experimentally in the same way. The parent molecule xanthine has more than one stable tautomer, which might cause the discrepancy between the calculation and experiment. With an additional methyl group, 7-methylxanthine is "locked" into a structure analogous to xanthine tautomer X137. The PA of 7-methylxanthine is calculated to be 210.1 kcal mol^{-1} (Figure 2.10) at B3LYP/6-31+G(d) level of theory. If the hypothesis that the common structural component in xanthine and uracil caused the discrepancy between calculation and experiment is true, the experimental PA of 7-methylxanthine will also be different from the calculated value.
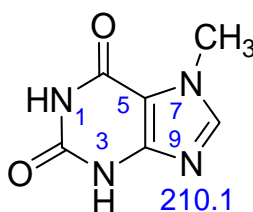
Figure 2.10. PA of 7-methylxanthine calculated at B3LYP/6-31+G(d), ΔH in kcal mol^{-1} at 298 K.

The bracketing results of 7-methylxanthine are shown in Table 2.7 and PA of 7-methylxanthine is bracketed to be 215 ± 3 kcal mol^{-1}. The experimental value is again higher than the calculated value by 5 kcal mol^{-1}. Thus experimental PA value of xanthine 211-212 kcal mol^{-1} is correct. In addition, it seems that the PA of xanthine cannot be accurately calculated by the methods we used here (B3LYP/6-31+G(d)).

Table 2.7. Summary of results for proton affinity bracketing of 7-methylxanthine.

Reference compound	PA[a]	Proton transfer[b]	
		Ref. base	Conj. acid
n-butylamine	220.2 ± 2.0	+	–
N-methylaniline	219.1 ± 2.0	+	–
3-bromopyridine	217.5 ± 2.0	+	–
3-fluoropyridine	215.6 ± 2.0	+	+
2-chloropyridine	215.3 ± 2.0	+	+
m-toluidine	214.1 ± 2.0	–	+
DMSO	211.4 ± 2.0	–	+
aniline	210.9 ± 2.0	–	+
pyrrole	209.2 ± 2.0	–	+

[a]PA is in kcal mol^{-1}.[115] [b]A "+" indicates the occurrence and a "–" indicates the absence of proton transfer

2.4.2 Biological Implications

To test our hypothesis, I compared the acidities of xanthine to that of the normal nucleobases. N9H acidity of xanthine is 315.6 kcal mol^{-1}, which is about 20 kcal mol^{-1} more acidic than the normal nucleobases adenine and guanine. This indicates that the *N*-glycosidic bond of xanthine is weaker than that of guanine and adenine, thus xanthine can be recognized and cleaved by AlkA.

It is also hypothesized that the active site of AlkA can provide a hydrophobic environment, which would increase the acidity difference between the damaged nucleobases and the normal bases. The non-polar environment of the active site can thus facilitate the excision of the damaged nucleobases by AlkA. We compare the gas phase and solution phase (water) N9-H acidities for xanthine (Table 2.8).

In the gas phase, ΔH_{acid} of xanthine is 315.6 kcal mol^{-1}; in aqueous phase its pK_a is 7.3. The normal nucleobase adenine has a gas phase ΔH_{acid} of 334.8 kcal mol^{-1}. In the gas phase, xanthine is more acidic than adenine by 19 kcal mol^{-1}. Based on the experimental pKa values, xanthine is more acidic than adenine by only 3.4 kcal mol^{-1} in the aqueous phase. This comparison supports our hypothesis that AlkA has a nonpolar active site, which could enhance the acidity differences between damaged nucleobases and the normal bases, and thus facilitate the cleavage of the damaged bases such as xanthine.

Table 2.8. Summary of calculated N9-H acidity values (in the gas phase ($\varepsilon=1$), experimental pK_a values (in water) for AlkA.[a,b,c]

Substrate	Acidity (kcal mol^{-1})[a,b]	pK$_a$[c]
	$\varepsilon=1$	
xanthine	315.6	7.3[d]
adenine	334.8[d] (19.2)	9.8[e](3.4)

[a]The values in parentheses are the differences between a adenine's acidity and that of xanthine, in kcal mol^{-1}. [b]Calculated using B3LYP/6-31+G(d) level of theory; [c]pK_a values in water are experimental for adenine, calculated for xanthine; [d]Reference [120]; [e]References [121,122]

2.5 Conclusions.

The gas phase thermodynamic properties (tautomerism, PA, and acidity) of xanthine has been studied by both computational and experimental methods. Experimental and computational results are compared to discuss the gas phase stabilities of the xanthine tautomers. These properties are used to probe the mechanism by which *N*-glycosylase (AlkA) cleaves the damaged bases.

Xanthine is more acidic than the normal nucleobases (adenine and guanine) and are cleaved more easily. Our results also support our hypothesis that AlkA provides a nonpolar hydrophobic site which facilitates the discrimination of damaged nucleobases from normal nucleobases. The acidity difference between the damaged and normal nucleobases is enhanced in such a nonpolar hydrophobic site.

Note: Major parts of the this chapter have been published: K. Wang, M. Chen, Q. Wang, X. Shi, J. K. Lee, "1,2,3-Triazoles: Gas Phase Properties", *J. Org. Chem.*, **2013**, *78*, 7249-7258.

Reprinted (adapted) with permission from K. Wang, M. Chen, Q. Wang, X. Shi, J. K. Lee, "1,2,3-Triazoles: Gas Phase Properties", *J. Org. Chem.*, **2013**, *78*, 7249-7258. Copyright 2013 American Chemical Society (see the end of this dissertation for the permission)

Chapter 3 Gas Phase Studies of 1,2,3-Triazoles

3.1 Introduction

1,2,3-Triazoles are a group of *N*-heterocyclic aromatic compounds (Figure 3.1). With the development of "click chemistry" discovered by Sharpless and, 1,2,3-triazoles have been heavily investigated for various applications. For example, since they are stable compounds under physiological conditions, 1,2,3-triazoles have long been studied and used in medicinal chemistry.[22,23] In addition, a large library of 1,2,3-triazole and its derivatives have been prepared as energetic materials[24], drug-delivery nanoparticles[25], fluorescent dyes for cancer chemotherapy[27] and bioimaging[28].

4-phenyl-2*H*-1,2,3-triazole

2-methyl-4-phenyl
-2*H*-1,2,3-triazole

2-(4-phenyl-2*H*-1,2,3
-triazol-2-yl)-ethanol

benzotriazole

1-methylbenzotriazole

1-phenylbenzotriazole
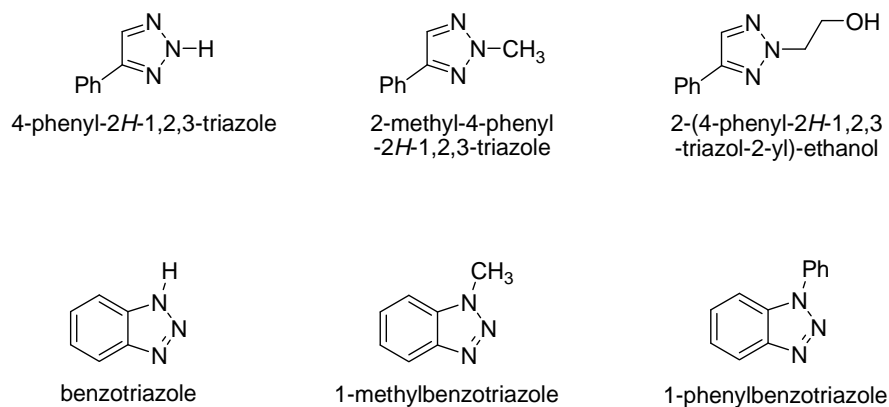
Figure 3.1. Structures of several 1,2,3-triazoles

As compared to *N*-heterocyclic singlet carbenes (NHCs), which are widely used as ligands in organometallic catalysts, 1,2,3-triazoles can be easily prepared and used as good ligands, since they are both N σ-donors and good π-acceptors. Our collaborator Dr. Shi[31,123-129] and coworkers used benzotriazole and 1-methyl-benzotriazole to bind to gold in complex catalysts for the intramolecular furan-alkyne cyclization and received high yield (95% with 1% cat.) and selectivity (>20:1) (Scheme 3.1). They also used anions of triazoles as ligands in Au(I) complexes to catalyze the intermolecular alkyne hydroamination and also received high yield (91% with 1% cat.).
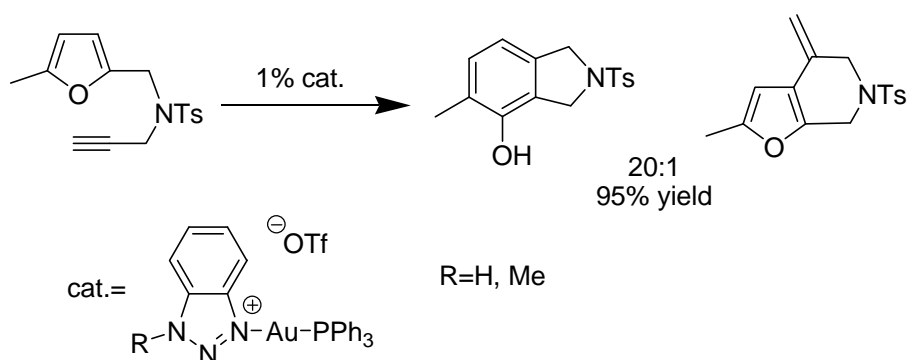
Scheme 3.1. 1,2,3-Triazoles (benzotriazole and 1-methyl-benzotriazole) used as ligands to gold metal

Since 1,2,3-triazoles bind to metals in both neutral and anionic forms, their instrinsic fundamental properties such as tautomerism, acidity, and proton affinity are important for the understanding of complexation of 1,2,3-triazoles to metals. However, many of these properties are still unknown.[32]

In this chapter, computational and experimental studies of 4-phenyl-1,2,3-triazole, 1-methylbenzotriazole and 1-methylphenylbenzotriazoles are described. The fundamental properties studied herein (tautomerism, acidity, and PA) are potentially useful in developing new methods for the synthesis of 1,2,3-triazoles and design of new organometallic catalysts.

3.2 Experimental

Bracketing measurements of the PA and acidity of the triazoles are conducted using the Fourier Transform Mass Spectrometer (FTMS) as described in chapter 1. Solid 4-phenyl-2H-1,2,3-triazole is introduced into the cell via a solids probe without heating. Other solid triazoles are also introduced via the heatable solids probe. Liquid reference bases or acids are introduced via a leak valve or a batch inlet system.

To measure the PA and acidity of the triazoles, the same bracketing method described in chapter 1 has been used.

Cooks kinetic method as described in chapter 1 is used for PA and acidity measurement of several triazoles. 1-methyl-benzotriazole and 4-phenyl-2H-1,2,3-triazole are first dissolved in 1:1 methanol/H_2O and then mixed with the reference base or acid.

^{31}P-NMR experiments are used by our collaborator Dr. Xiaodong Shi to measure the chemical shift of the phosphine in PPh$_3$Au(triazole)OTf. A solution of 0.05 M PPh$_3$Au(triazole)OTf in CDCl$_3$ is used for the measurement. The complexes are prepared and purified (through recrystallization) as previously reported by the Shi group.[31] For accurate chemical shift measurement, 85% H$_3$PO$_4$ is used as an internal standard (0 ppm) in a sealed capillary. The ^{31}P-NMR experiments are conducted at ambient temperature by the Shi group and I include their results here for the discussion of my results.

B3LYP/6-31+G(d) is used to calculated the thermodynamic properties of the triazoles using Gaussian03 and Gaussian09. All geometries are fully optimized and vibrational frequencies are calculated. No scaling factor is applied. All values described in this chapter are enthalpies (ΔH) at 298 K.

3.3 Results

This project is completed in collaboration with Kai Wang in our group. The results and discussion part focus on the triazoles characterized by Mu Chen. However, the work of Kai Wang is also mentioned briefly where necessary, since our data are both integral components of the project.

3.3.1 1-Methylbenzotriazole

To assess the accuracy of our calculations for the gas phase porperties of benzotriazole, 1-methylbenzotriazole (**1**) is examined since there is only one tautomer for this compound. PA of 1-methylbenzotriazole is calculated to be 222.4 kcal mol^{-1} (N3

position, Figure 3.2); acidity of 1-methylbenzotriazole is calculated to be 379.1 kcal mol^{-1} (CH$_3$ on the N1 position, Figure 3.2).
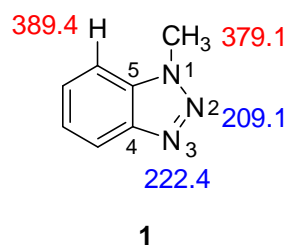
Figure 3.2. Calculated properties of 1-methylbenzotriazole. Gas phase acidities are in red; gas phase proton affinities are in blue. The values are ΔH (kcal mol^{-1}) at B3LYP/6-31+G(d), 298 K.

Experimentally, gas phase acidity of this compound is measured by bracketing method (Table 3.1). The proton transfer reactions happen in both directions when ethanol is used as the reference acid (ΔH$_{acid}$=379.2 kcal mol^{-1}). Thus, the gas phase acidity of this compound is bracketed to be 379 ± 3 kcal mol^{-1}. This result is consistent with the calculated value (379.1 kcal mol^{-1}). The PA of 1-methylbenzotrizole is measured to be 223 ± 3 kcal mol^{-1}, which is also consistent with the calculated value (222.4 kcal mol^{-1}). These data indicate that the calculations are accurate.[130]

Table 3.1. Summary of results for acidity bracketing of 1-methylbenzotriazole (**1**).

Reference compound	ΔH$_{acid}$[a]	Proton transfer[b]	
		Ref. acid	Conj. base
acetone	368.8 ± 2.1	–	+
DMSO	373.5 ± 2.1	–	+

butanol	375.3 ± 2.0	–	+
ethanol	379.2 ± 1.0	+	+
methanol	382.0 ± 1.0	+	–

[a] Acidities are in kcal mol^{-1}.[131,132] [b] A "+" indicates the occurrence and a "–" indicates the absence of proton transfer

Cooks kinetic method has been used to measure the PA of 1-methylbenzotriazole, which was previously measured by Abboud and coworkers (222.6 kcal mol^{-1}).[33] Seven reference bases are used, yielding a PA of 223 ± 3 kcal mol^{-1}. This value is consistent with Abboud's results.

3.3.2 4'-Methyl-1-phenylbenzotriazole

To probe how substituents affect the PA of the triazoles, a series of 1-phenylbenzotriazoles (**2a-f**, Figure 3.3) with different substitution have been studied. My study focused on the PA of 4'-methyl-1-phenylbenzotriazole (**2e**, Figure 3.3).
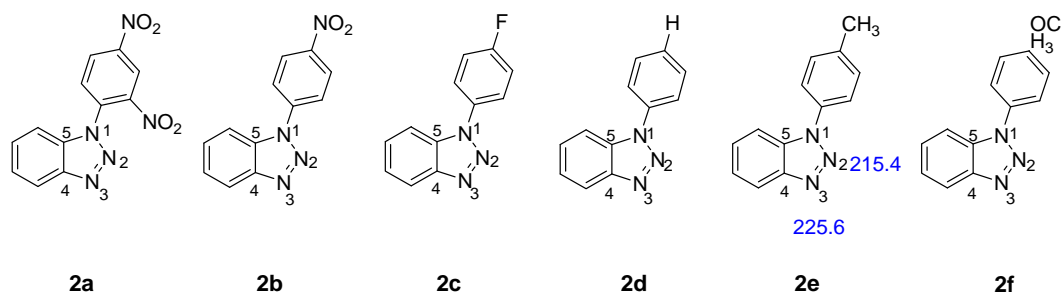
Figure 3.3. Calculated PAs of a series of 1-phenylbenzotriazoles at B3LYP/6-31+G(d); ΔH (kcal mol^{-1}) at 298 K.

The most basic site of 4'-methyl-1-phenylbenzotriazole (**2e**) is the N3 site with a calculated PA of 225.6 kcal mol^{-1}. The less basic site is the N2 site with a PA of 215.4

kcal mol^{-1}. PA of 4'-methyl-1-phenylbenzotriazole is measured by using bracketing method (Table 3.2). The proton transfer reaction happens in both directions when 3-picoline (PA = 225.5 ± 2.0 kcal mol^{-1}) is used as the reference base. The PA of 4'-methyl-1-phenylbenzotriazole is thus bracketed to be 226 ± 3 kcal mol^{-1}.

Table 3.2. Summary of results for PA bracketing of 4'-methyl-1-phenylbenzotriazole.

Reference compound	PA[a]	Proton transfer[b]	
		Ref. base	Conj. acid
pyrrolidine	226.6 ± 2.0	+	−
4-picoline	226.4 ± 2.0	+	−
3-picoline	225.5 ± 2.0	+	+
cyclohexylamine	223.3 ± 2.0	−	+
pyridine	222.3 ± 2.0	−	+

[a]Proton affinities are in kcal mol^{-1} and come from NIST[115]. [b]A "+" indicates the occurrence and a "-" indicates the absence of proton transfer.

Cooks kinetics method are also conducted to measure the PA of 4'-methyl-1-phenylbenzotriazole. Five reference bases are used, yielding a PA of 227 ± 3 kcal mol^{-1}. This result is consistent with the calculated value (225.6 kcal mol^{-1}).

3.3.3 4-Phenyl-2,3-triazole

4-Phenyl-1,2,3-triazole (**3**) has been previously studied by Abboud and coworkers. However, their study generated some ambiguous results.[33] It has eight possible tautomers,

the five most stable ones are shown in Figure 3.4. B3LYP/6-31+G(d) level of theory is used to calculate the relative stabilities, PA, and acidity of 4-phenyl-1,2,3-triazole.
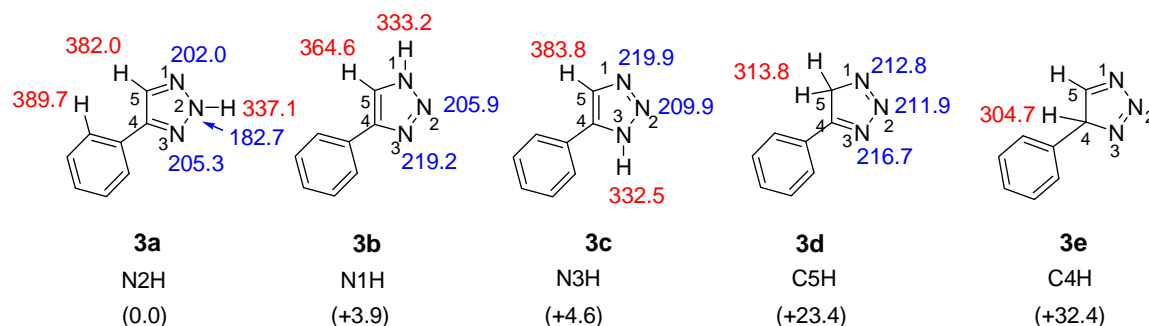
Figure 3.4. The first five most stable tautomers of 4-phenyl-1,2,3-triazole (**3**). Gas phase acidities are in red; gas phase PAs are in blue. Relative stabilities are also listed in parentheses. All values are enthalpy values ΔH (kcal mol^{-1}) calculated at B3LYP/6-31+G(d), 298 K.

Bracketing method is again used to measure the acidity of 4-phenyl-1,2,3-triazole. The conjugate base of 4-phenyl-1,2,3-triazole deprotonates 2-chloropropionic acid (ΔH_{acid} = 337.0 ± 2.1 kcal mol^{-1}); however, the reaction in the opposite direction (2-chloropropionate with 4-phenyl-1,2,3-triazole) does not take place (Table 3.3). Deprotonated 4-phenyl-1,2,3-triazole is unable to deprotonate trifluoromethyl-*m*-cresol (ΔH_{acid} = 339.3 ± 2.1 kcal mol^{-1}) but the cresolate does deprotonate 4-phenyl-1,2,3-triazole. We therefore bracket the ΔH_{acid} of 4-phenyl-1,2,3-triazole as 338 ± 3 kcal mol^{-1}.

Table 3.3. Summary of results for acidity bracketing of 4-phenyl-1,2,3-triazole (**3**).

Reference compound	$\Delta H_{acid}{}^a$	Proton transfer[b]	
		Ref. acid	Conj. base
methylcyanoacetate	340.80 ± 0.60	–	+
trifluoromethyl-*m*-cresol	339.3 ± 2.1	–	+
2-chloropropionic acid	337.0 ± 2.1	+	–
malononitrile	335.8 ± 2.1	+	–
per-fluoro-tert-butanol	331.6 ± 2.2	+	–

[a] Acidities are in kcal mol^{-1}.[131,132] [b]A "+" indicates the occurrence and a "–" indicates the absence of proton transfer

Bracketing method is also used to measure the PA of 4-phenyl-1,2,3-triazole (Table 3.4). The PA of 3 is bracketed between 3-fluoropyridine and 3-bromo-pyridine. Thus, its PA is measured to be 217 ± 3 kcal mol^{-1}.

Table 3.4. Summary of results for PA bracketing of 4-phenyl-1,2,3-triazole (**3**).

Reference compound	PA^a	Proton transfer[b]	
		Ref. base	Conj. acid
pyridine	222.3 ± 2.0	+	–
butylamine	220.2 ± 2.0	+	–
3-bromopyridine	217.5 ± 2.0	+	–

3-fluoropyridine	215.6 ± 2.0	–	+
2-chloropyridine	215.3 ± 2.0	–	+
o-toluidine	212.9 ± 2.0	–	+
aniline	210.9 ± 2.0	–	+
2,4-pentadione	208.8 ± 2.0	–	+

[a] PAs are in kcal mol^{-1}.[131] [b] A "+" indicates the occurrence and a "–" indicates the absence of proton transfer

3.4 Discussion

3.4.1 1-Phenylbenzotriazoles as ligands

A summary of the calculated and experimental values for the proton affinities of the 1-phenylbenzotriazoles studied herein are shown in Table 3.5. The experimental and computational values correlate, indicating the accuracy of the computational method for these species. As would be expected, more electron donating substituents correlate to an increase in the PA.

Table 3.5. Calculated (B3LYP/6-31+G(d); 298 K) and experimental proton affinity data for 1-phenylbenzotriazoles (**2**), in kcal mol^{-1}.

Substrate	Calculated value	Experimental value[a]
2',4'-dinitro-1-phenylbenzotriazole (**2a**)	214.0	213
4'-nitro-1-phenylbenzotriazole (**2b**)	215.4	216

4'-fluoro-1-phenylbenzotriazole (**2c**)	221.7	222
1-phenylbenzotriazole (**2d**)	224.0	223
4'-methyl-1-phenylbenzotriazole (**2e**)	225.6	226
4'-methoxy-1-phenylbenzotriazole (**2f**)	226.9	226

[a]Experimental value is obtained by bracketing; error is ± 3 kcal mol^{-1}.

One of our primary interests is to use triazoles as ligands to bind with transition metals. Our collaborator (Dr. Xiaodong Shi) have in recent years reported the application of triazole ligands for tuning the reactivity of cationic gold(I) catalysts.[31,124-129] We wondered if there is a correlation between the ligand basicity and catalyst efficacy. Thus, we carried out a study to compare the PA data to the binding affinity data.[31] In this experiment, we measured the ^{31}P-NMR shift for the binding of the 1-phenylbenzotriazoles to AuPPh$_3$, using chloroform as the solvent (Figure 3.5).[133] The Au(I) complexes are generally two-coordination linear complexes and the X-ray crystallographic structures from our previous studies have confirmed this conformation for the triazole-gold complexes.[31,125,127,128] Therefore, we expect that the ^{31}P-NMR should serve as a direct measurement of the binding ability of various triazoles toward gold cations.[134] The results show that there is a strong correlation between the triazole PA and the ^{31}P-NMR chemical shift. This is probably due to the deshielding effects (toward the P-ligand) provided by the strong coordination of triazole to the opposite side of the gold cation. These results indicate that gas phase PA values can be used as a predictor of ligand binding.
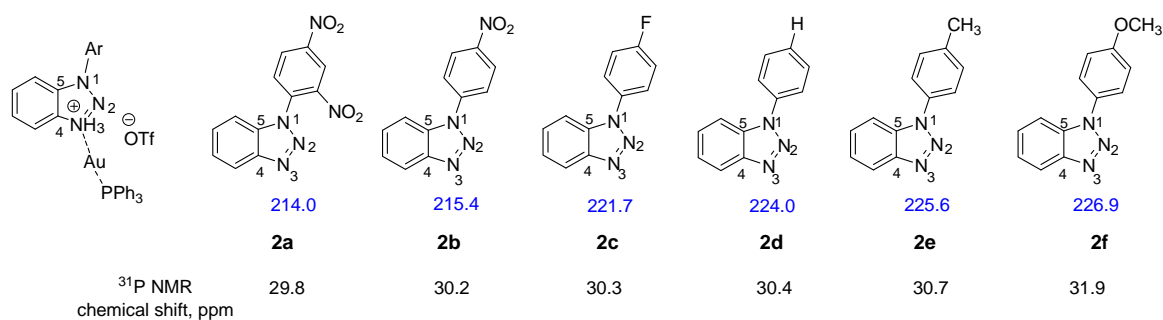
Figure 3.6. Calculated (B3LYP/6-31+G(d), ΔH, kcal mol^{-1}) PAs for a series of 1-phenylbenzotriazoles and experimental ^{31}P-NMR shifts in ppm for those triazoles bound to AuPPh$_3$, in CDCl$_3$.

3.5 Conclusions

The proton affinity of benzotriazole, 4'-methyl-1-phenylbenzotriazoles, and 4-phenyl-1,2,3-triazole have been characterized. A correlation between gas phase proton affinity and binding to Au(I) in solution (as measured by ^{31}P-NMR shifts) is established, showing that PA can be used as an indicator of the binding ability of 1,2,3-triazoles to metal cations. These studies are thus useful for the design of catalysts containing this interesting new class of ligands.

Note: Major parts of the this chapter have been published: M. Liu, <u>M. Chen</u>, S. Zhang, I. Yang, B. Buckley, and J. K. Lee, "Reactivity of Carbene•Phosphine Dimers: Proton Affinity Revisited", *J. Phys. Org. Chem.*, **2011**, *24*, 929-936.

<u>M. Chen</u>, J. P. Moerdyk, C. W. Bielawski, J. K. Lee, "Assessing the Proton Affinities of *N,N'*-Diamidocarbenes", *J. Org. Chem.*, **2013**, *78*, 10452-10458.

Reprinted (adapted) with permission from M. Liu, <u>M. Chen</u>, S. Zhang, I. Yang, B. Buckley, and J. K. Lee, "Reactivity of Carbene•Phosphine Dimers: Proton Affinity Revisited", *J. Phys. Org. Chem.*, **2011**, *24*, 929-936. Copyright 2011 John Wiley& Sons, Ltd. and <u>M. Chen</u>, J. P. Moerdyk, C. W. Bielawski, J. K. Lee, "Assessing the Proton Affinities of *N,N'*-Diamidocarbenes", *J. Org. Chem.*, **2013**, *78*, 10452-10458. Copyright 2013 American Chemical Society (see end of this dissertation for the permissions)

Chapter 4 Gas Phase Studies of *N*-heterocyclic carbenes (NHCs) and *N,N'*-diamidocarbenes (DACs)

4.1 Introduction

Traditional carbenes such as methylene (CH_2:) are electrophilic and display chemical reactivities including C-H insertion, H_2 activation, cyclopropanation of olefins, and so on.[37-40] However, the application of electrophilic carbenes is limited because they require *in situ* generation. Scientists have for decades been looking for stable carbenes until the first ones were reported by Bertrand[41] and Arduengo (NHCs).[42] The *N*-heterocyclic carbenes (NHCs) have a basic structure as shown in Figure 4.1. When

compared to traditional carbenes, NHCs are more nucleophilic and do not have electrophilic reactivities. For example, NHCs cannot activate H_2 nor fix carbon monoxide to make ketenes.[51]
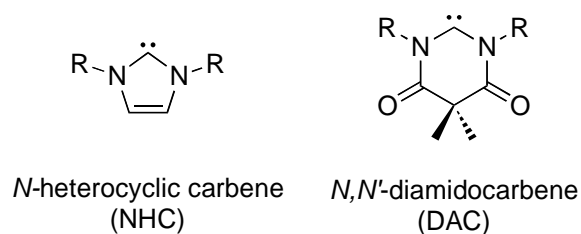
Figure 4.1. General structures for *N*-heterocyclic carbene (NHC) and

N,N'-diamidocarbene (DAC)

Our collaborator Dr. Bielawski and coworkers made the NHCs more electrophilic by introducing the carbonyl groups (DACs, Figure 4.1), which draw electron density of the adjoining nitrogen atoms away from the carbenic carbon.[52,53,135-137] The electrophilic reactivities of the DACs were reported, such as: C-H insertions,[52] CO fixation,[52,53,138] and NH_3 activation[53]. Although the DACs display electrophilic reactivities, they are still nucleophilic and are observed to be able to coordinate to transition metals and to electrophilic heteroallenes.[52,139,140] Since there is usually a correlation between basicity and nucleophilicity, I measured the PA of the DACs in order to make the comparisons between DACs and other carbenes easier. I also expect the PA characterization could help the design of novel electrophilic carbenes.

Figure 4.2. NHCs and DACs studied in this chapter

4.2 Experimental

For NHCs **1a**, **1b** and **1d**, the corresponding precursors (1,3-dimethylimidazolium tetrafluoroborate, 1-ethyl-3-methylimidazolium tetrafluoroborate, and 1,3-di*iso*propyl -imidazolium tetrafluoroborate) were used as received (Sigma Aldrich). The precursor to
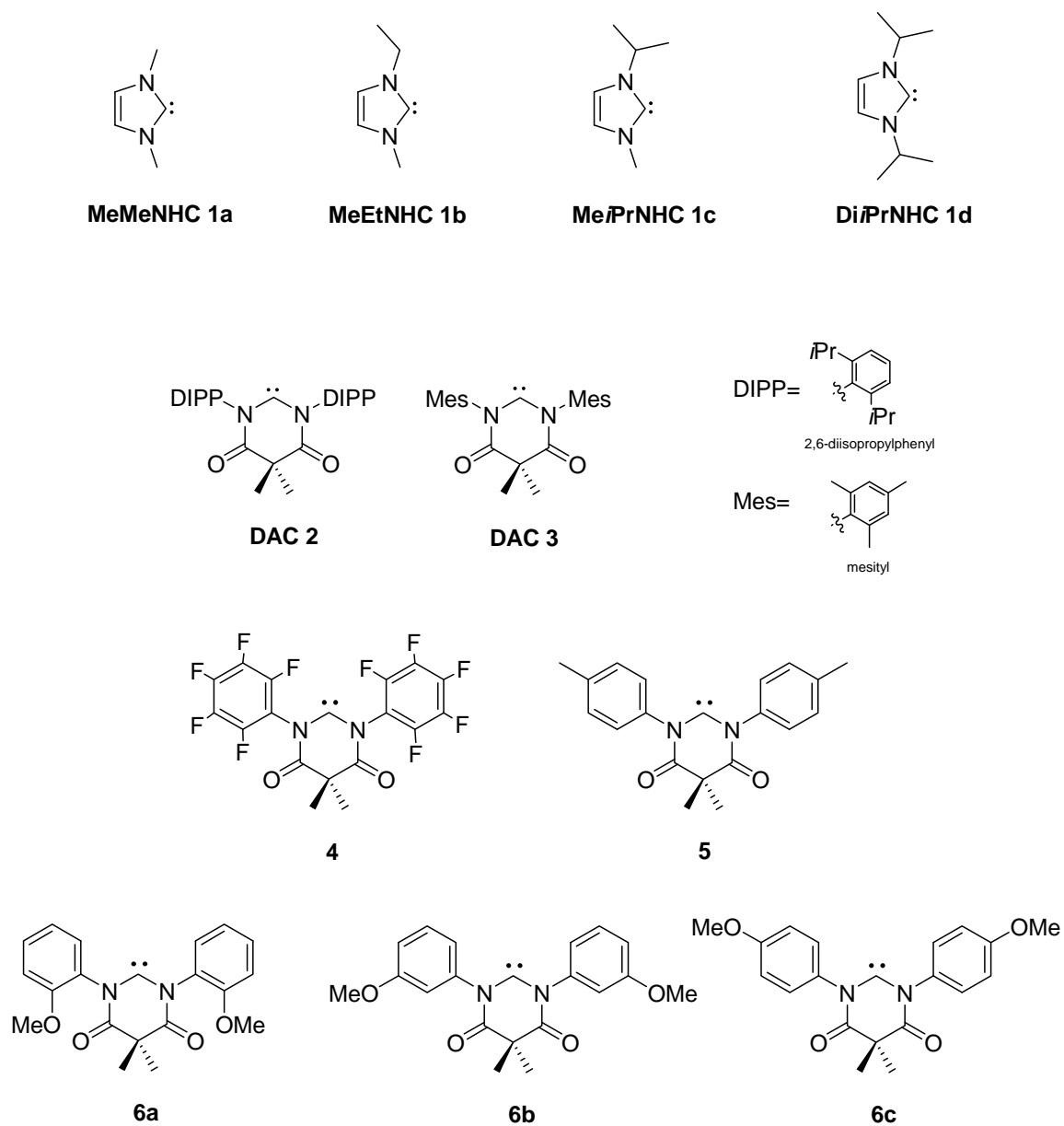
1c, 1-methyl-3-*iso*propyl-imidazolium iodide, was synthesized according to a literature procedure.[141] Bis(4-methylphenyl)formamidine,[142] bis(2-methoxyphenyl)formamidine,[143] bis(perfluorophenyl)formamidine,[144] 2-chloro-1,3-bis(2,6-diisopropylphenyl)-4,6-diketo -5,5 -dimethylpyrimidine (**2·HCl**),[53] and the formally hydrated carbene adduct **3·H$_2$O**[53] were synthesized according to literature procedures by the Bielawski group. All reference bases were used as received (Sigma Aldrich).

To generate the protonated carbene species via electrospray, the formally hydrated DACs were dissolved in formic acid or a mixture of formic acid/water (1:10 v/v) ([DAC]$_0$ ~10^{-4} M). Standard Schlenk techniques under an atmosphere of nitrogen or in a nitrogen-filled glove box were used by our collaborator (the Bielawski group) for the condensation reactions needed to prepare **2-6·H$_2$O**.

Bracketing experiments were conducted using a house-modified quadrupole ion trap mass spectrometer as described in chapter 1.[145] Protonated carbene ions were generated by electrospray ionization (ESI) from a ~10^{-4} M solution using a flow rate of 15~25 μL/min. The analyzed solutions were prepared by dissolving the conjugate acids of NHCs **1a**, **1b**, **1c**, and **1d** in methanol; dissolving the formally hydrated DACs **2**, **4**, and **5** in pure formic acid; or dissolving the formally hydrated DACs **3**, **6** in pure formic acid followed by dilution (10×) using DI water. Final concentrations of these solutions for ESI were ~10^{-4} M.

The capillary temperature was 150 °C. Neutral reference bases were added with the helium gas flow. The protonated carbene ions were allowed to react with neutral reference bases for 0.03-1000 ms. The unreactive DACs **2** and **3** were allowed to react up to 10,000 ms with BEMP to ensure that proton transfer was not occurring. The

occurrence of proton transfer was regarded as evidence that the reaction was exothermic ("+" in Tables); otherwise the reaction was regarded as endothermic ("−" in Tables). The typical electrospray needle voltage was ~4.5 kV. A total of 10 scans were collected and averaged.

All calculations were performed using density functional theory (B3LYP/6-31+G(d))[92-96] as implemented in Gaussian 09.[91] All the geometries were fully optimized and vibrational frequencies were calculated; no scaling factor was applied. The optimized structures had no negative vibrational frequencies. All calculations were done at 298 K. GaussView 5.0 was used to generate the electrostatic potential maps of the protonated carbenes based on their optimized structures in the gas phase. Density isovalues for the surfaces were set to 0.0004. The color range for the surfaces was set to -0.19 to +0.19.

4.3 Results and Discussion

I first calculated the proton affinities of carbenes **2** and **3** at B3LYP/6-31+G(d) level of theory. Proton affinities of **2** and **3** are calculated to be 258.1 kcal mol^{-1} and 257.8 kcal mol^{-1}, respectively (Figure 4.3).
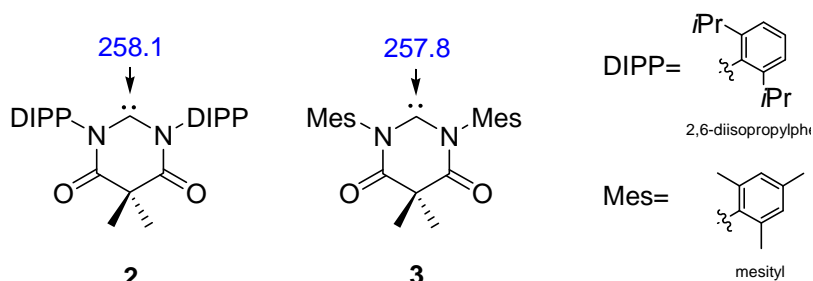

Figure 4.3. Calculated PAs of *N,N'*-diamidocarbenes **2** and **3**, in blue, at B3LYP/6-31+G(d) level, in kcal mol^{-1}, 298 K

Since the electrophilic properties of **2** and **3** were observed by our collaborators, the carbonyl groups are expected to drive the electron density away from the carbene center. Based on this, we expect PAs of DACs **2** and **3** to be much lower than that of traditional NHCs. However, the calculated PA values of **2** and **3** are around 258 kcal mol^{-1}, which are not that much lower than traditional NHCs. When I compared these values to the calculated PA of NHCs **1a** and **1b** (Figure 4.4), which are 259.9 and 261.4 kcal mol^{-1} respectively, PA of **2** and **3** are only ~3 kcal mol^{-1} less basic. In addition, the first generation of Grubbs catalysts (PCy$_3$) has a calculated PA of 243.3 kcal mol^{-1} and was experimentally measured to be 249 ± 3 kcal mol^{-1} by a former group member in Dr. Lee's group.[146] Based on the calculated values, DACs **2** and **3** are much more basic than PCy$_3$ by more than 14 kcal mol^{-1}. This indicates the high electron-donating ability of DACs **2** and **3**.

I also conducted the PA bracketing experiment on a LCQ mass spectrometer in order to measure the PAs of these two diamidocarbenes. The method is described in detail in the experimental part of this chapter and in the introduction chapter. I used several reference bases with high PAs to react with the protonated DACs **2** and **3** (Table 4.1). Proton transfer was not observed for all these reference bases, even with the most basic reference base used (PA=263.8 kcal mol^{-1}), which is more basic than the calculated PA of carbene **2** by 5 kcal mol^{-1}. The experimental result is not consistent with the expectation based on the calculations.

I have observed the same discrepancy between computational and experimental PAs of carbene **3**. Even very basic reference bases (more basic than 260 kcal mol^{-1}) are not able to deprotonate the protonated carbene **3**, whose calculated PA is 257.8 kcal mol^{-1}

(Table 4.1). This observation indicates two possibilities. One is the PA of 3 is higher than the calculated value; the second is that our gas phase experiments are not accurate.

Table 4.1. Summary of the PA bracketing results for DACs **2**, **3** and NHCs **1c**, **1d**.

Reference base[147]	PA (kcal mol^{-1})	Proton transfer to reference base[a]			
		1H$^+$	**2H$^+$**	**3cH$^+$**	**3dH$^+$**
BEMP	263.8 ± 2.0	–	–	+	–
tOctP$_1$(dma)	262.0 ± 2.0	–	–	–	–
tBuP$_1$(dma)	260.6 ± 2.0	–	–	–	–
HP$_1$(dma)	257.4 ± 2.0	–	–	–	–

BEMP = 2-*tert*-Butylimino-2-diethylamino-1,3-dimethylperhydro-1,3,2-diaza-phosphorine; tOctP$_1$(dma) = *tert*-Octylimino-tris(dimethylamino)phosphorane; tBuP$_1$(dma) = *tert*-Butylimino-tris(dimethylamino)phosphorane; HP$_1$(dma) = Imino-tris(dimethylamino)phosphorane. [a]The "+" symbol indicates that the proton transfer happens and the "–" symbol indicates that the proton transfer did not happen.

In a previous work, we proved that our gas phase bracketing method is accurate and gives results that are consistent with the results at B3LYP/6-31+G(d) level of theory.[145] To further test the accuracy of our bracketing method, I carried out the bracketing of another two NHCs, **1c** (Me*i*PrNHC) and **1d** (di*i*PrNHC) (Figure 4.4).
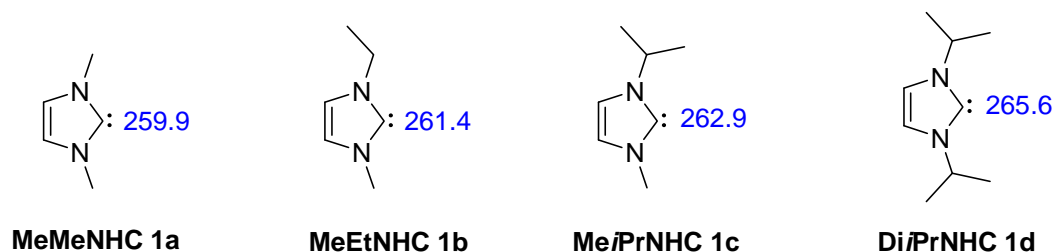
Figure 4.4. Structures of the NHCs studied in this chapter. Proton affinities are in blue, at B3LYP/6-31+G(d), in kcal mol^{-1}, 298K

I first calculated the PAs of **1c** and **1d** at the B3LYP/6-31+G(d) level of theory. Their PAs are calculated to be 262.9 kcal mol^{-1} and 265.6 kcal mol^{-1} respectively. As can be seen in Figure 4.4, the NHCs with larger substituents on the nitrogens tend to have a higher PA.

Then we used the same bracketing method to measure the PAs of methyl isopropyl carbene **1c** and diisopropyl carbene **1d**. As shown in Table 4.1, protonated **1c** can be deprotonated by 2-*tert*-butylimino-2-diethylamino-1,3-dimethylperhydro-1,3,2-diaza-phosphorine (PA=263.8 ± 2.0 kcal mol^{-1}). However, the rest of the reference bases cannot deprotonate the protonated **1c**. Thus, I bracket the PA of **1c** be 262.0-263.8 kcal mol^{-1}. This result is consistent with the calculated value. I also tried to bracket the PA of diisopropyl carbene **1d**. However, the reference bases above 263.8 kcal mol^{-1} are not volatile enough to be used in our instrument. As shown in Table 4.1, none of the reference bases that I used are able to deprotonated the protonated **1d**. Even with 2-*tert*-butylimino-2-diethylamino-1,3-dimethylperhydro-1,3,2-diaza-phosphorine (263.8 ± 2.0 kcal mol$^{-1,}$ the most basic in the series), I did not observe proton transfer between the base and protonated **1d**. These observations are all consistent with the calculated PA of **1d**, which is 265.6 kcal mol^{-1} at B3LYP/6-31+G(d) level of theory. However, without

testing with more reference bases at even higher ranges, I am not able to conclude that the PA bracketing result for **1d** is consistent with calculation.

When comparing the structures of DACs **2** and **3** to the structures of NHCs **1a-1d**, it should be noticed that the substituents (on the nitrogens) on the DACs are a lot bulkier than the substituents on the NHCs. For the proton transfer reaction between DACs **2** and **3** and the reference bases that have lower PAs, the reaction is exothermic, from the thermodynamic point of view. However, from the kinetic point of view, the steric hindrance from the bulkier substituents on DACs **2** and **3** can prevent the proton on the protonated **2** or **3** from being accessed by the reference bases. This might explain why the proton transfer does not happen even if they are predicted to happen by PA calculations. In addition, the reference bases that are used in these bracketing experiments are also sterically bulky. This can also contribute to the overall steric effect of the reaction.

Aue and coworkers have actually reported similar steric effects when they looked at the reaction between protonated 2,6-disubstituted-*tert*-butyl pyridine (2,6-DTBP) and other bases in the solution phase.[148] Ion cyclotron resonance results from the same group show that the proton transfer reaction involving 2,6-DTBP are much slower than that involving 2,4-DTBP, although 2,4-DTBP has the same PA as 2,6-DTBP.[149] Their observations support the existence of steric effect in the proton transfer reactions.

To further test the hypothesis that the steric effect plays a role in the gas phase proton transfer reactions, I designed several more DACs (our collaborators synthesized them). They include DACs **4, 5,** and **6a-c** in Figure 4.5. As compared to mesityl and DIPP groups, perfluorophenyl group in DAC **4** and tolyl group in carbene **5** are less hindered. Thus, I expect the reference bases with higher PAs than these DACs are able to

deprotonate the protonated species of these DACs. In addition, for diamidocarbenes **6a-c**, when the methoxy group is located at the *ortho-*, *meta-*, and *para-* positions respectively, the steric effect is expected to be different. *O*-anisidyl diamidocarbene **6a** is the most sterically hindered in the three, thus it is expected that **6a** will have the strongest steric effect.
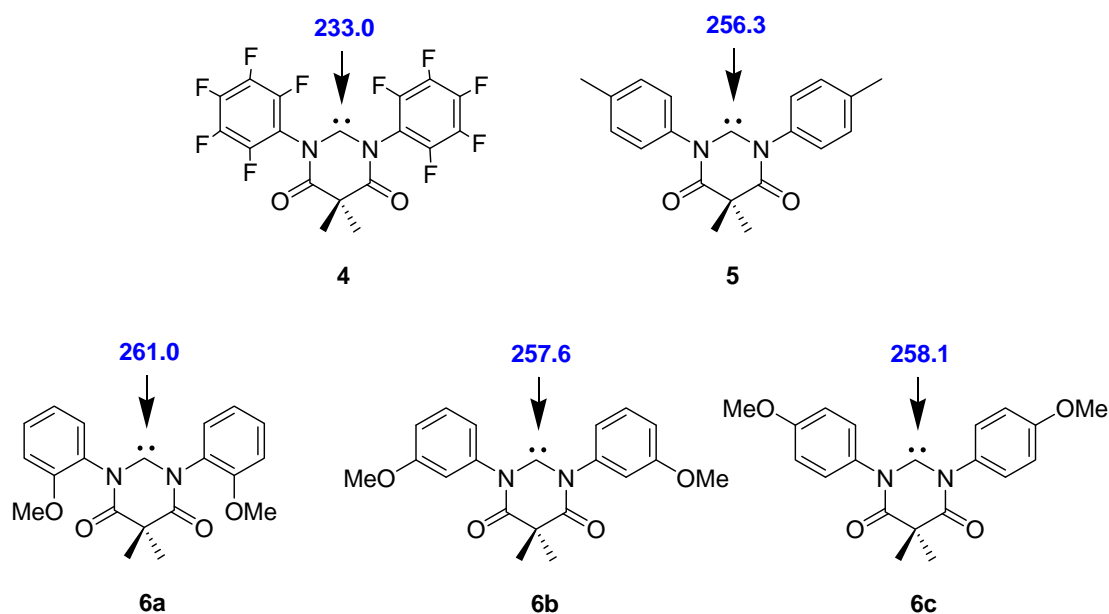

Figure 4.5. *N,N'*-Diamidocarbenes designed with different substituents to study the steric effect. Proton affinities of the carbenic carbon are in blue, B3LYP/6-31+G(d), in kcal mol^{-1}, 298K

I first calculated the PA of DACs **4** and **5** at the same level of theory (B3LYP/6-31+G(d)) and measured experimentally by using the same bracketing method. PA of **4** is calculated to be 233.0 kcal mol^{-1}. The bracketing results are shown in Table 4.2. The reference bases with PAs larger than 234 kcal mol^{-1} can deprotonate protonated

DAC **4**, while reference bases that are less basic than 233 kcal mol^{-1} cannot deprotonate protonated **4**. Thus, proton affinity of **4** is bracketed to be 232.1-234.7 kcal mol^{-1}. This experimental result is consistent with the calculated PA. It is likely that the reduced steric effect in DAC **4** makes the proton more available for the reference bases than the protons in DACs **2** and **3**.

Table 4.2. Summary of bracketing results for PA of perfluorophenyl DAC **4**.

Reference base[115]	PA (kcal mol^{-1})	Proton transfer (between protonated **4H$^+$** and reference base)^a
N,N-dimethylcyclohexylamine	235.1 ± 2.0	+
triethylamine	234.7 ± 2.0	+
N-methylpiperidine	232.1 ± 2.0	–
N-methylpyrrolidine	230.8 ± 2.0	–
piperidine	228.0 ± 2.0	–

^{a}The "+" symbol indicates the observation of proton transfer and the "–" symbol indicates the lack of observed proton transfer.

Calculated PA of tolyl DAC **5** is 256.3 kcal mol^{-1}. The experimental results are summarized in Table 4.3: PA of tolylDAC is bracketed to be 247.4-260.6 kcal mol^{-1}, which is consistent with the calculated value. For the gas phase reactions of protonated **5** and the reference bases, reference bases are the same as those used in the bracketing of

DACs **2** and **3**. Thus, the steric effect from the reference bases are the same. This indicates that by simply reducing the steric bulkiness in the protonated DAC, the carbenic carbon can be made to be more accessible for the attack of neutral reference bases.

Table 4.3. Summary of bracketing results for the PA of tolylDAC **5**.

Reference base[115,147]	PA (kcal mol^{-1})	Proton transfer (between **5H$^+$** and reference base)^a
BEMP	263.8 ± 2.0	+
tOctP$_1$(dma)	262.0 ± 2.0	+
tBuP$_1$(dma)	260.6 ± 2.0	+
N,N,N',N'-tetramethyl-1,3-propanediamine	247.4 ± 2.0	−

^{a}The "+" symbol indicates the observation of proton transfer and the "−" symbol indicates the lack of observed proton transfer.

For the PA bracketing experiments of the anisidyl substituted DACs **6a**, **6b**, and **6c**, the same group of bases that are used in the bracketing of DACs **2** and **3** are used. Among these three anisidyl DACs, **6a** is the most sterically hindered because the methoxy group is at the *ortho* position, closest to the carbenic carbon. Thus, it is expected that **6a** has the most significant steric effect. However, in Table 4.4 where all experimental results are summarized, *tert*-octylimino-tris(dimethylamino)-phosphorane (262.0 kcal mol^{-1}) can deprotonate protonated **6a** while *tert*-butylimino-tris(dimethylamino)phosphorane (260.6 kcal mol^{-1}) cannot. Thus I bracket the PA of **6a** to be 260.6-262.0 kcal mol^{-1}. This result

is consistent with the calculated value (261.0 kcal mol^{-1}). The expected significant steric

effect is not observed for **6a**. This is probably because the *o*-anisidyl group is not as

bulky as the 2,6-diisopropylphenyl group or mesityl group in DACs **2** and **3**.

Table 4.4. Summary of PA bracketing results for the anisidyl-based DACs **6**.

Reference base[115,147]	PA (kcal mol^{-1})	Proton transfer (between protonated **6H$^+$** and reference base)[a]		
		6a	**6b**	**6c**
		(261.0)[b]	(257.6)[b]	(258.1)[b]
BEMP	263.8 ± 2.0	+	+	+
tOctP$_1$(dma)	262.0 ± 2.0	+	+	+
tBuP$_1$(dma)	260.6 ± 2.0	–	+	+
HP$_1$(dma)	257.4 ± 2.0	complex	complex	complex
MTBD^c	254.0 ± 2.0	complex	complex	complex
N,N,N′,N′-tetramethyl-1,4-butanediamine	250.1 ± 2.0	–	–	–

^{a} The "+" symbol indicates the observation of proton transfer and the "–" symbol indicates the lack of observed proton transfer. ^{b} Calculated at the B3LYP/6-31+G(d) level of theory. ^{c} MTBD = 7-Methyl-1,5,7-triazabicyclo[4.4.0]dec-5-ene

For the other two anisidyl DACs **6b** and **6c**, as shown in Table 4.4, both protonated DACs can be deprotonated by *tert*-butylimino-tris (dimethylamino)phosphorane (PA=260.6 kcal mol^{-1}), but cannot be deprotonated by N,N,N′,N′-tetramethyl-1,4-butanediamine (PA=250.1 kcal mol^{-1}). The reference bases in

between these two reference bases can form dimers with the DAC, thus these results are not informative. The PAs of both **6b** and **6c** are thus bracketed to be 250.1-260.6 kcal mol^{-1}. These results are again consistent with the calculated PAs at B3LYP/6-31+G(d) level of theory.

Electrostatic potential masps (ESP maps) are generated and used to visualize the steric effect in the protonated DACs (**2**, **3**, **4**, **5**, **6a-c**, Figure 4.6). For the DACs **2** and **3**, it is obvious that the high electrostatic potential part (blue) of the proton is submerged in the ESP surface of the DIPP and mesityl groups. In contrast, for the protonated DACs **4** and **5**, the proton (high electrostatic potential, blue part) is not blocked by the tolyl groups or C$_6$F$_5$ groups on the nitrogen atoms (more accessible). As compared to the ESP of **2** and **3**, protonated DACs **4** and **5** are significantly less hindered at the protonated carbenic carbon center.

For the protonated *o*-anisidyl DAC **6a**, the proton at the carbene center is more hindered than the protons in DACs **4** and **5**. However, proton in **6a** looks less hindered than the protonated **2** and **3**. This might be because the methoxy group on the phenyl ring is not as bulky as the DIPP and mesityl groups in DACs **2** and **3**.

These ESP maps support our hypothesis that the steric effect can influence the gas phase proton transfer reaction.
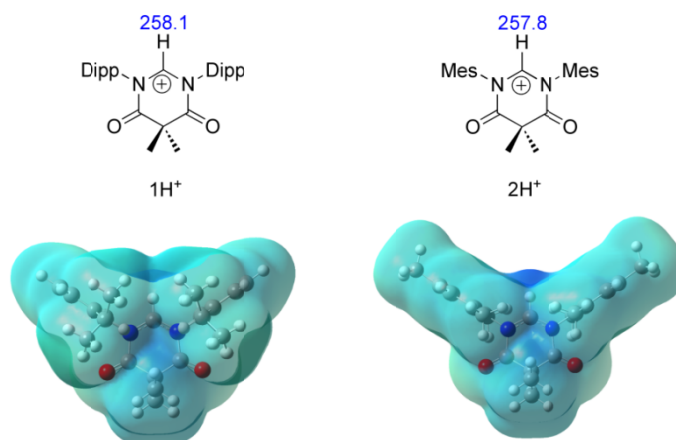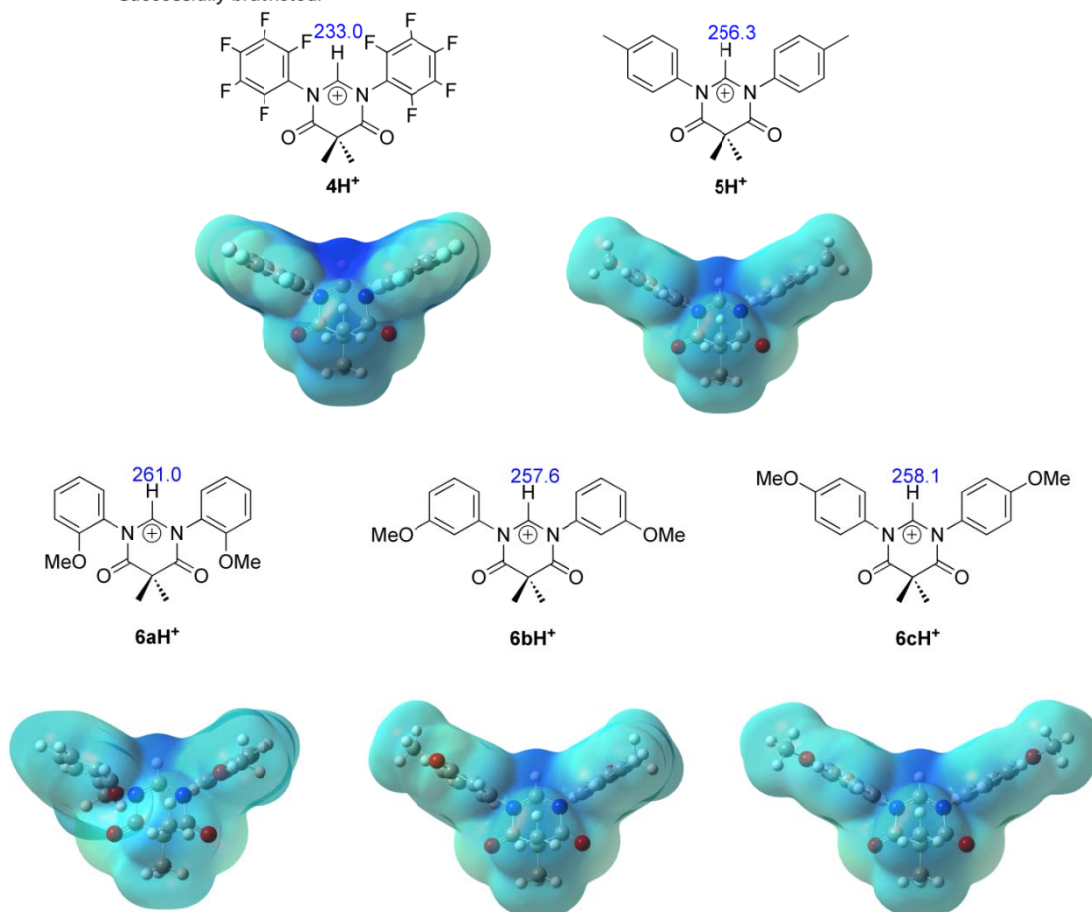
Figure 4.6. Calculated electrostatic potential maps for various protonated DACs. Values in blue are calculated PAs for the corresponding carbenes (B3LYP/6-31+G(d), kcal mol^{-1})

In addition, the HOMO and LUMO energies for the DACs and NHCs are calculated at the B3LYP/6-31+G(d) level of theory. Our collaborator have previously predicted that the HOMO energies of DACs and NHCs should be close, while the LUMO energies should be quite different.[150] By my calculation, DAC **2** has a HOMO that is only 7 kcal mol^{-1} lower than that of NHC **1a**. However, the LUMO energy of DAC **2**, is 54 kcal mol^{-1} lower than that of the NHC. Similarly HOMO of DAC **3** is calculated to be close to that of NHC **1a** (within 6 kcal mol^{-1}). However, the LUMO of the DAC **3** was 51 kcal mol^{-1} lower than that of **1a**.

4.4 Conclusions

To summarize, the gas phase PA of novel diamidocarbenes (DACs) have been characterized both computationally and experimentally. The substituents on the nitrogens adjacent to the carbene center are hypothesized to have a steric effect in the gas phase proton transfer reactions. This is supported by the calculated electrostatic potential maps (ESP).

Our bracketing results are consistent with the calculated results at B3LYP/6-31+G(d) level of theory when the steric effect is taken into account. Our gas phase studies show that the novel *N,N'*-diamidocarbenes (DACs) have close basicity to the NHCs. This is supported by the fact that the HOMO energy level of DACs is also close to that of NHCs. However, the LUMO energies of the DACs are about 50 kcal mol^{-1} lower than that of NHCs. This might be used to explain the novel reactivity of DACs as compared to the NHCs.

Chapter 5 Differentiating Covalent Bond and Hydrogen Bond for the Gas Phase Characterization of Nucleophilicity and Electrophilicity

5.1 Introduction

Nucleophilicity and electrophilicity are important factors that decide the rate of many organic reactions. Many studies have been done to describe these two factors quantitatively by using various parameters and equations.[58-61] Mayr and coworkers developed a systematic set of paramenters to describe the nucleophilicity and electrophilicity of a neutral nucleophile and cation electrophile, respectively.[62] They demonstrated that the relative rate constant of such a nucleophilic reaction can be described by the following equation (Equation 5.1). In this system, two parameters s and N are used for the nucleophile; one parameter E is used for the electrophile. This equation can precisely predict the rate constants of many nucleophilic reactions, covering a reactivity range of eighteen orders of magnitude.

$$\log k = s(N+E) \qquad\qquad \textbf{Eq. 5.1}$$

However, all the parameters developed by previous researchers are for solution phase reactions. These parameters do not reveal the intrinsic properties of the nucleophiles and electrophiles since the solvents have a strong effect on the nucleophilic

reactions. The gas phase provides a good environment to exclude the influence of the solvents. By using the equation developed by Mayr, Denekamp and coworkers reported a systematic gas phase study of the reactions between cation electrophiles and neutral nucleophiles.[63] They found that the linear selectivity described by the equation is still true in the gas phase.

One typical reaction studied by Denekamp and coworkers is between diphenylmethylium cation and neutral pyridine (Scheme 5.1). The experiments were carried out by monitoring the disappearance of the reactant cation and appearance of the product ion. Mass-to-charge ratio is used to represent concentrations of the ions in the gas phase. However, Denekamp and coworkers did not show evidence for the structure of the product ion. In fact, based on our previous experiences with gas phase ion-molecule reactions, diphenylmethylium cation can also form a proton-bound dimer with the neutral pyridine (Path 2, Scheme 5.1). The formation of a covalent bond (Path 1, Scheme 5.1) might not be the only reaction pathway of this reaction.
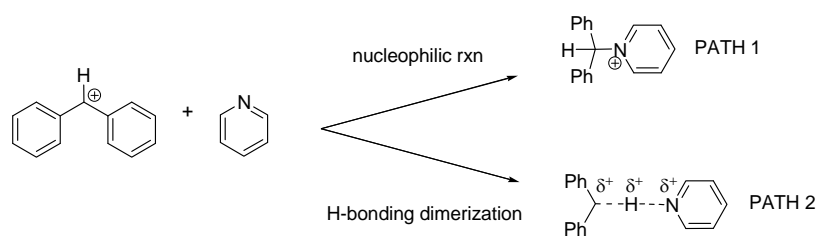
Scheme 5.1. Two possible reaction pathways of the reaction between diphenylmethylium cation and pyridine

In order to use this reaction to probe the gas phase nucleophilicity and electrophilicity, one need to prove that the structure of the cluster is covalent bonded. Only when the cluster formed in the gas phase is proven to be a covalent bonded ion, one

can be sure that the gas phase reaction observed is a nucleophilic reaction. Otherwise, the gas phase reaction could be a proton-bound dimerization, which cannot be used to probe the nucleophilicity and electrophilicity of the reactants. To probe the structure of the cluster, we monitored gas phase ion-molecule reactions of a series of diphenylmethylium cations and neutral electrophile (pyridine) in a 3D ion trap mass spectrometer. Several physical organic methods, including Hammett plot, kinetic isotope effect, and H/D exchange reactions, have been used to elucidate the structure of the cluster in the gas phase.

5.2 Experiments

The diphenylmethylium cation is generated in the gas phase by electrospraying a solution of benzhydrol (100 uM). Neutral pyridine is introduced into the 3D ion trap with the flow of helium. A Finnigan LCQ mass spectrometer is modified as described in chapter 1 and used for the gas phase reactions in this chapter. In order to find out the pressure of pyridine in the ion trap, a much less basic base such as *m*-chloroaniline (PA=207.5 kcal mol^{-1}) is isolated to react with pyridine. This reaction is considered to undergo at 100% efficiency. The rate constant of this reaction is measured and used to "back up" the pressure of pyridine.

All compounds are commercially available (Sigma Aldrich and TCI) and used as received. Deuterated benzhydrol is synthesized according to literature procedures.[151]

All calculations are performed at B3LYP/6-31+G(d) level of theory[92-96], as implemented in Gaussian 09.[91] All the geometries were fully optimized and vibrational frequencies were calculated; no scaling factor was applied. All calculation results were at

298 K. GaussView 5.0 was used to generate the electrostatic potential maps (ESP) of the diphenylmethylium cation, pyridine, and possible clusters. Density isovalues were set to be 0.0004. Color range is -0.19 to +0.19.

5.3 Results and Discussion

5.3.1 Charge change and Hammett plot

One way to differentiate the covalent bond versus H-bonding is the Hammett plot. In the nucleophilic reaction pathway (Scheme 5.2), positive charge diminishes and negative charge "builds up" at the carbon center. Thus, a large ρ is expected in the Hammett plot. In contrast, little positive charge diminishes and little negative charge "builds up" at the carbon center in the H-bonding dimerization pathway. Thus, a small ρ is expected in the Hammett plot.

CHELPG charge distribution is used to calculate the charge change. As shown in Scheme 5.2, in the nucleophilic reaction pathway, the CHELPG charge on the methylene carbon change from -0.08 to -0.31. The diminished positive charge transfers to the nitrogen on pyridine (from -0.67 to +0.13). However, in the H-bonding dimerization pathway, the change in charge is not obvious. The charge on the methylene carbon only changes from -0.08 to +0.04.
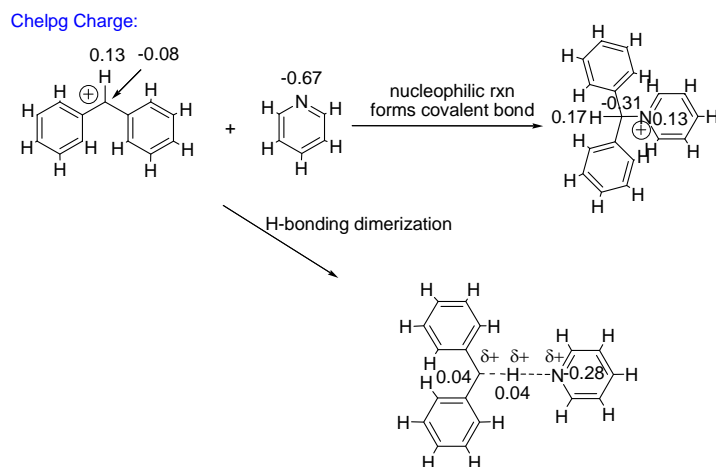
Scheme 5.2. CHELPG charge distribution in the two pathways, B3LYP/6-31+G(d)

The CHELPG calculation is supported by the electrostatic potential maps (ESPs) (Figure 5.1). The blue part indicates higher electrostatic potential (relatively more positive charge), while the red part indicates lower electrostatic potential (relatively more negative charge). In the covalent bonded product (Figure 5.1 c), positive charge on the carbon transfers to the pyridine. In the H-bonding product (Figure 5.1 d), positive charge is still distributed on the diphenylmethylium system and less positive charge transfers to the pyridine. Thus, the CHELPG charge calculation and ESP maps support that the two different reaction pathways have different charge distribution changes. Thus, Hammett plot might be used to differentiate them.

c   **d**
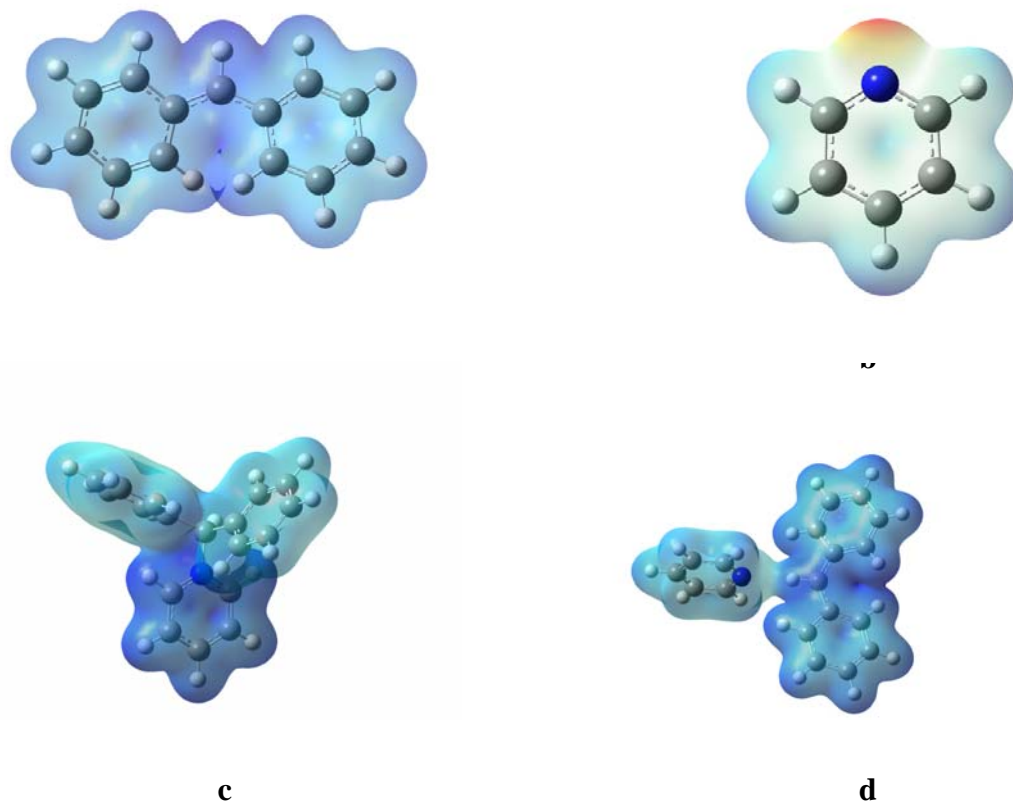
Figure 5.1. ESPs of the species in the reaction between diphenylmethylium and pyridine: **a** - diphenylmethylium cation, **b** - pyridine, **c** - covalent bonded cluster, **d** - proton-bound cluster

Hammett plot is made for the reaction between 4-substituted diphenylmethylium cations and pyridine. Seven different substituents are used in the plot: methoxy, methyl, fluoro, hydrogen (non-substituted), chloro, trifluoromethyl, and nitro group (Figure 5.2). The Hammett plot from calculated data for the covalent bonding pathway has a slope of 5.4374. The Hammett plot from calculated data for H-bonding has a slope of 0.9139. This difference in the slope is consistent with the different charge change patterns in the two pathways. The Hammett plot from experimental data has a slope of 0.3161, which is

closer to the calculated H-bonding pathway. This indicates that the product we observed in our LCQ experiments might be hydrogen bonded dimer, although it has the same m/z as the covalently bonded product.
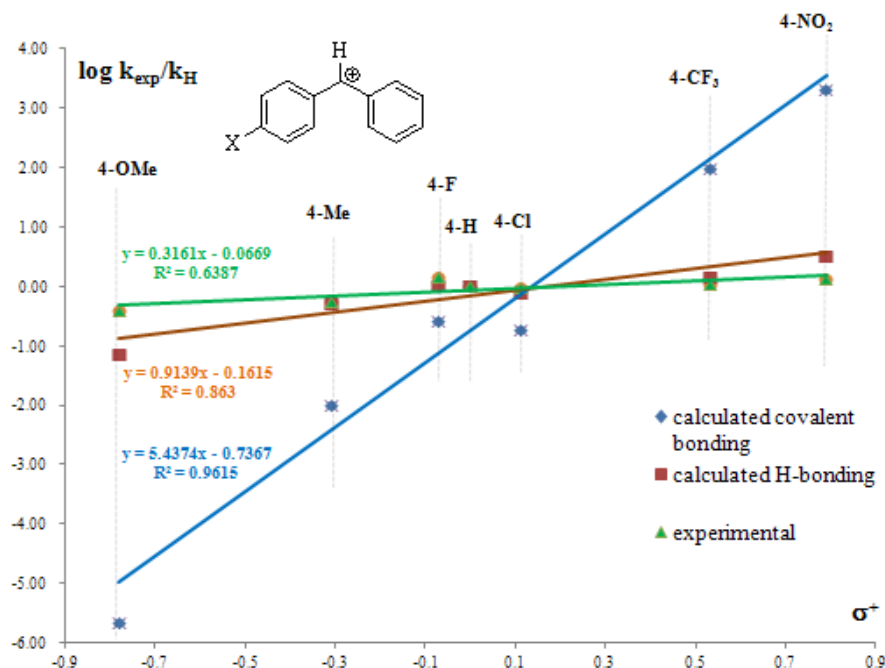
Figure 5.2. Calculated and experimental Hammett plot for the reaction of substituted diphenylmethylium cation with pyridine

5.3.2 Secondary kinetic isotope effect

Another difference between the covalent bonded product and the proton-bound dimer is that they have different hybridization states for the methylene carbon. In the pathway that leads to the covalent bond product, hybridization of the methylene carbon changes from sp^2 (in reactant, diphenylmethylium cation) to sp^3 (in the covalent bond product). In contrast, in the H-bonding dimerization pathway, hybridization of the methylene carbon does not change. (Scheme 5.3)

If we use deuterated diphenylmethylium cation (Scheme 5.3) to react with pyridine and compare the rate constant with that of non-deuterated diphenylmethylium cation, we expect to get a secondary KIE of the reaction. If covalent bond is formed in the product, we expect to see an inverse secondary KIE ($k_H/k_D<1$). However, if proton-bound dimer is formed in the product, we expect to see a very small KIE ($k_H/k_D \sim 1$).
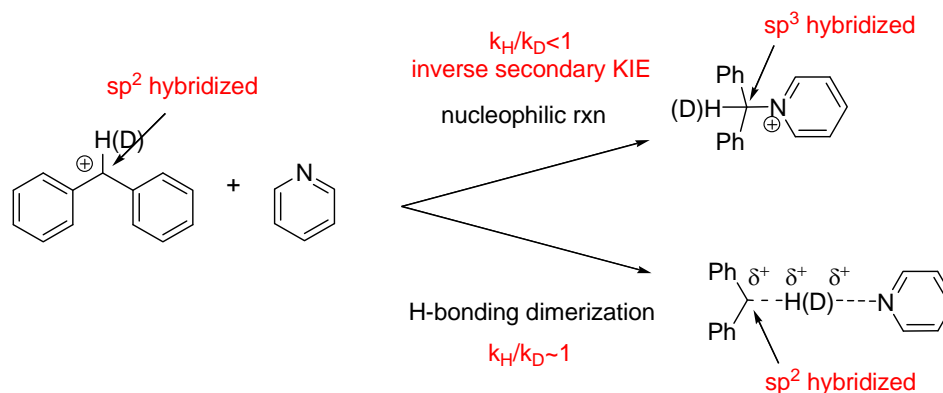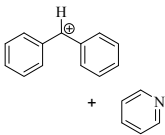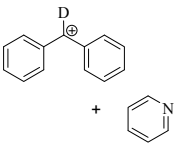
Scheme 5.3. Hybridization of the methylene carbon and KIE of the two different pathways

Deuterated diphenylmethylium cation has been synthesized by Yiejie Niu in our group and reaction between it and pyridine has been carried out in our LCQ. The reaction between H-diphenylmethylium/D-diphenylmethylium cations and pyridine are carried out and the k_{exp} and efficiencies are calculated (Table 5.1). Three trials of reactions between the H-diphenylmethylium cation and pyridine are carried out. The efficiencies and k_{exp} from these three trials are very consistent with an average k_{exp} of $7.83*10^{-10}$ cm^3 molecule^{-1} s^{-1}. Only two trials of D-diphenylmethylium cation and pyridine are carried out and the k_{exp} are not very consistent ($1.22*10^{-9}$ vs $8.28*10^{-10}$ cm^3 molecule^{-1} s^{-1}). The average of these two trials is $1.034*10^{-9}$ cm^3 molecule^{-1} s^{-1}. It seems the deuterated diphenylmethylium cation reacts faster than the non-deuterated one. The KIE from the

average k_{exp} is 0.783/1.034=0.76. If this KIE is substantial, it supports that the product in the reaction is covalently bonded rather than non-covalently bonded. However, more trials of experiments are needed to validate this result.

Table 5.1. Reaction of H(D)-diphenylmethylium cation with pyridine

reaction	trial	efficiency	$k_{exp}/10^{-9}$ [a]	Average $k_{exp}/10^{-9}$ [a]
	1	45.29%	0.794	
	2	44.03%	0.772	0.783
	3	44.73%	0.784	
	1	69.80%	1.22	
	2	48.40%	0.848	1.034

[a] Unit for k_{exp} is cm^3 molecule^{-1} s^{-1}

5.3.3 Exchange reactions with d_5-pyridine

An H/D exchange experiment is suggested by Professor Steven Kass to differentiate the covalent and proton-bound products. Since the hydrogen bond in the proton-bound dimer is weaker than the covalent bond, the non-covalent complex should be more willing to exchange out the whole pyridine. We isolate the complex and let it react with perdeuterated pyridine ($d5$-pyridine). If the complex is non-covalent in nature, we expect the pyridine to exchange in and out, thus a +5 increase in mass-to-charge ratio could be observed. If the complex is covalent in nature, the +5 increase in mass-to-charge would not happen (Scheme 5.4).
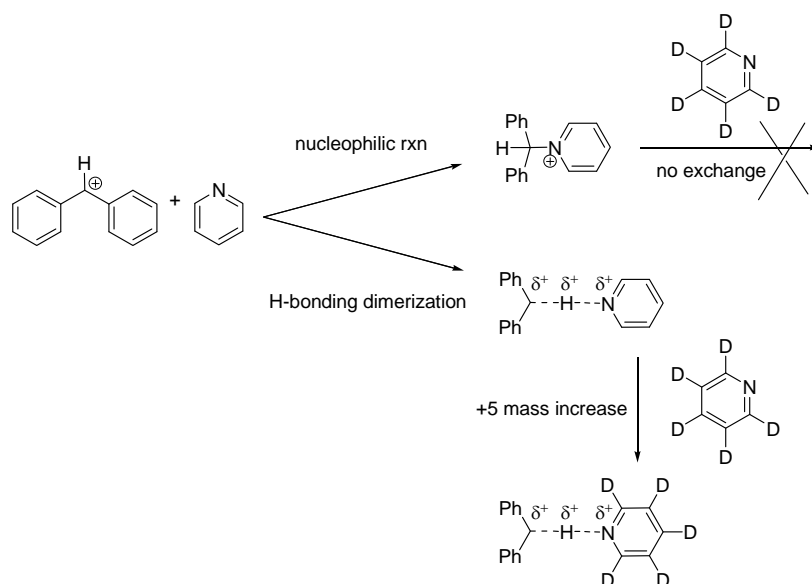
Scheme 5.4. Exchange of the complex with d_5-pyridine

In the actual experiment, pyridine and d_5-pyridine are introduced into the ion trap at the same time. Diphenylmethylium cation (m/z=167) is first isolated to react with both pyridine and d_5-pyridine, yielding the clusters at two different mass-to-charge ratios (m/z=246 and m/z=251). The cluster with mass-to-charge ratio of 246 is then isolated and given a certain time to interact with the pyridine and d_5-pyridine in the ion trap. If the d_5-pyridine exchange happens, a peak at m/z=251 should be observed. However, at the reaction time of 8000 ms, no peak at mass-to-charge ratio of 251 is observed. Similarly, the cluster with d_5-pyridine (m/z=251) is isolated and allowed to react with pyridine and d_5-pyridine. No exchange of the pyridine in the cluster is observed. The d_5-pyridine exchange is not observed experimentally, which might indicate that the bond between diphenylmethylium cation and pyridine is strong and a covalent bond under our experimental conditions.

5.3.4 Collision induced dissociation of the clusters

Another way to differentiate covalent bonded cluster and proton-bound dimer is to apply collision induced dissociation (CID) energy on the cluster. Since covalent bond is stronger than the hydrogen bond, the covalent bonded cluster would be harder to be fragmented under CID conditions as compared to the proton-bound dimer.

Diphenylmethylium cation (m/z=167) is first isolated and allowed to react with pyridine. The cluster between diphenylmethylium cation and pyridine (m/z=246) is observed and then isolated for CID. When 12% CID is applied to the cluster, ions at mass-to-charge ratio of 167 and 251 can be observed (Scheme 5.5 and Figure 5.3 a). Ion at 167 is the diphenylmethylium cation. Ion at 251 is the cluster formed from the reaction of the diphenylmethylium cation and d_5-pyridine, which is also present in the ion trap. When 19% CID is applied, the ions at 167 and 251 become very apparent (Figure 5.3 b), indicating more fragmentation. Similar observations have been made for the CID experiment of the cluster of diphenylmethylium and d_5-pyridine (m/z=251). It seems that the cluster can be fragmented under CID conditions. However, this observation is not conclusive without knowing how much energy is needed to fragment a covalent bond under our gas phase conditions. More experiments are ongoing in our group to find out the CID energy required to fragment a covalent bond in ions of similar structure to the clusters we studied herein.
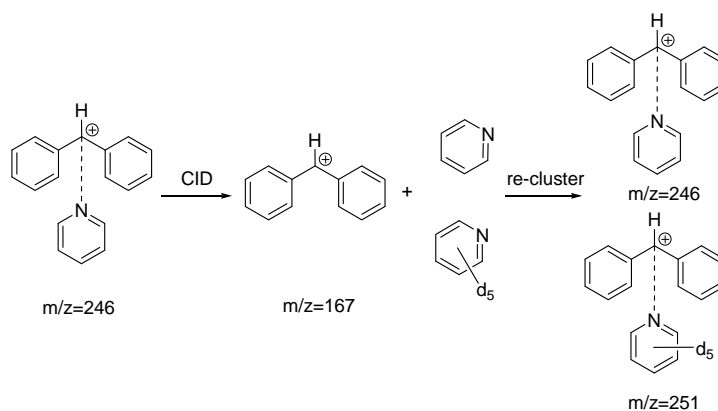
Scheme 5.5. CID fragmentation of the cluster between diphenylmethylium and pyridine
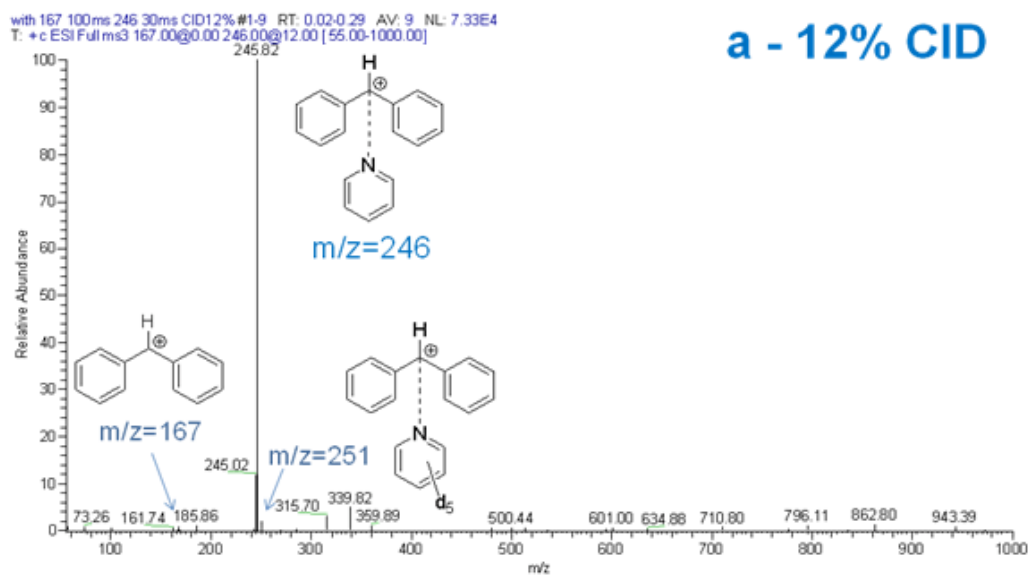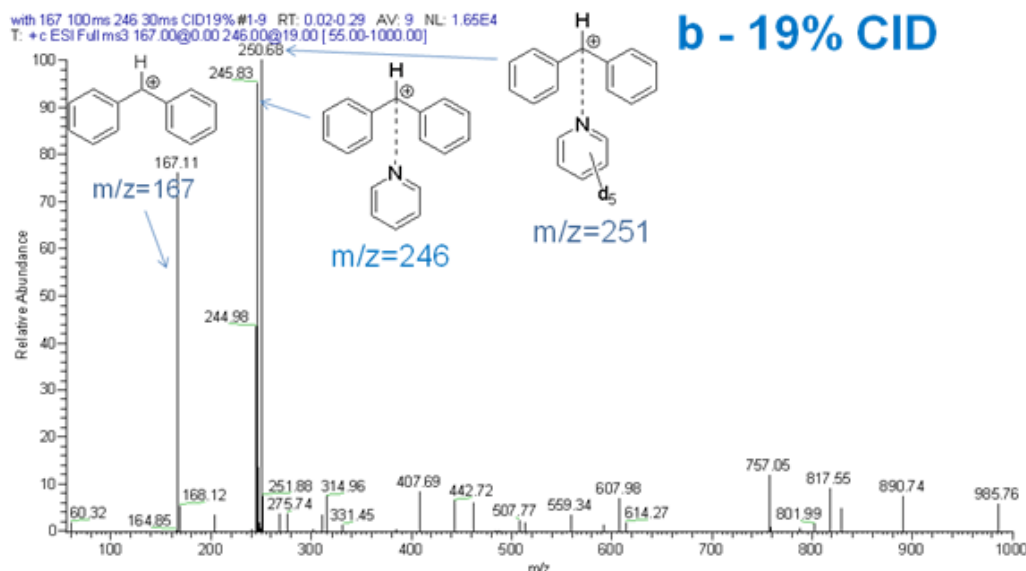
Figure 5.3. Mass Spectrum for the CID fragmentation of the cluster at m/z=246. **a** − 12%CID; **b** − 19% CID.

5.4 Conclusions

The structure of the gas phase cluster formed between diphenylmethylium cation and pyridine is studied by using several physical organic methods. Based on the charge change of the reactions, Hammett plot is used to probe the mechanism of the ion-molecule reaction. Comparison between calculated and experimental Hammett plot indicates that the cluster might be a proton-bound dimer. Kinetic isotope effect (KIE) is observed when the hydrogen on the methylium carbon is deuterated. The KIE is less than 1, which supports the covalent bond feature of the cluster. d_5-Pyridine exchange reactions show that the pyridine in the cluster cannot be easily exchanged (at least within the timescale of our experiments), which indicates that the cluster might be covalently bonded. In addition, CID of the cluster was studied and shows that the cluster can be fragmented at around 12% energy level.

Based on the methods that are described above, the nature of the cluster is still not conclusive without further experimental data being collected. More experiments are ongoing in our group to lend support to resolve this issue. Our experiments and discussion herein are potentially helpful to better understand the structure of gas phase clusters and facilitate the proposed nucleophilicity and electrophilicity measurements in the gas phase.

Chapter 6 Collision Induced Dissociation of NanoRNAs in the Gas Phase

6.1 Introduction

Transcription, also known as RNA synthesis, is the initial step of gene expression.[64] During transcription, genetic information stored in DNA is transferred into a complementary RNA strand (mRNA), which carries the genes throughout the following expression procedures. The transcriptions in prokaryotes and eukaryotes, although different in many aspects, both follow complex mechanisms and are regulated by many factors.

The first step of transcription is referred to as pre-initiation in which many functional transcription factors bind to promoter region of DNA to form the pre-initiation complex. Then, with the presence of these transcription factors, the RNA polymerase binds to the promoter to initiate the synthesis of mRNA which completes during the following elongation and termination steps. When the RNA polymerase reaches the first gene, short RNA transcripts with 2-15 nucleobases (nanoRNAs) are sometimes synthesized and released. This "abortive initiation" process, which competes with the formation of full-length transcripts, is believed to play important functional roles in regulating transcription, even gene expression.[65]

Recently, our collaborator Nickels and coworkers reported the first direct detection of abortive transcripts *in vivo* by utilizing hybridization-based detection of short RNA nucleotides.[66] Their work further supported the possible functional roles played by these

short abortive nucleotides. For example, it is indicated by many *in vitro* experiments that small RNAs (2-5nt) can prime the transcription initiation step in both eukaryotic and prokaryotic cells. However, little is known about the functions of the abortive nucleotides *in vivo* due to the lack of information about their identities. Thus, developing a novel method to analyze these nanoRNAs (2-15 nt) is of great significance in understanding abortive transcription and its biological functions.

Mass spectrometry has been widely used in characterization of oligonucleotides.[67,68] The development of ionization techniques, especially ESI and MALDI, facilitated the identification of short nucleotides by their mass-to-charge ratio. Tandem mass spectrometry (MS/MS) serves as a good method of sequencing short nucleotides. In this project, we used a quadrupole ion trap mass spectrometer with an ESI probe to analyze simple short nucleotides. Signals in both positive and negative modes were compared and fragmentation patterns of different small RNAs were also investigated. Since the nanoRNAs exist at very low concentrations in real cells, we also optimized the lowest detection limit of triphosphate dinucleotides. Our method under development is potentially useful in characterizing nanoRNAs *in vivo* and understanding their biological functions.

6.2 Experiments

Small RNA samples are from our collaborator (either purchased or synthesized biologically) (Figure 6-1). All equipment used to handle these samples are RNAse free. All samples are dissolved in RNAse free water and stored at -20 °C. 40 mM Ammonium acetate is used as buffer in order to keep the pH of solutionFat constant value.

Ammonium cation also prevents metal cations (K$^+$, Na$^+$) from clustering with the samples and diluting the signals. 20% MeOH (V/V) is also added to help the ESI process.
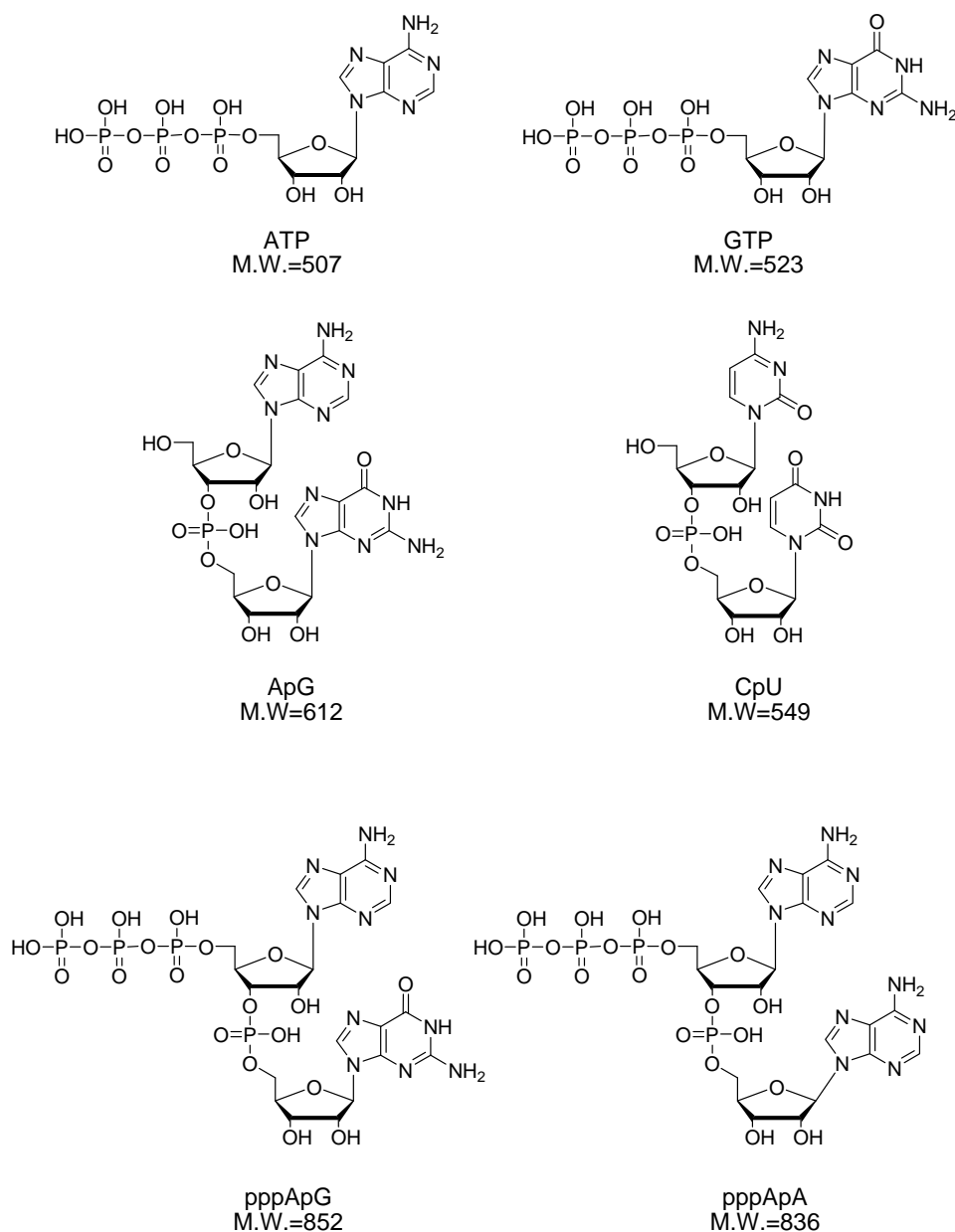
Figure 6.1. Structures of NanoRNAs studied in this chapter

Two quadrupole ion trap mass spectrometers (Thermo Finnigan LCQ Duo and LCQ Deca) with ESI probe were used to analyze the small RNAs. The small RNAs are

analyzed in both positive ion mode and negative ion mode and dissociation patterns are obtained by applying collision induced dissociation (CID).

To find out the lowest detection limit of triphosphate dinucleotide samples, a 580 μM stock solution of pppApG is prepared and diluted into different concentrations. Optimization of signal of pppApG in positive mode is conducted with a 0.5 μM solution, and the optimized conditions are used for the detection at lower concentrations.
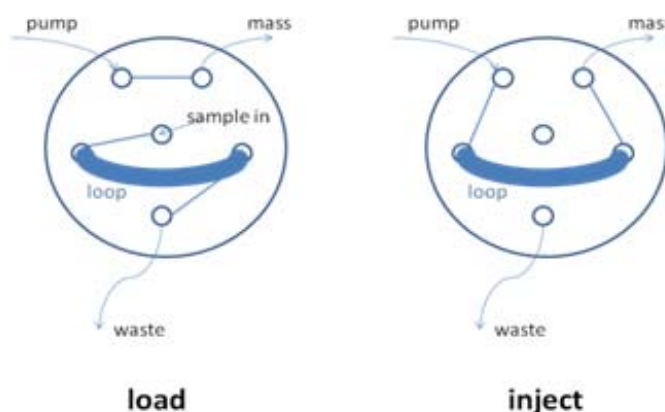
Figure 6.2. Loop injection mode

Two injection modes are used to compare their capability in detecting small RNAs at low concentrations. In the first mode, sample solution is injected by direct infusion to the ESI prove via a 500 μL syringe. The syringe is driven by an external pump at an adjustable rate. In the second injection mode, loop injection, sample solution is first loaded into a 10 μL metal loop on a conversion valve (Figure 6.2). As the flow route is changed (Figure 6.2, load to inject), the eluent can flow through the loop and bring the sample into the ESI probe.

6.3 Results and Discussion

6.3.1 Signal intensities in positive and negative modes

Analytes usually have different signal intensities in positive and negative ion modes. To start our analysis, we compare signal intensities of mononucleotides (ATP, GTP) and dinucleotides (ApG, CpU, pppApG, pppApA) in positive and negative modes. All RNA samples are ionized mainly into ions with only one charge (Table 6.1). Sometimes, very tiny amount of ions with two charges are observed. Higher charge states are not observed.

Table 6.1. Intensities of small RNAs in different ion modes

Sample	Ion mode	Charge number	Ion intensity/10^5
ATP	negative	1	2.9
	positive	1	5.8
GTP	negative	1	2.2
	positive	1	5.1
ApG	negative	1	2.0
	positive	1 and 2	8.0
CpU	negative	1	3.1
	positive	1	2.7
pppApG	negative	1 and 2	0.2
	positive	1	17
pppApA	negative	1 and 2	0.2
	positive	1	33

For ATP, GTP, ApG and CpU, ion intensities in the two modes are generally at the same level, with positive intensity being slightly higher than negative. Interestingly, for

triphosphate dinucleotides (pppApG, pppApA), positive ion intensity is much higher than negative intensity (by 2 orders of magnitude). Positive mode turned out to be better than negative mode for analysis of small RNA samples.

6.3.2 Fragmentation patterns of different nanoRNAs

By using CID, we compared fragmentation patterns of small RNA analogues in both positive mode and negative mode. Generally, similar RNA molecules follow the same fragmentation pattern.

The simplest analogues we studied were ATP and GTP. In negative ion mode (Figure 6.3, 6.4), both deprotonated ATP and GTP tends to lose phosphoric acid (98) as the major pathway. Also, loss of nucleobase directly or after loss of phosphoric acid was observed as a minor pathway. In positive mode (Figure 6.5, 6.6), loss of H_3PO_4 is one major pathway. However, loss of neutral base was not observed. Instead, loss of P160 (Figure 6.5, 6.6) and dimer formed by nucleobase and phosphoric acid were observed.
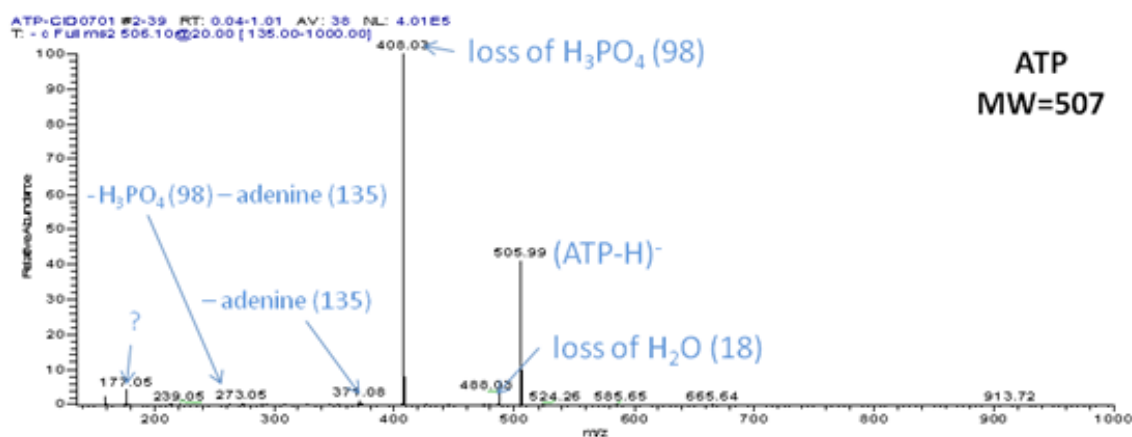
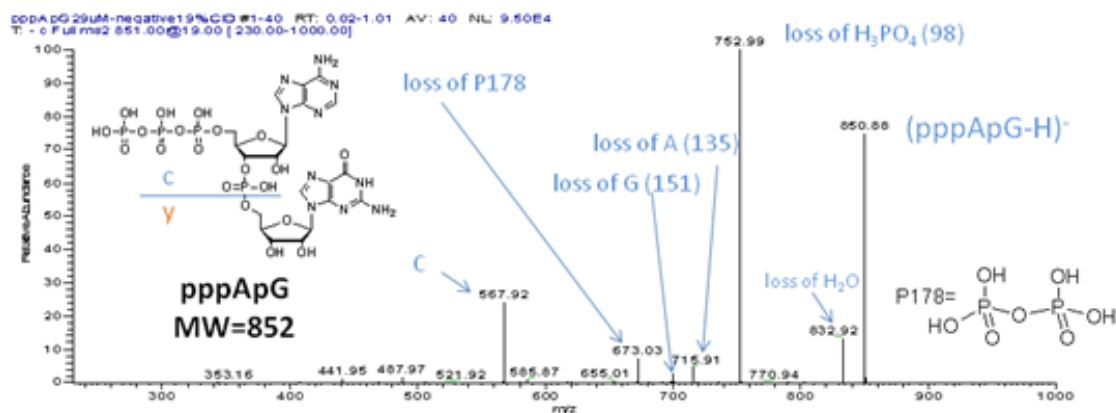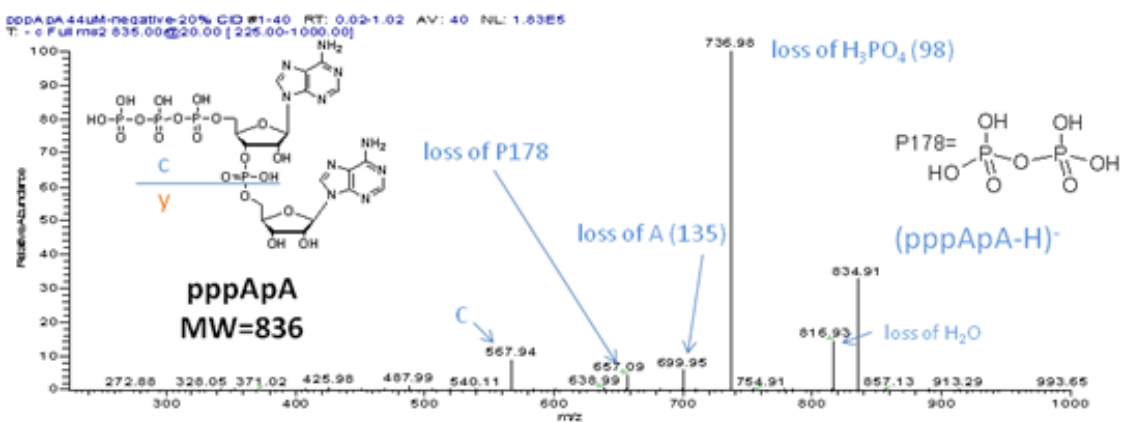**Figure 6.3.** Fragmentation of ATP in negative mode
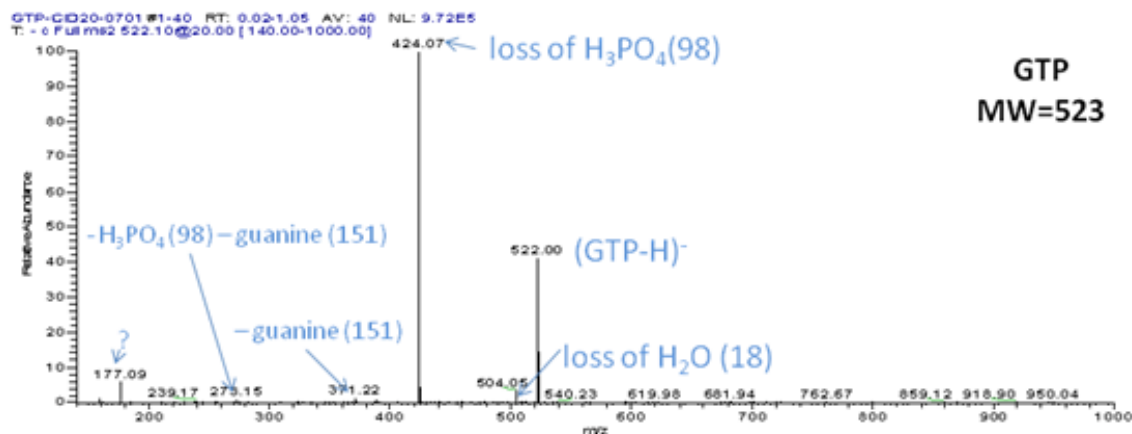
Figure 6.4. Fragmentation of GTP in negative mode
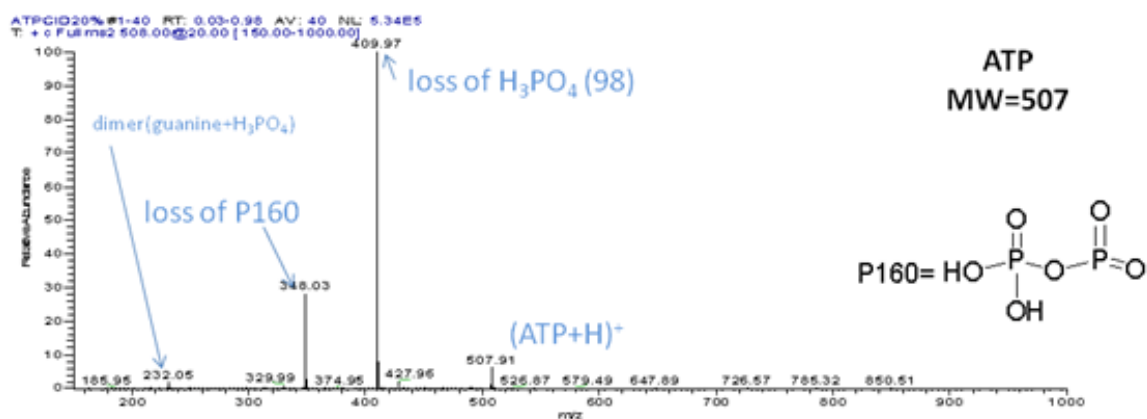
Figure 6.5. Fragmentation of ATP in positive mode
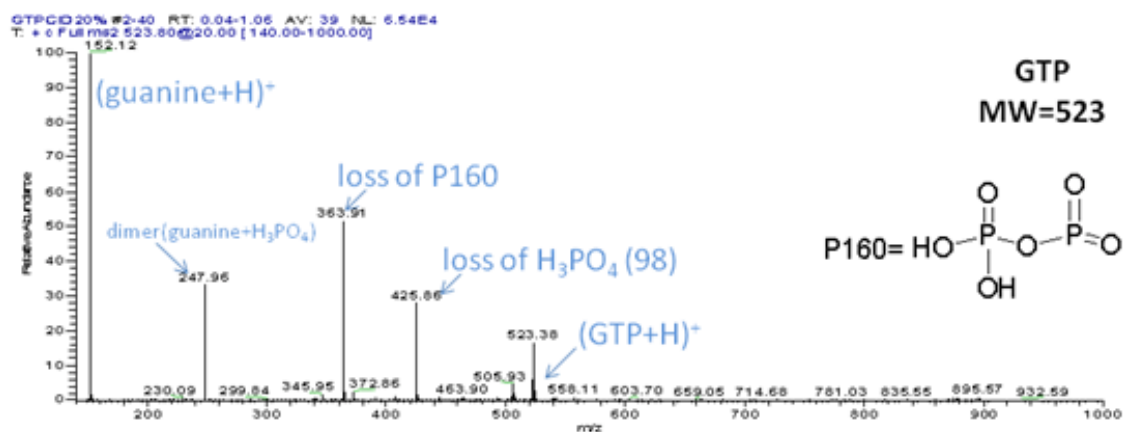
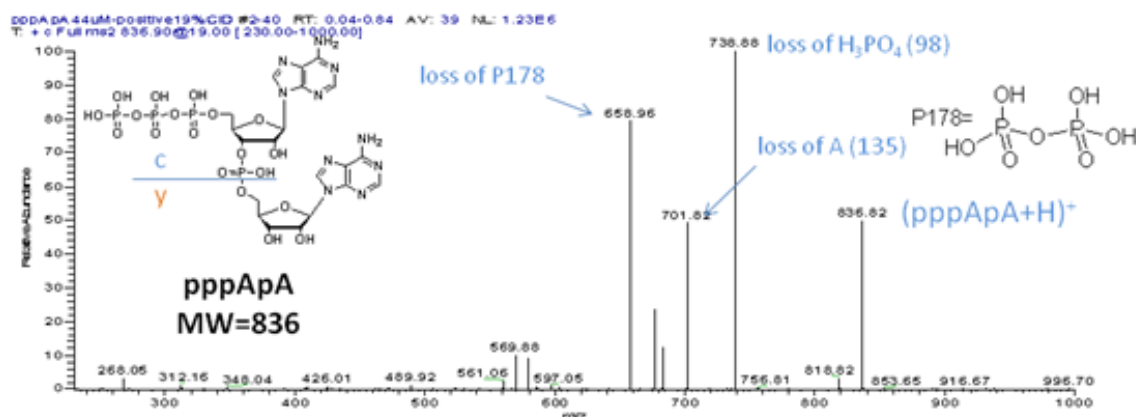**Figure 6.6.** Fragmentation of GTP in positive mode

Without a triphosphate group in their structures, dinucleotide ApG and CpU fragment mainly via the loss of one nucleobase. In negative mode (Figure 6.7, 6.8), only nucleobases on 5' side is fragmented. This selective loss of nucleobase can be used to differentiate dinucleotides which have the same composition but different sequences, such as ApG and GpA. However, in positive mode (Figure 6.9, 6.10), ApG loses its 3'-base (guanine) while CpU still loses the base on the 5' side (cytosine) as in negative mode.
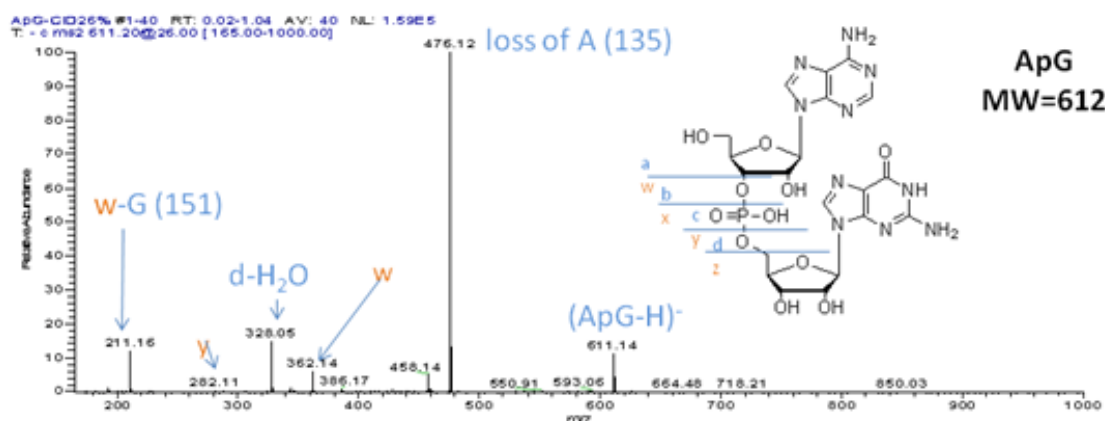
Figure 6.7. Fragmentation of ApG in negative mode
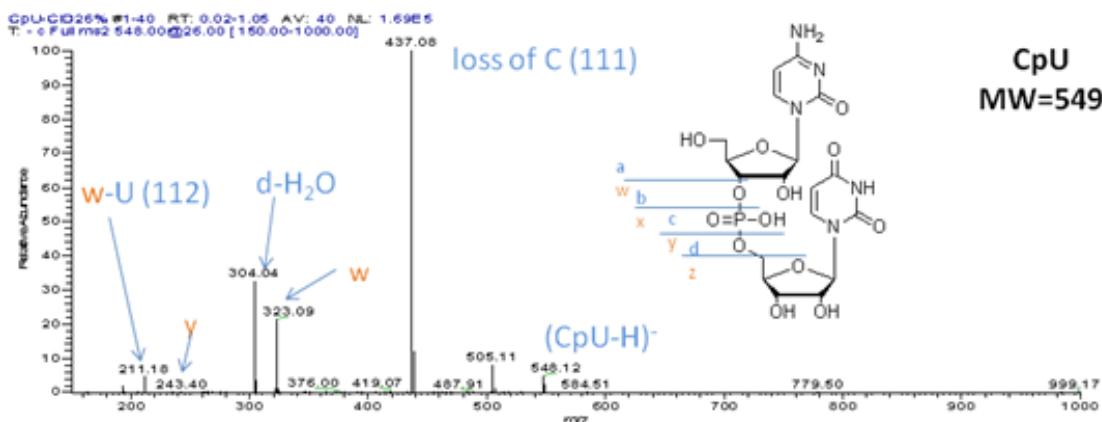
Figure 6.8. Fragmentation of CpU in negative mode
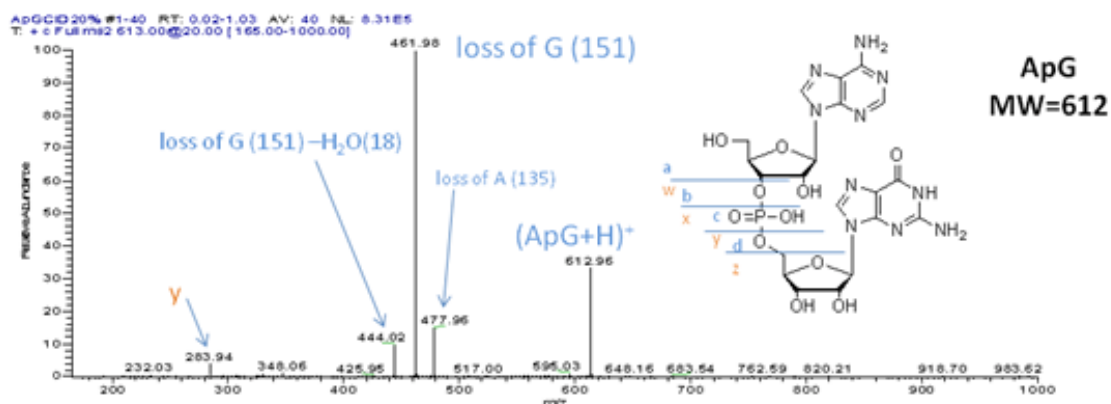
Figure 6.9. Fragmentation of ApG in positive mode
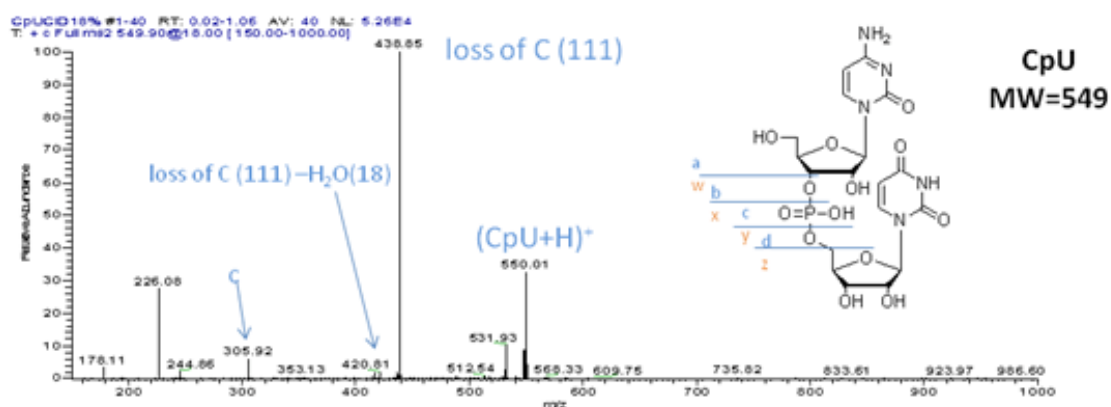
Figure 6.10. Fragmentation of CpU in positive mode

Triphosphate dinucleotides pppApG and pppApA gave the most complicated fragmentation patterns (Figure 6.11, 6.12, 6.13, 6.14). In both negative and positive modes, major pathways of both pppApG and pppApA include: loss of water, loss of phosphoric acid, loss of P178 (Figure 6.11). In negative mode (Figure 6.11, 6.12), loss of 5' and 3' base take place to the same extent. Both pppApG and pppApA are fragmented into their corresponding c ion (Figure 6.11). Since c ion contains the 5'-base, it is

possible to use it as a characteristic ion to differentiate triphosphate dinucleotides which consist of the same bases but in different sequences, such as pppApG and pppGpA. In positive mode (Figure 6.13, 6.14), loss of 3' base happens more readily than loss of 5' base. Thus, loss of 3'-base can be used as a characteristic peak in positive mode and it has higher ion intensity than the c ion in negative mode.

Figure 6.11. Fragmentation of pppApG in negative mode

Figure 6.12. Fragmentation of pppApA in negative mode
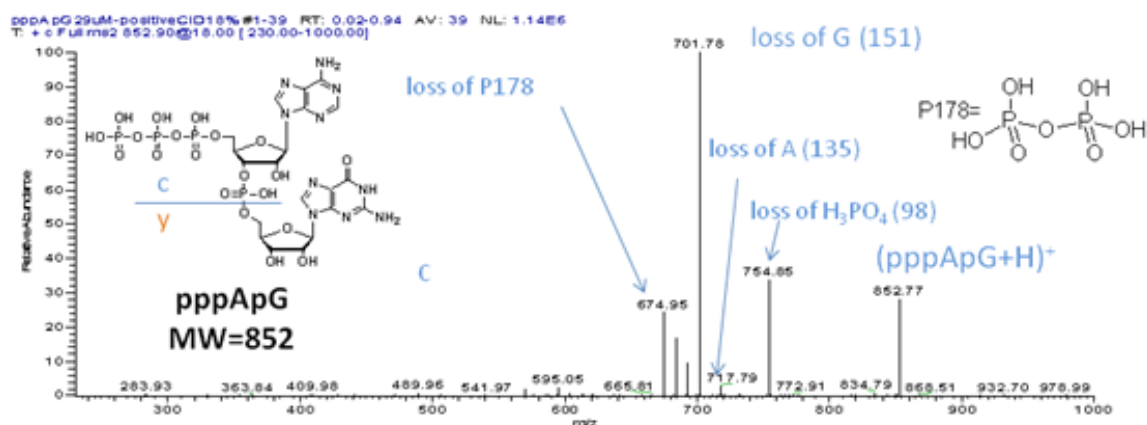
Figure 6.13. Fragmentation of pppApG in positive mode

Figure 6.14. Fragmentation of pppApA in positive mode

6.3.3 Lowest detection limit of pppApG

Since nanoRNAs are at low concentrations in real cells or cell lysates, it is important to optimize the detection conditions and lower the detection limits of these small RNAs. A 0.5μM solution of pppApG is used to optimize the instrument parameters for higher signal intensity. The optimized parameters are listed in Table 6.2.

Table 6.2. Optimized LCQ parameters for pppApG

Capillary temp/°C	Sheath gas flow rate	Spray voltage/kV	Sample flow rate μL/min
250	70	4.5	25

Under the optimized conditions, pppApG solution was diluted into lower concentrations and the molecular ion intensities at different concentrations were recorded (Table 6.3). The lowest detection limit is found to be 0.01μM. No molecular ion signal was observed for the 0.001μM solution.

Table 6.3. Signal intensities of pppApG at different concentrations

Concentration/μM	Signal intensity
0.1	9.32E3
0.01	1.75E3
0.001	No signal

Since the direct injection mode requires a relatively large amount of material (pppApG), we considered the loop injection mode which requires only 10μL solution for each load. Single ion monitoring (SIM) at m/z=853 was used to monitor the ion intensity at different time after the injection valve was moved to the inject position (Figure 6.15). pppApG cannot be detected when concentration is lower than 0.5 μM.
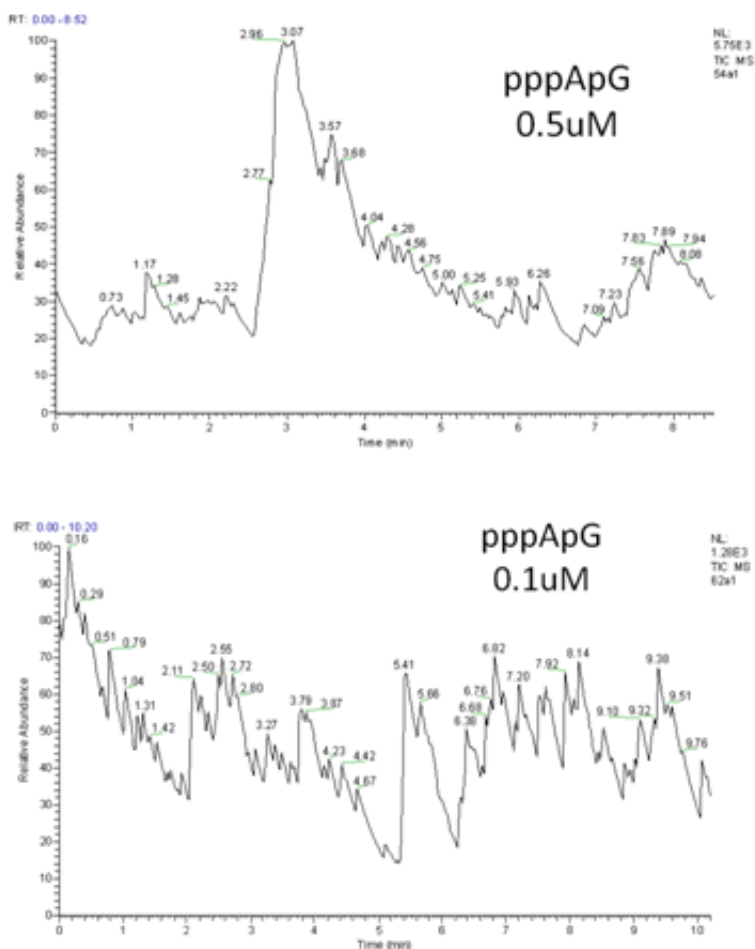
Figure 6.15. Lowest detection limit for pppApG is 0.5μM by loop injection

6.4 Conclusions

Several nanoRNAs have been studied by using mass spectrometry (ESI-MS). Mass parameters for highest signal intensity have been optimized. Intensities in positive ion mode and negative ion mode have been compared. The results show that positive mode give higher ion intensity of triphosphate dinucleotide ions. Lowest detection limit under different injection modes is also studied and compared for pppApG. In addition, CID in both positive and negative modes have been studied. The characteristic CID fragments of the dinucleotides could potentially be used for the sequencing of the nanoRNAs. LC-MS

method for the separation and quantification of nanoRNAs is currently being developed in our lab to facilitate the detection of nanoRNAs in cell lysates.

References

(1) Watson, J. D. **1968**, The Double Helix: A Personal Account of the Discovery of the Structure of DNA; Norton Critical Editions.

(2) Stone M. P., H. H., Brown K. L., Shanmugam G. *Chemistry & Biodiversity* **2011**, *8*, 1571.

(3) *DNA Damage and Repair, Vol 1: DNA Repair in Procaryotes and Lower Eucaryotes*; Humana Press, Inc.: Totowa, NJ, 1998.

(4) Berti, P. J.; McCann, J. A. B. *Chem. Rev.* **2006**, *106*, 506.

(5) Milanowska K., R. K., Bujnicki J. M. *Mol. Biol. Internat.* **2011**, 1.

(6) Friedberg, E. C.; Walker, G. C.; Siede, W.; Wood, R. D.; Schultz, R. A.; Ellenberger, T. *DNA Repair and Mutagenesis: 2nd ed.*; ASM Press: Washington, DC, 2006.

(7) Stivers, J. T.; Jiang, Y. L. *Chem. Rev.* **2003**, *103*, 2729.

(8) *DNA Damage and Repair, Vol. 1: DNA Repair in Procaryotes and Lower Eucaryotes*; Nickoloff, J. A.; Hoekstra, M. F., Eds.; Humana Press, Inc.: Totowa, NJ, 1998.

(9) Liu, M.; Xu, M.; Lee, J. K. *J. Org. Chem.* **2008**, *73*, 5907.

(10) Sun, X.; Lee, J. K. *J. Org. Chem.* **2007**, *72*, 6548.

(11) Lee, J. K. *International Journal of Mass Spectrometry* **2005**, *240*, 261.

(12) Sharma, S.; Lee, J. K. *J. Org. Chem.* **2002**, *67*, 8360.

(13) Bennett, M. T.; Rodgers, M. T.; Hebert, A. S.; Ruslander, L. E.; Eisele, L.; Drohat, A. C. *J. Am. Chem. Soc.* **2006**, *128*, 12510.

(14) Kurinovich, M. A.; Lee, J. K. *J. Am. Chem. Soc.* **2000**, *122*, 6258.

(15) Zhachkina, A.; Liu, M.; Sun, X.; Amegayibor, S.; Lee, J. K. *J. Org. Chem.* **2009**, *74*, 7429.

(16) Sun X., L. J. K. *J. Org. Chem.* **2010**, *75*, 1848.

(17) Kurinovich, M. A.; Lee, J. K. *Journal of the American Society for Mass Spectrometry* **2002**, *13*, 985.

(18) Kurinovich, M. A.; Phillips, L. M.; Sharma, S.; Lee, J. K. *Chemical Communications* **2002**, 2354.

(19) Sharma, S.; Lee, J. K. *J. Org. Chem.* **2004**, *69*, 7018.

(20) Liu, M.; Li, T.; Amegayibor, F. S.; Cardoso, D. S.; Fu, Y.; Lee, J. K. *J. Org. Chem.* **2008**, *73*, 9283.

(21) Zhachkina, A.; Lee, J. K. *J. Am. Chem. Soc.* **2009**, *131*, 18376.

(22) Tron, G. C. *Medicinal Research Reviews* **2008**, *28(2)*, 278.

(23) Kolb H. C., F. M. G., Sharpless K. B. *Angew. Chem., Int. Ed.* **2001**, *40*, 2004.

(24) Ye C., G. L., Winter R. W., Syvret R. G., Twamly B., Shreeve J. M. *Org. Lett.* **2007**, *9(19)*, 3841.

(25) Zink, J. *Angew. Chem., Int. Ed.* **2008**, *47*, 2222.

(26) Sivakumar K., X. F., Cash B. M., Long S., Barnhill H., Wang Q. *Org. Lett.* **2004**, *6(24)*, 4603.

(27) Camarasa, A. R. *Eur. J. Med. Chem.* **1980**, *15*, 105.

(28) Purnell L. G., S. J. C., Hodgson D. J. *J. Am. Chem. Soc.* **1975**, *9*, 2376.

(29) Reinaud, O. *Org. Lett.* **2007**, *9(24)*, 4987.

(30) Karthikeyan T., S. S. *Tetrahedron Lett.* **2009**, *50*, 5834.

(31) Duan, H.; Sengupta, S.; Petersen, J. L.; Akhmedov, N. G.; Shi, X. *Journal of the American Chemical Society* **2009**, *131*, 12100.

(32) Tomas, F.; Abboud, J. L. M.; Laynez, J.; Notario, R.; Santos, L.; Nilsson, S. O.; Catalan, J.; Claramunt, R. M.; Elguero, J. *J. Am. Chem. Soc.* **1989**, *111*, 7348.

(33) Abboud, J.-Luis M.; Foces-Foces, C.; Notario, R.; Trifonov, Rostislav E.; Volovodenko, Anna P.; Ostrovskii, Vladimir A.; Alkorta, I.; Elguero, J. *European Journal of Organic Chemistry* **2001**, *2001*, 3013.

(34) Ichino, T.; Andrews, D. H.; Rathbone, G. J.; Misaizu, F.; Calvi, R. M. D.; Wren, S. W.; Kato, S.; Bierbaum, V. M.; Lineberger, W. C. *J. Phys. Chem. B* **2008**, *112*, 545.

(35) Ichino, T.; Kato, S.; Wren, S. W.; Bierbaum, V. M.; Lineberger, W. C. *J. Phys. Chem. A* **2008**, *112*, 9723.

(36) Anslyn, E. V.; Dougherty, D. A. *Modern Physical Organic Chemistry*; University Science Books, 2006.

(37) Tomioka, H.; Mizutani, K.; Matsumoto, K.; Hirai, K. *J. Org. Chem.* **1993**, *58*, 7128.

(38) Hirai, K.; Komatsu, K.; Tomioka, H. *Chem. Lett.* **1994**, *23*, 503.

(39) Robinson, G. C. *Tetrahedron Lett.* **1965**, *6*, 1749.

(40) Sander, W.; Bucher, G.; Wierlacher, S. *Chem. Rev.* **1993**, *93*, 1583.

(41) Igau, A.; Grutzmacher, H.; Baceiredo, A.; Bertrand, G. *J. Am. Chem. Soc.* **1988**, *110*, 6463.

(42) Arduengo, A. J. I.; Harlow, R. L.; Kline, M. *J. Am. Chem. Soc.* **1991**, *113*, 361.

(43) Enders, D.; Niemeier, O.; Henseler, A. *Chem. Rev.* **2007**, *107*, 5606.

(44) Struble, J. R.; Kaeobamrung, J.; Bode, J. W. *Org. Lett.* **2008**, *10*, 957.

(45) Trnka, T. M.; Grubbs, R. H. *Acc. Chem. Res.* **2001**, *34*, 18.

(46) Marion, N.; Nolan, S. P. *Acc. Chem. Res.* **2008**, *41*, 1440.

(47) Tekavec, T. N.; Louie, J. *Top. Organomet. Chem.* **2007**, *21*, 159.

(48) Lord, R. L.; Wang, H.; Vieweger, M.; Baik, M.-H. *J. Organomet. Chem.* **2006**, *691*, 5505.

(49) Dröge, T.; Glorius, F. *Angew. Chem., Int. Ed.* **2010**, *49*, 6940.

(50) Herrmann, W. A. *Angew. Chem., Int. Ed.* **2002**, *41*, 1290.

(51) Dixon, D. A.; Arduengo, A. J. I.; Dobbs, K. D.; Khasnis, D. V. *Tetrahedron Lett.* **1995**, *36*, 645.

(52) Hudnall, T. W.; Bielawski, C. W. *J. Am. Chem. Soc.* **2009**, *131*, 16039.

(53) Hudnall, T. W.; Moerdyk, J. P.; Bielawski, C. W. *Chem. Commun.* **2010**, *46*, 4288.

(54) Ingold, C. K. *Chem. Rev.* **1934**, *1934*, 225.

(55) Ingold, C. K. *Recl. Trav. Chim. Pays-Bas* **1929**, *48*, 797.

(56) L. G. Wade, J. *Organic Chemistry*; Pearson Prentice Hall: Upper Saddle River, NJ 07458, 2010.

(57) Ingold, C. K. *J. Chem. Soc.* **1933**, 1120.

(58) Swain, C. G.; Scott, C. B. *J. Am. Chem. Soc.* **1953**, *75*, 141.

(59) Edwards, J. O. *J. Am. Chem. Soc.* **1954**, *76*, 1540.

(60) Kane-Maguire, L. A. P.; Honig, E. D.; Sweigard, D. A. *Chem. Rev.* **1984**, *84*, 525.

(61) Mayr, H.; Schneider, R.; grabis, U. *Angew. Chem., Int. Ed. Engl.* **1986**, *25*, 1017.

(62) Mayr, H.; Patz, M. *Angew. Chem., Int. Ed. Engl.* **1994**, *33*, 938.

(63) Denekamp, C.; Sandlers, Y. *Angew Chem Int Ed* **2006**, *45*, 2093.

(64) Miller, A. D.; Tanner, J. *Essentials of Chemical Biology, Structure and Dynamics of Biological Macromolecules*; John Wiley and Sons: New York, 2008.

(65) Murakami, K. S.; Darst, S. A. *Curr. Opin. Struct. Biol.* **2003**, *13*, 31.

(66) Goldman, S. R.; Ebright, R. H.; Nickels, B. E. *Science* **2009**, *324*, 927.

(67) Fitzgerald, M. C.; Smith, L. M. *Annu. Rev. Biophys. Biomol. Struct.* **1995**, *24*, 117.

(68) Lin, Z. P.; Li, W.; Dai, G. *Journal of Pharmaceutical and Biomedical Analysis* **2007**, 330.

(69) Amster, I. J. *J. Mass Spectrom* **1996**, *31*, 1325.

(70) Marshall, A. G.; Grosshans, P. B. *Anal. Chem.* **1991**, *63*, 215.

(71) Yamashita, M.; Fenn, J. B. *Phys. Chem.* **1988**, *88*, 4451.

(72) Yamashita, M.; Fenn, J. B. *Phys. Chem.* **1988**, *88*, 4671.

(73) Kebarle, P.; Tang, L. *Anal. Chem.* **1993**, *65*, 972A.

(74) Kebarle, P.; Tang, L. *Analytical Chemistry* **1993**, *65*, 972A.

(75) Chen, H.; Justes, D. R.; Cooks, R. G. *Org. Lett.* **2005**, *7*, 3949.

(76) Lee, M.-T.; Hu, C.-H. *Organometallics* **2004**, *23*, 976.

(77) Herrmann, W. A.; Kocher, C. *Angew. Chem., Int. Ed. Engl.* **1997**, *36*, 2162.

(78) Paul, W.; Steinwedel, H. S. *Naturforsch* **1953**, *8a*, 448.

(79) Finnigan, R. E. *Anal. Chem.* **1994**, *66*, 969A.

(80) Ferguson, R. E.; McKulloh, K. E.; Rosenstock, H. M. *J. Chem. Phys.* **1965**, *42*, 100.

(81) Kienitz, H. *Massenspektrometrie*; Verlag Chemie: Weinheim, 1968.

(82) Douglas, D. J.; Frank, A. J.; Mao, D. *Mass Spectrometry Reviews* **2005**, *24*, 1.

(83) Todd, J. F. J. *Mass Spectrometry Rev.* **1991**, *10*, 3.

(84) Stafford, G. C.; Kelley, P. E.; Syka, J. E.; Reynolds, W. W.; Todd, J. F. J. *International Journal of Mass Spectrometry Ion Processes* **1984**, *60*, 85.

(85) Cooks, R. G.; Kruger, T. L. *J. Am. Chem. Soc.* **1977**, *99*, 1279.

(86) McLuckey, S. A.; Cameron, D.; Cooks, R. G. *J. Am. Chem. Soc.* **1981**, *103*, 1313.

(87) Green-Church, K. B.; Limbach, P. A. *J. Am. Soc. Mass Spectrom* **2000**, *11*, 24.

(88) Ervin, K. M. *Chem. Rev.* **2001**, *101*, 391.

(89) Gronert, S.; Feng, W. Y.; Chew, F.; Wu, W. *Int. J. Mass Spectrom. Ion Proc.* **2000**, *196*, 251.

(90) Frisch, M. J.; et al. Gaussian 03; Gaussian, Inc., Wallingford, CT 2004.

(91) Frisch, M. J.; et al. Gaussian 09; Gaussian, Inc., Wallingford, CT 2009.

(92) Lee, C.; Yang, W.; Parr, R. G. *Phys. Rev. B* **1988**, *37*, 785.

(93) Kohn, W.; Becke, A. D.; Parr, R. G. *J. Phys. Chem.* **1996**, *100*, 12974.

(94) Becke, A. D. *J. Chem. Phys.* **1993**, *98*, 5648.

(95) Becke, A. D. *J. Chem. Phys.* **1993**, *98*, 1372.

(96) Stephens, P. J.; Devlin, F. J.; Chabalowski, C. F.; Frisch, M. J. *J. Phys. Chem.* **1994**, *98*, 11623.

(97) Zhao, Y.; Truhlar, D. G. *Theor. Chem. Acc.* **2008**, *120*, 215.

(98) Zhao, Y.; Truhlar, D. G. *Acc. Chem. Res.* **2008**, *41*, 157.

(99) Head-Gordon, M.; Pople, J. A.; Frisch, M. J. *J. Chem. Phys. Lett.* **1988**, *1988*, 503.

(100)   Saebo, S.; Almlof, J. *J. Chem. Phys. Lett.* **1989**, *154*, 83.

(101)   Moller, C.; Plesset, M. S. *Phys. Rev.* **1934**, *46*, 618.

(102)   Frisch, M. J.; Head-Gordon, M.; Pople, J. A. *Chem Phys. Lett.* **1990**, *166*, 275.

(103)   Frisch, M. J.; Head-Gordon, M.; Pople, J. A. *Chem. Phys. Lett.* **1990**, *166*, 281.

(104)   Head-Gordon, M.; Head-Gordon, T. *Chem Phys. Lett.* **1994**, *220*, 122.

(105)   Montgomery, J. A., Jr.; Frisch, M. J.; Ochterski, J. W.; Petersson, G. A. *J. Chem. Phys.* **1999**, *110*, 2822.

(106)   Montgomery, J. A., Jr.; Frisch, M. J.; Ochterski, J. W.; Petersson, G. A. *J. Chem. Phys.* **2000**, *112*, 6532.

(107)   Barone, V.; Cossi, M. *J. Phys. Chem. A* **1998**, *102*, 1995.

(108)   Cossi, M.; Rega, N.; Scalmani, G.; Barone, V. *J. Comput. Chem.* **2003**, *24*, 669.

(109)   Takano, Y.; Houk, K. N. *J. Chem. Theory Comput.* **2005**, *1*, 70.

(110)   Radzicka, A.; Wolfenden, R. *Science* **1995**, *267*, 90.

(111)   Lee, J. K.; Houk, K. N. *Science* **1997**, *276*, 942.

(112)   Kurinovich, M. A.; Lee, J. K. *J. Am. Chem. Soc.* **2000**, *122*, 6258.

(113)   Sun, X.; Lee, J. K. *J. Org. Chem.* **2007**, *72*, 6548.

(114)   Sponer, J.; Leszczynski, J. *Structural Chemistry* **1995**, *6*, 4.

(115)   NIST Chemistry WebBook, NIST Standard Reference Database Number 69; retrieved in 2011. Linstrom, P. J.; Mallard, W. G., Eds.; National Institute of Standards and Technology: Gaithersburg, MD 20899, http://webbook.nist.gov.

(116)   Callahan, M. P.; Crews, B.; Abo-Riziq, A.; Grace, L.; de Vries, M. S.; Gengeliczki, Z.; Holmes, T. M.; Hill, G. A. *Phys. Chem. Chem. Phys.* **2007**, *9*, 4587.

(117)   Wheeler, S. E.; Moran, A.; Pieniazek, S. N.; Houk, K. N. *J. Phys. Chem. A* **2009**, *113*, 10376.

(118)   Crenshaw, J. D.; Phillipot, S. R.; Iordanova, N.; Sinnott, S. B. *Chem. Phys. Lett.* **2011**, *510*, 197.

(119)   Riffet, V.; Frison, G.; Bouchoux, G. *Phys. Chem. Chem. Phys.* **2011**, *13*, 18561.

(120)   Rogstad, K. N.; Jang, Y. H.; Sowers, L. C.; Goddard, W. A. *Chem. Res.Toxicol.* **2003**, *16*, 1455.

(121)   Taylor, H. F. W. *J. Chem. Soc.* **1948**, 765.

(122)   Albert, A.; Brown, D. J. *J. Chem. Soc.* **1954**, 2060.

(123)   Duan, H.; Sengupta, S.; Petersen, J. L.; Shi, X. *Organometallics* **2009**, *28*, 2352.

(124)   Duan, H.; Yan, W.; Sengupta, S.; Shi, X. *Bioorg. Med. Chem. Lett.* **2009**, *19*, 3899.

(125)   Wang, D.; Ye, X.; Shi, X. *Org. Lett.* **2010**, *12*, 2088.

(126)   Wang, D.; Zhang, Y.; Harris, A.; Gautam, L. N. S.; Chen, Y.; Shi, X. *Adv. Synth. Catal.* **2011**, *353*, 2584.

(127)   Wang, D.; Gautam, L. N. S.; Bollinger, C.; Harris, A.; Li, M.; Shi, X. *Org. Lett.* **2011**, *13*, 2618.

(128)   Wang, D.; Zhang, Y.; Cai, R.; Shi, X. *Beilstein J. Org. Chem.* **2011**, *7*, 1014.

(129)   Wang, Q.; Aparaj, S.; Akhmedov, N. G.; Petersen, J. L.; Shi, X. *Org. Lett.* **2012**, *14*, 1334.

(130)   Öfele, K.; Herrmann, W. A.; Mihalios, D.; Elison, M.; Herdtweck, E.; Scherer, W.; Mink, J. *J. Organomet. Chem.* **1993**, *459*, 177.

(131)   Rodgers, M. T.; Campbell, S.; Marzluff, E. M.; Beauchamp, J. L. *International Journal of Mass Spectrometry and Ion Processes* **1995**, *148*, 1.

(132)   Eyet, N.; Villano, S. M.; Bierbaum, V. M. *Int. J. Mass Spectrom.* **2009**, *283*, 26.

(133)   Meljon, A.; Watson, G. L.; Wang, Y.; Shackleton, C. H. L.; Griffiths, W. J. *Biochemical Pharmacology* **2013**, *86*, 43.

(134)   Hashmi, A. S. K.; Lothschütz, C. *ChemCatChem* **2010**, *2*, 133.

(135)   César, V.; Lugan, N.; Lavigne, G. *Eur. J. Inorg. Chem.* **2010**, 361.

(136)   Hobbs, M. G.; Forster, T. D.; Borau-Garcia, J.; Knapp, C. J.; Tuononen, H. M.; Roesler, R. *New J. Chem.* **2010**, *34*, 1295.

(137)   Braun, M.; Frank, W.; Reiss, G. J.; Ganter, C. *Organometallics* **2010**, *29*, 4418.

(138)   Hudnall, T. W.; Tennyson, A. G.; Bielawski, C. W. *Organometallics* **2010**, *29*, 4569.

(139)   Moerdyk, J. P.; Bielawski, C. W. *Organometallics* **2011**, *30*, 2278.

(140)   Lee, Y.-G.; Moerdyk, J. P.; Bielawski, C. W. *J. Phys. Org. Chem.* **2012**, *25*, 1027.

(141)   Schaub, T.; Backes, M.; Radius, U. *Organometallics* **2006**, *25*, 4196.

(142)   Cole, M. L.; Junk, P. C.; Louis, L. M. *J. Chem. Soc., Dalton Trans.* **2002**, 3906.

(143)   Binobaid, A.; Iglesias, M.; Beetstra, D. J.; Kariuki, B.; Dervisi, A.; Fallis, I. A.; Cavell, K. J. *Dalton Trans.* **2009**, 7099.

(144)   Abdou, H. E.; Mohamed, A. A.; López-de-Luzuriaga, J. M.; Monge, M.; Fackler, J. P., Jr. *Inorg. Chem.* **2012**, *51*, 2010.

(145)   Liu, M.; Chen, M.; Zhang, S.; Yang, I.; Buckley, B.; Lee, J. K. *J. Phys. Org. Chem.* **2011**, *24*, 929.

(146)   Liu, M.; Yang, I.; Buckley, B.; Lee, J. K. *Org. Lett.* **2010**, *12*, 4764.

(147)   Kaljurand, I.; Koppel, I. A.; Kutt, A.; Room, E.-I.; Rodima, R.; Koppel, I.; Mishima, M.; Leito, I. *J. Phys. Chem. A* **2007**, *111*, 1245.

(148)   Hopkins, H. P., Jr.; Jahagirdar, D. V.; Moulik, P. S.; Aue, D. H.; Webb, H. M.; Davidson, W. R.; Pedley, M. D. *J. Am. Chem. Soc.* **1984**, *106*, 4341.

(149)   Jasinski, J. M.; Brauman, J. I. *J. Am. Chem. Soc.* **1980**, *102*, 2906.

(150)   Hudnall, T. W.; Moorhead, E. J.; Gusev, D. G.; Bielawski, C. W. *J. Org. Chem.* **2010**, *75*, 2763.

(151)   Brown, A. R.; Kuo, W.-H.; Jocobsen, E. N. *J. Am. Chem. Soc.* **2010**, *132*, 9286.

ACS Publications
High quality. High impact.

Title: Gas-Phase Studies of Purine 3-Methyladenine DNA Glycosylase II (AlkA) Substrates

Author: Anna Zhachkina Michelson, Mu Chen, Kai Wang, and Jeehiun K. Lee

Publication: Journal of the American Chemical Society

Publisher: American Chemical Society

Date: Jun 1, 2012

Copyright © 2012, American Chemical Society

Title: Reactivity of carbene•phosphine dimers: proton affinity revisited

Author: Min Liu,Mu Chen,Sisi Zhang,Ill Yang,Brian Buckley,Jeehiun K. Lee

Publication: Journal of Physical Organic Chemistry

Publisher: John Wiley and Sons

Date: Jul 18, 2011

Copyright © 2011 John Wiley & Sons, Ltd.

Logged in as:
Mu Chen

LOGOUT

Order Completed

Thank you very much for your order.

This is a License Agreement between Mu Chen ("You") and John Wiley and Sons ("John Wiley and Sons"). The license consists of your order details, the terms and conditions provided by John Wiley and Sons, and the payment terms and conditions.

Get the printable license.

License Number	3274320689950
License date	Nov 22, 2013
Licensed content publisher	John Wiley and Sons
Licensed content publication	Journal of Physical Organic Chemistry
Licensed content title	Reactivity of carbene•phosphine dimers: proton affinity revisited
Licensed copyright line	Copyright © 2011 John Wiley & Sons, Ltd.
Licensed content author	Min Liu,Mu Chen,Sisi Zhang,Ill Yang,Brian Buckley,Jeehiun K. Lee
Licensed content date	Jul 18, 2011
Start page	929
End page	936
Type of use	Dissertation/Thesis
Requestor type	Author of this Wiley article
Format	Print and electronic
Portion	Full article
Will you be translating?	No
Total	0.00 USD

ORDER MORE... | CLOSE WINDOW

This is a License Agreement between Mu Chen ("You") and John Wiley and Sons ("John Wiley and Sons") provided by Copyright Clearance Center ("CCC"). The license consists of your order details, the terms and conditions provided by John Wiley and Sons, and the payment terms and conditions.

All payments must be made in full to CCC. For payment instructions, please see information listed at the bottom of this form.

License Number	3274320689950
License date	Nov 22, 2013
Licensed content publisher	John Wiley and Sons
Licensed content publication	Journal of Physical Organic Chemistry
Licensed content title	Reactivity of carbene•phosphine dimers: proton affinity revisited
Licensed copyright line	Copyright © 2011 John Wiley & Sons, Ltd.
Licensed content author	Min Liu,Mu Chen,Sisi Zhang,Ill Yang,Brian Buckley,Jeehiun K. Lee
Licensed content date	Jul 18, 2011
Start page	929
End page	936
Type of use	Dissertation/Thesis
Requestor type	Author of this Wiley article
Format	Print and electronic
Portion	Full article
Will you be translating?	No
Total	0.00 USD
Terms and Conditions	

TERMS AND CONDITIONS

This copyrighted material is owned by or exclusively licensed to John Wiley & Sons, Inc. or one of its group companies (each a "Wiley Company") or a society for whom a Wiley Company has exclusive publishing rights in relation to a particular journal (collectively "WILEY"). By clicking "accept" in connection with completing this licensing transaction, you agree that the following terms and conditions apply to this transaction (along with the billing and payment terms and conditions established by the Copyright Clearance Center Inc., ("CCC's Billing and Payment terms and conditions"), at the time that you opened your RightsLink account (these are available at any time at http://myaccount.copyright.com).

Terms and Conditions

8. IN NO EVENT SHALL WILEY OR ITS LICENSORS BE LIABLE TO YOU OR ANY OTHER PARTY OR ANY OTHER PERSON OR ENTITY FOR ANY SPECIAL, CONSEQUENTIAL, INCIDENTAL, INDIRECT, EXEMPLARY OR PUNITIVE DAMAGES, HOWEVER CAUSED, ARISING OUT OF OR IN CONNECTION WITH THE DOWNLOADING, PROVISIONING, VIEWING OR USE OF THE MATERIALS REGARDLESS OF THE FORM OF ACTION, WHETHER FOR BREACH OF CONTRACT, BREACH OF WARRANTY, TORT, NEGLIGENCE, INFRINGEMENT OR OTHERWISE (INCLUDING, WITHOUT LIMITATION, DAMAGES BASED ON LOSS OF PROFITS, DATA, FILES, USE, BUSINESS OPPORTUNITY OR CLAIMS OF THIRD PARTIES), AND WHETHER OR NOT THE PARTY HAS BEEN ADVISED OF THE POSSIBILITY OF SUCH DAMAGES. THIS LIMITATION SHALL APPLY NOTWITHSTANDING ANY FAILURE OF ESSENTIAL PURPOSE OF ANY LIMITED REMEDY PROVIDED HEREIN.

9. Should any provision of this Agreement be held by a court of competent jurisdiction to be illegal, invalid, or unenforceable, that provision shall be deemed amended to achieve as nearly as possible the same economic effect as the original provision, and the legality, validity and enforceability of the remaining provisions of this Agreement shall not be affected or impaired thereby.

10. The failure of either party to enforce any term or condition of this Agreement shall not constitute a waiver of either party's right to enforce each and every term and condition of this Agreement. No breach under this agreement shall be deemed waived or excused by either party unless such waiver or consent is in writing signed by the party granting such waiver or consent. The waiver by or consent of a party to a breach of any provision of this Agreement shall not operate or be construed as a waiver of or consent to any other or subsequent breach by such other party.

11. This Agreement may not be assigned (including by operation of law or otherwise) by you without WILEY's prior written consent.

12. Any fee required for this permission shall be non-refundable after thirty (30) days from receipt

13. These terms and conditions together with CCC's Billing and Payment terms and conditions (which are incorporated herein) form the entire agreement between you and WILEY concerning this licensing transaction and (in the absence of fraud) supersedes all prior agreements and representations of the parties, oral or written. This Agreement may not be amended except in writing signed by both parties. This Agreement shall be binding upon and inure to the benefit of the parties' successors, legal representatives, and authorized assigns.

14. In the event of any conflict between your obligations established by these terms and conditions and those established by CCC's Billing and Payment terms and conditions, these terms and conditions shall prevail.

15. WILEY expressly reserves all rights not specifically granted in the combination of (i) the license details provided by you and accepted in the course of this licensing transaction, (ii) these terms and conditions and (iii) CCC's Billing and Payment terms and conditions.

16. This Agreement will be void if the Type of Use, Format, Circulation, or Requestor Type was misrepresented during the licensing process.

17. This Agreement shall be governed by and construed in accordance with the laws of the State of New York, USA, without regards to such state's conflict of law rules. Any legal action, suit or

proceeding arising out of or relating to these Terms and Conditions or the breach thereof shall be instituted in a court of competent jurisdiction in New York County in the State of New York in the United States of America and each party hereby consents and submits to the personal jurisdiction of such court, waives any objection to venue in such court and consents to service of process by registered or certified mail, return receipt requested, at the last known address of such party.

Wiley Open Access Terms and Conditions

Wiley publishes Open Access articles in both its Wiley Open Access Journals program [http://www.wileyopenaccess.com/view/index.html] and as Online Open articles in its subscription journals. The majority of Wiley Open Access Journals have adopted the [Creative Commons Attribution License](#) (CC BY) which permits the unrestricted use, distribution, reproduction, adaptation and commercial exploitation of the article in any medium. No permission is required to use the article in this way provided that the article is properly cited and other license terms are observed. A small number of Wiley Open Access journals have retained the [Creative Commons Attribution Non Commercial License](#) (CC BY-NC), which permits use, distribution and reproduction in any medium, provided the original work is properly cited and is not used for commercial purposes.

Online Open articles - Authors selecting Online Open are, unless particular exceptions apply, offered a choice of Creative Commons licenses. They may therefore select from the CC BY, the CC BY-NC and the [Attribution-NoDerivatives](#) (CC BY-NC-ND). The CC BY-NC-ND is more restrictive than the CC BY-NC as it does not permit adaptations or modifications without rights holder consent.

Wiley Open Access articles are protected by copyright and are posted to repositories and websites in accordance with the terms of the applicable Creative Commons license referenced on the article. At the time of deposit, Wiley Open Access articles include all changes made during peer review, copyediting, and publishing. Repositories and websites that host the article are responsible for incorporating any publisher-supplied amendments or retractions issued subsequently. Wiley Open Access articles are also available without charge on Wiley's publishing platform, **Wiley Online Library** or any successor sites.

Conditions applicable to all Wiley Open Access articles:

- The authors' moral rights must not be compromised. These rights include the right of "paternity" (also known as "attribution" - the right for the author to be identified as such) and "integrity" (the right for the author not to have the work altered in such a way that the author's reputation or integrity may be damaged).

- Where content in the article is identified as belonging to a third party, it is the obligation of the user to ensure that any reuse complies with the copyright policies of the owner of that content.

- If article content is copied, downloaded or otherwise reused for research and other purposes as permitted, a link to the appropriate bibliographic citation (authors, journal, article title, volume, issue, page numbers, DOI and the link to the definitive published version on Wiley Online Library) should be maintained. Copyright notices and disclaimers must not be deleted.
    - Creative Commons licenses are copyright licenses and do not confer any other rights,

including but not limited to trademark or patent rights.

- Any translations, for which a prior translation agreement with Wiley has not been agreed, must prominently display the statement: "This is an unofficial translation of an article that appeared in a Wiley publication. The publisher has not endorsed this translation."

Conditions applicable to non-commercial licenses (CC BY-NC and CC BY-NC-ND)

For non-commercial and non-promotional purposes individual non-commercial users may access, download, copy, display and redistribute to colleagues Wiley Open Access articles. In addition, articles adopting the CC BY-NC may be adapted, translated, and text- and data-mined subject to the conditions above.

Use by commercial "for-profit" organizations

Use of non-commercial Wiley Open Access articles for commercial, promotional, or marketing purposes requires further explicit permission from Wiley and will be subject to a fee. Commercial purposes include:

- Copying or downloading of articles, or linking to such articles for further redistribution, sale or licensing;

- Copying, downloading or posting by a site or service that incorporates advertising with such content;

- The inclusion or incorporation of article content in other works or services (other than normal quotations with an appropriate citation) that is then available for sale or licensing, for a fee (for example, a compilation produced for marketing purposes, inclusion in a sales pack)

- Use of article content (other than normal quotations with appropriate citation) by for-profit organizations for promotional purposes

- Linking to article content in e-mails redistributed for promotional, marketing or educational purposes;

- Use for the purposes of monetary reward by means of sale, resale, license, loan, transfer or other form of commercial exploitation such as marketing products

- Print reprints of Wiley Open Access articles can be purchased from: corporatesales@wiley.com

  The modification or adaptation for any purpose of an article referencing the CC BY-NC-ND License requires consent which can be requested from RightsLink@wiley.com .

Other Terms and Conditions:

BY CLICKING ON THE "I AGREE..." BOX, YOU ACKNOWLEDGE THAT YOU HAVE READ AND FULLY UNDERSTAND EACH OF THE SECTIONS OF AND PROVISIONS SET FORTH IN THIS AGREEMENT AND THAT YOU ARE IN AGREEMENT WITH AND ARE WILLING TO ACCEPT ALL OF YOUR OBLIGATIONS AS SET FORTH IN THIS AGREEMENT.

v1.8

ACS Publications
High quality. High impact.

Title: Assessing the Proton Affinities of N,N'-Diamidocarbenes

Author: Mu Chen, Jonathan P. Moerdyk, Garrett A. Blake, Christopher W. Bielawski, and Jeehiun K. Lee

Publication: The Journal of Organic Chemistry

Publisher: American Chemical Society

Date: Oct 1, 2013

Copyright © 2013, American Chemical Society

Logged in as:
Mu Chen

LOGOUT